POLITECNICO DI MILANO

DIPARTIMENTO DI INGEGNERIA IDRAULICA, AMBIENTALE,
INFRASTRUTTURE VIARIE E RILEVAMENTO

DOCTORAL PROGRAMME IN ENVIRONMENTAL AND
INFRASTRUCTURE ENGINEERING

THEORETICAL AND NUMERICAL UPSCALING OF SOLUTE TRANSPORT IN POROUS MEDIA

Doctoral Dissertation of:

Sergey Chaynikov

Matricola: 754463

Director of doctorate program : **Prof. Alberto Guadagnini**

Tutor: **Prof. Alberto Guadagnini**

Advisors: **Prof.Alberto Guadagnini**

Prof. Monica Riva

Dot.Giovanni Porta

2013 - XXV CYCLE

Contents

INTRODUCTION

1. Relevance

Understanding and quantifying the chemical and physical processes involved in flow and transport scenarios through porous media is of utmost importance. Relevant challenges are related to environmental sustainability and energy generation and exploitation, such as climate change and safe disposal of nuclear waste. Increasing greenhouse gases caused by human activities is often considered as one of the major causes of global warming. The carbon dioxide (CO2) sequestration where industrially-produced CO2 are stored using subsurface saline aquifers and reservoirs is considered as one of the possible options which may be implemented to reduce greenhouse gases. The other important issues currently being addressed are related to the increasing demand for fresh water and oil. These include for instance remediation of contaminated water sources for drinking and irrigation, prevention of salt water intrusion into fresh water bodies, locating new oil deposits and optimizing recovery of hydrocarbons. All these crucial targets involve fluid flow and solute transport processes in natural porous media. Moreover, porous media are used widely in many manmade systems such as fuel cells (porous diffusion layer), packed columns, filtration, paper pulp drying, textiles etc. Besides their potential applications in environmental and industrial processes, they also find an important place in biological sciences (e.g., blood flow in the human body). Modeling flow and transport in porous media therefore has wide theoretical and applied interest. However, its simulation and predictions are very challenging because of the complexity involved in these processes and the (conceptual and practical) description of the host porous media at multiple scales of interest.

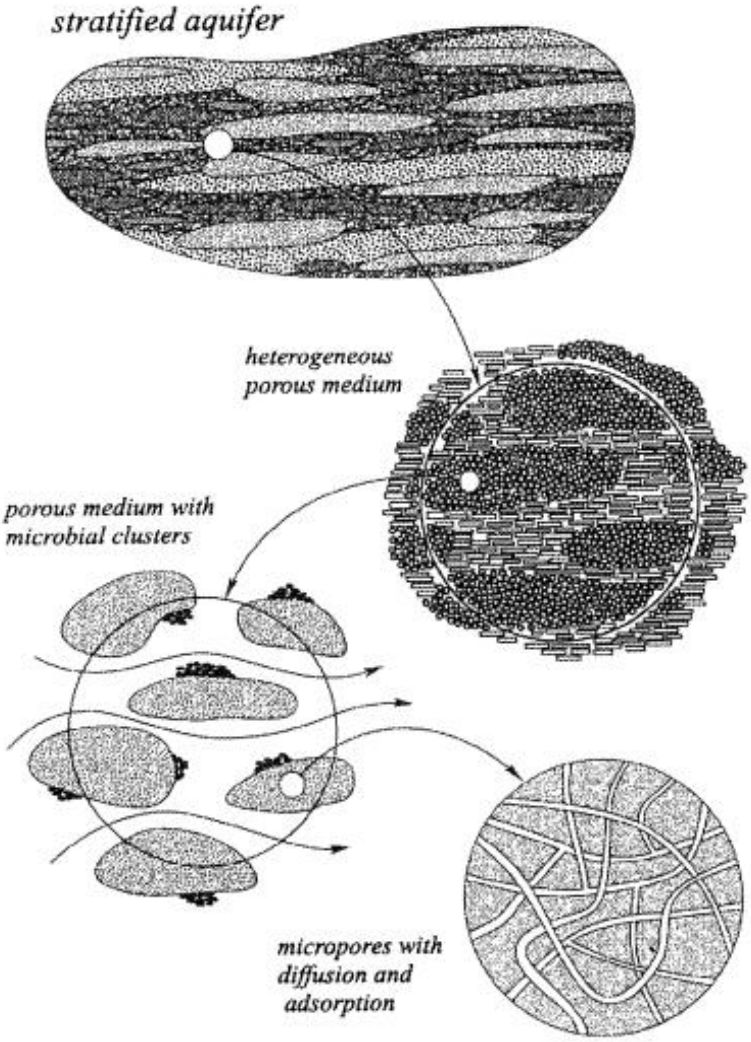

Figure 1.Length scales in geological systems [Whitaker, S. ,1999]

2. Scales

In porous media, complex physical phenomena often occur on a wide range of scales. Length scale magnitude may vary from the pore-level (in the order of few micro meters) to the field level (in the order of kilometers). Hence, a continuing challenge in mathematical and

computational modeling is to handle these relevant scales properly. In general, the appropriate modeling approach is a function of the scale at which the porous medium and the key processes of interest are described. As an example, Figure 1 provides an illustration of complexities associated with the description of a porous medium over multiple observation scales.

a. Pore-scale modeling

The pore-scale or micro scale typically ranges from 10^{-6} to 10^{-3} m. At this scale of resolution, the description of individual pores is considered. Flow at these scales is driven by the specific geometry of the solid phase (which determines the boundary with the fluid phases) and obeys local conservation laws such as the Navier–Stokes equations. Given the appropriate boundary conditions for the surface of the solid grains (e.g., no-slip), the velocity and pressure field in the pore-space can be determined by solving the Navier–Stokes equation. However for the groundwater flow inertial forces are assumed to be negligible with respect to viscous forces and the Stokes problem is frequently solved. Pore-scale modeling is appealing as the approach directly accounts for the fundamental physical processes that affect the fluid behavior thus providing improved understanding of flow and transport processes. Despite its attractiveness, the major difficulty involved in this approach is the presence of complex pore geometries.

In principle, pore-scale modeling may be used to improve the prediction of parameters of large scale models. For instance, pore scale simulations have been used to characterize absolute and relative permeability [*Blunt,* 2001], dispersion coefficients [*Wood et al.,* 2003; *Salles et al*., 1993], and effective reaction rates [*Lichtner and Tartakovsky,* 2003; *Tartakovsky et al* 2009].

b. Continuum-Scale Modeling

The solution of practical problems of flow and transport in porous media is virtually impossible at the pore scale. Therefore, continuum modeling approaches are typically introduced. In this framework the porous medium is reproduced by a continuum approximation, where the key characteristics of the underlying pore network are included through effective properties. The format of continuum scale equations for porous media has been supported both through experimental/phenomenological observations (e.g., Darcy law) and theoretical analyses. Theoretical approaches enable one to derive continuum scale systems of equations starting from pore scale equations. This typically relies on a set of appropriate hypotheses. Among the widely used approaches to derive continuum scale systems are volume Averaging and homogenization.

The classical volume averaging method, based on ideas of laid down by *Whitaker* [1967] and *Slattery* [1967] starts with a set of microscopic equations which are assumed to old at a point in space. By averaging the microscopic equations in a volume of space, a corresponding set of macroscopic equations are developed over the fluid region or over the entire region. Other than averaging the governing equations of flow and transport, directly averaging a parameter over a domain of interest is also widely implemented for upscaling. This method has been used to upscale dispersion [*Plumb and Whitaker*, 1988; *Wood et al*., 2003] and transport for fractured media [*Quintard and Whitaker*, 1996]. Recently, by examining the difference between the mathematical processes of averaging and upscaling, *Wood* [2009] revealed that the process of the volume averaging is not sufficient to reduce the number of degrees of freedom as required by upscaling [*Cushman et al*., 2002]. This target is then achieved by introducing so called scaling laws [*Wood 2009*], which allow to formulate closure relationships and typically involve the definition of the physical and chemical features of the considered problem.

Homogenization method has also been largely employed for upscaling flow and transport processes in porous media [*Auriault and Adler,* 1995; *Battiato et al.,* 2009]. a porous medium with microscopic structure characterized by period l and a macroscopic structure with the characteristic length of L. A spatial scale parameter can be defined as $\varepsilon = l / L$. Instead of working on one function u, a family of functions u^{ε} is considered to find the limit of u^{ε} when $\varepsilon \to 0$. The limit is considered as the result of upscaling procedure for homogenization. The asymptotic condition $\varepsilon \to 0$ requires separation of spatial scales. The upscaling by the homogenization is completed by making the microscopic scale approximate to zero [*Hornung*, 1997].

Typically continuum or macroscopic (or lab) scale is in the order of 10^{-2} to 10 m. Owing to the difficulty to observe and characterize properties at the pore-scale, in this approach, the effective macroscopic variables are defined by averaging the microscopic properties over a volume. Most of the laboratory experiments are conducted at this scale to obtain required parameters and hence it is widely used for modeling in porous media. Proper characterization of continuum scale effective parameters is often a challenging task (e.g. permeability, dispersion coefficients, capillary pressure, relative permeability etc.), as these may depend on the pore structure and pore-level physical processes.

3. Motivation

The pore structure and the physical characteristics of the porous medium and of the fluids that occupy the pore spaces determine several macroscopic or continuum parameters of the medium, e.g. permeability and dispersion coefficients. Understanding the relation between the

pore-scale properties and these continuum parameters is therefore a great interest both theoretically and practically in many fields. Flow and transport processes show a large dependence on the geometrical details of the porous media at the pore-scale while the physical properties of interest are observed at a larger scale.

We consider upscaling of reactive/conservative solute transport. Upscaling from pore to continuum scale: it can be performed through both theoretical and numerical methods. In particular focus of the work are the following targets: (a) theoretical derivation of a double continuum model starting from pore scale equations (Chapter 1) and (b) micro-scale numerical simulation and upscaling of a reactive transport process (Chapter 2).

CHAPTER 1. UPSCALING OF SOLUTE TRANSPORT IN POROUS MEDIA TO A DUAL CONTINUUM FORMULATION

I. Modeling techniques

1. Introduction

Transport of conservative solutes in porous and fractured media is often described at the continuum (Darcy-) scale by the advection dispersion equation (ADE). This formulation is based on the so-called Fickian analogy to model hydrodynamic dispersion. The ability of the ADE to represent observed processes at various scales has been largely discussed in the literature through theoretical, numerical and experimental analyses. *Salles et al*. [1993] present a comprehensive theoretical and numerical study and clearly identify the limits under which dispersion can be considered Gaussian/Fickian in a porous medium. Non Gaussian dispersion is observed at early times, when the solute has not sampled completely the heterogeneous pore scale velocity distribution [*e.g.*, *Gelhar et al.*, 1992; *Berkowitz et al*., 2000]. This behavior has relevant implications in the modeling of solute breakthrough curves observed, *e.g*., at the field scale under natural and/or forced gradient tracer tests [*e.g*., *Riva et al*., 2008 and references therein].

Anomalous (non-Fickian) behavior associated with observed solute breakthrough curves can be attributed to spatial variability of the velocity field, which is generally distributed over a wide range of scales. Several approaches have been proposed to deal with anomalous transport in heterogeneous porous media at different (continuum) scales of observation [*e.g*., *Berkowitz et al*., 2006; *Neuman and Tartakovsky*, 2009; and *Zhang et al*., 2009]. These include theoretical frameworks based on the continuous time random walk (CTRW) model [*Berkowitz et al*., 2006 and references therein], time and/or space-time fractional derivative formulations of the system

[*Zhang et al*, 2009 and references therein], and double- [*e.g*., *Coats and Smith*, 1964] or multi-rate mass transfer models [e.g., *Haggerty et al*., 2000, 2004]. These modeling approaches are usually supported by numerical and experimental findings [*e.g*., *Bjielic and Blunt*, 2006; *Haggerty et al*., 2004]. However, to the best of our knowledge they are still not directly grounded on a theoretical upscaling of micro-scale advective-diffusive processes.

The chapter 1 is organized as follows: Section I provides a brief introduction of several available techniques for modeling solute transport in porous media; Section II provides the formulation of the pore-scale system, the formulation of the closure system and the final upscaled equations with a comparison with DRMT/MRMT standard models; Section III illustrates our application example.

2. Theoretical framework. Advection-dispersion equation

The mass conservation equation constitutes the basis for describing the flow and solute transport in the subsurface. It is basically a mass balance equation which expresses that the net mass flux across the boundaries of a control volume must be equal to the accumulated mass.

$$\frac{\partial \Gamma}{\partial t} + \nabla \cdot \bar{\Omega} = G \tag{1.1}$$

Where Γ is the conserved fluid concentration in units per unit volume, $\bar{\Omega}$ is the flux vector in units of mass/conserved parameter per unit time per unit area and G is the source/sink term with units of concentration per unit time.

In the case of porous media flows the pore-scale Reynolds number is usually smaller than 1, consequently it is possible to assume Darcy's law to account for the relationship between pressure and flow. For a single phase, Darcy's law can be written as:

$$\Omega_i = q_i = \frac{Q_i}{A} = -\frac{K}{\mu}\left(\frac{\partial \psi}{\partial x_i}\right) \tag{1.2}$$

where q is the Darcy velocity in units of length per unit time, Q is the flow rate in volume per unit time, K is the permeability in length squared, A is the cross-sectional area in length squared, μ is the viscosity in pressure-time, $\frac{\partial \psi}{\partial x_i}$ is the pressure gradient and Ψ is given by:

$$\Psi = P + \rho g z \tag{1.3}$$

where P is the pressure in force per unit area, ρ is the fluid density in units of mass per unit volume which can be related to the system pressure and temperature by an equation of state, g is the acceleration due to gravity in the units of length squared per unit time and z is depth in units of length. We can now substitute equation (1.2) into (1.1) to obtain the governing equation for the solvent phase flowing through an isotropic porous medium:

$$\frac{\partial(\phi\rho)}{\partial t} + \frac{\partial}{\partial x}\left(\frac{K\rho}{\mu}\frac{\partial \Psi}{\partial x}\right) + \frac{\partial}{\partial y}\left(\frac{K\rho}{\mu}\frac{\partial \Psi}{\partial y}\right) + \frac{\partial}{\partial z}\left(\frac{K\rho}{\mu}\frac{\partial \Psi}{\partial z}\right) = G \tag{1.4}$$

The flux of an individual solute contains contributions from advection and diffusion. This is modeled by including the effect of the local velocity field to Fick's law using:

$$\Omega = \Omega_a + \Omega_D = q_i C + \left(-\phi D \frac{\partial C}{\partial x_i}\right) \tag{1.5}$$

where q_i is the local Darcy velocity in direction i given in units of distance per unit time, ϕ is the porosity of the medium, C is the concentration in units of mass/quantity per unit volume, $\frac{\partial C}{\partial x_i}$ is the concentration gradient in the i^{th} direction and D is the dispersion tensor in units of distance squared per unit time which is typically defined in two or three dimensions by

$$\phi D_i = \phi D_d \tau + \alpha_i |\bar{q}| \tag{1.6}$$

where D_d is the molecular diffusion coefficient (assumed isotropic), τ is the tortuosity, D_i are the eigenvalues of D, and α_i are the local dispersivity coefficients , they are associated to the principal directions of the tensor, which is aligned with the directions parallel and perpendicular to flow, and referred to as longitudinal and transverse dispersivities, α_L and α_T .

Substituting (1.5) into (1.1) we get the governing equation for the solute or the ADE [*Bear*,1972]:

$$\phi \frac{\partial C}{\partial t} + \nabla \cdot (\bar{q} C) = \phi \nabla \cdot \left(D \nabla C \right) + G \tag{1.7}$$

3. Multi-rate Mass Transfer model

Double- and multi-rate mass transfer continuum-scale models (DRMT/MRMT) represent the porous medium through an effective description which is formed by a collection of overlapped mobile and immobile sub-regions. Immobile regions can also comprise low velocity zones which are accessible to the solute and where solute can temporarily be delayed with respect to processes developing within other mobile portions of the domain. These different regions are characterized by their own transport parameters and solute mass transfer takes place between

these continua. Anomalous behavior is then attributed to delayed storage of the solute within immobile regions and solute channeling through mobile regions. Long tails and early arrival times characterizing observed breakthrough curves of concentrations have been successfully reproduced through this conceptual picture and its mathematical representations. This improved modeling capability with respect to the standard ADE is associated with an increased model complexity, *i.e.*, additional transport parameters are introduced, in the form of mass transfer coefficients describing solute exchanges between continua.

Basically one may consider Multi-Rate Mass Transfer (MRMT) model as a modified advection-dispersion equation where an additional term takes into account the exchange between high and low conductivity regions. This description implies that the pore space is decomposed into a mobile and immobile zones. The two quantities ϕ_{im} and ϕ_m identify the porosities corresponding to the mobile and the immobile regions, respectively. In the mobile zone the advective transport mechanism is predominant whereas in immobile zones advection plays negligible role. The rate at which solute moves between these two domains is controlled by a mass transfer coefficient α. One defines C_m and C_{im} , the concentrations in the mobile and immobile regions respectively. The ADE is typically used to describe the solute at mobile region, C_m. Concentration at immobile zones, C_{im}, is influences by the source/sink term which represents the mass transfer exchange between a mobile zone and a of immobile zones.

The simple form of MRMT is a double rare mass transfer(DRMT)(double porosity/double region) model. In DRMT one assumes that the porous media can be divided only into two regions: one mobile region and one immobile region. Then the model can be written as follows

$$\phi_m \frac{\partial C_m}{\partial t} + \nabla \cdot (\bar{q} C_m) = \phi_m \nabla \cdot \left(D \nabla C_m \right) - \alpha \left(C_m - C_{im}(\alpha) \right) + G \tag{1.8}$$

$$\phi_{im} \frac{\partial C_{im}(\alpha)}{\partial t} = \alpha \left(C_m - C_{im}(\alpha) \right) \tag{1.9}$$

The MRMT model provides an extension of the DRMT, where transport between mobile and immobile regions is not described by a single coefficient. This representation may be explained by assuming that due to geometrical complexity a single coefficient can hardly represent the whole mechanism of mass exchange between mobile and immobile regions(stagnant zones, pores/fractures, cavities, liquid inclusion etc).The MRMT can be written in the following form

$$\phi_m \frac{\partial C_m}{\partial t} + \nabla \cdot (\bar{q} C_m) = \phi_m \nabla \cdot \left(D \nabla C_m \right) + \phi_{im} \int_0^\infty f(\alpha) \frac{\partial C_{im}(\alpha)}{\partial t} d\alpha + G \tag{1.10}$$

$$\phi_{im} \frac{\partial C_{im}(\alpha)}{\partial t} = \alpha \left(C_m - C_{im}(\alpha) \right) \quad \forall \alpha \tag{1.11}$$

where α is the mass transfer coefficient between the immobile zones and mobile zone, $f(\alpha)$ is the density function of mass transfer rates, ϕ_m and ϕ_{im} are the volume fractions of the mobile and immobile zones.

The memory function can be interpreted as the particle resident time distribution function in the immobile zone. In other words, the memory function represents the mass flux to the immobile zones per unit volume of aquifer, for a unit change in concentration in the mobile zones [*Haggerty et al*., 2000; *Carrera et al*., 1998]. The formulation of this term depends on the geometry of the immobile zones and on the variability of the mass transfer or diffusion rates [*Haggerty et al*., 2000].

Various researches [e.g. *Zinn and Harvey*., 2003] have demonstrated that MRMT models are able to improve the results of the ADE in the case of solute transport through heterogeneous porous media.

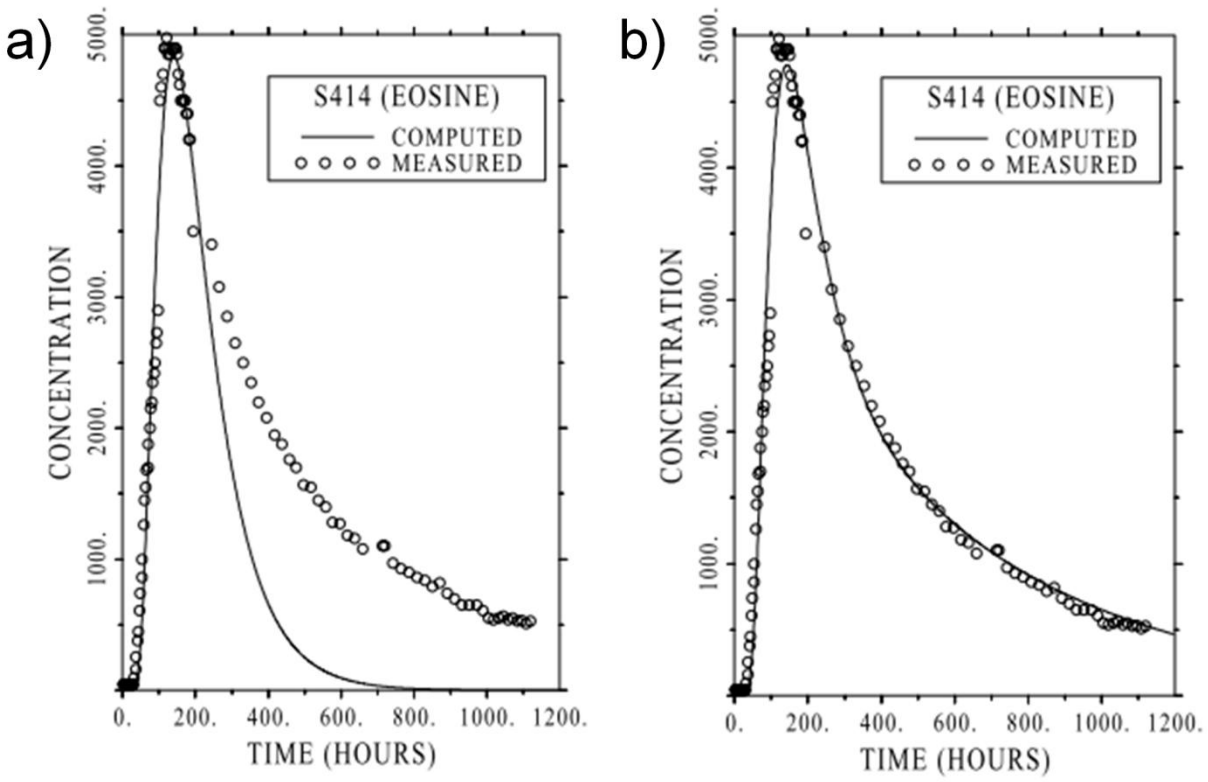

Figure 2. Comparison of experimental results and breakthrough curves predicted by a) ADE and b) DRMT models (Sanchez-Villa and Carrera, 2004).

Figure 2 shows that the DRMT model is able to reproduce the concentration profile while the ADE fails. However relationships between memory functions and physical properties of the aquifer are not clearly established yet, the appropriate format of the memory function has been shown to be a function of the medium heterogeneity. The formulation of the memory function

depends on the geometry of immobile zones and on the variability of mass transfer or diffusion rates [*Haggerty et al*., 2000].

For idealized cases, some a priori estimates of the mass exchange coefficient have been proposed [*Van Genuchten and Dalton.*, 1986; *Gwo et al*., 1998]. Numerical simulation of local-scale transport can be used to evaluate macroscopic properties [*Lessoff and Dagan*, 2001]. However, in general, these properties are derived through experiments interpretation. With this approach, macroscopic properties of a heterogeneous sample are obtained using a curve-fitting procedure.

Volume averaging approach has been used to provide theoretical foundation of DRMT and MRMT models in bimodal porous media. These works focus on the analysis of transport in heterogeneous porous media where the anomalous transport behavior may be due to the heterogeneity of the permeability field. *Ahmadi et al*.[1998] derived a two-equation model using the large-scale volume averaging method. This method provides three closure problems that give an explicit link between the different scales, and makes it possible to determine directly the macroscopic properties associated with bimodal porous media, constituted by high and low permeability regions. *Cherblanc et al*. [2003] proposed an original numerical procedure to solve these three closure problems. The developed tools were used to discuss the influence of the local-scale characteristics on the large-scale properties, in the case of a nodular system. Later *Cherblanc et al*. [2007] analyzed ability of the proposed DRMT model to represent the non-ideal behavior of more general heterogeneous systems. The need for a time-evolving effective mass transfer process has been identified previously in the literature, as summarized in the introduction. *Chastaned and Wood*[2008] using unsteady closure assumption derived an expression for mass transfer term which includes convolution product between the time

derivative of a concentration and a closure function (memory function). The expression is equivalent to the expressions proposed at other works [*Moyne*, 1997; *Landereau et al*., 2001; *Haggerty et al*., 2000]

II. Upscaling transport through volume averaging

1. Introduction

This section aims at providing a theoretical foundation of double- and multi-rate mass transfer continuum-scale models (DRMT/MRMT). As such, we consider pore-to-Darcy scale upscaling of solute transport in macroscopically homogeneous porous media and identify the pore scale velocity field as the primary source of continuum-scale observed anomalous features of transport. We start from a pore scale advective-diffusive system and derive a two-equation continuum model through an application of the volume averaging method [*Whitaker*, 1999]. The fraction of the averaging volume occupied by the fluid phase is subdivided into two sub-regions, according to the relative influence of advective and diffusive transport terms. Similar strategies have been pursued in the literature, *e.g.*, in the framework of biofilm growth modeling in porous media [*Orgogozo et al.*, 2010].

As anticipated in previous Section I theoretical and numerical works grounded on volume averaging arguments [*Ahmadi et al*., 1998; *Quintard et al*., 2001; *Cherblanc et al*., 2003, 2007; *Golfier et al*., 2011] consider upscaling from Darcy- to field- scale in bimodal porous media, *i.e.*, systems which are characterized by the occurrence of high and low hydraulic conductivity regions. These authors assume that a continuum scale description of the transport process based on the ADE holds within each sub-region. Numerical simulations are then employed to study the validity of different single- or two-equation models which have the same format of Darcy-scale single- or dual-continuum equations and can be derived upon invoking different assumptions on

local concentration equilibrium. In this context, non-Fickian behavior of the solute is assumed to be due to the heterogeneity of the hydraulic conductivity field. Recent pore scale numerical studies and experimental observations show that the complex micro-scale structure of rock samples can give rise to persistent anomalous behavior even within media which appear to be homogenous at the continuum scale [*e.g.*, *Bijeljic et al*., 2011].

Upscaling through volume averaging typically requires suitable closure relationships. These provide the link between small scale variation of velocity and concentrations and volume averaged quantities. While steady-state closure approximations are generally assumed to hold, here we rely on an unsteady (time-dependent) closure following *Moyne* [1997], *Chastanet and Wood* [2008], *Porta et al*. [2012], and *Wood and Valdes-Parada* [2012]. An unsteady closure formulation allows to (*a*) retrieve closed form equations explicitly embedding nonlocal temporal behavior and (*b*) include these in the final upscaled equations through time convolutions. We pursue an approach similar to the one presented by *Chastanet and Wood* [2008], who employ a time-dependent closure while considering Darcy- to field-scale upscaling of solute transport in heterogeneous bimodal porous media through volume averaging. These authors (*a*) show that such an unsteady closure leads to a time dependent formulation of the (upscaled) mass transfer coefficient and (*b*) provide a solution of the unsteady closure problem through a Laplace transform for a simplified geometry of the domain. In this work we provide a direct link between pore scale quantities and the coefficients of the upscaled two-equation model. The derived upscaled model embeds a minimal set of assumptions. Therefore, it is possible to identify the assumptions which are implicitly embedded in DRMT/MRMT models by direct comparison of our upscaled formulation with the standard DRMT/MRMT model equations.

2. *Problem description*

We consider transport of a passive solute through a single phase flow field taking place in a fully saturated porous domain, Ω. The latter comprises a solid (Ω_α) and a liquid (Ω_l) phase. We assume steady-state Stokes flow to take place in the pore space with a given velocity distribution $\hat{\mathbf{u}}(\hat{\mathbf{x}})$, $\hat{\mathbf{x}}$ denoting the vector of space coordinates and $\hat{\cdot}$ indicating dimensional quantities. The liquid-solid phase boundary surface is assumed to be impervious. We consider the solute to be diluted so that diffusion in the liquid space is governed by Fick's law. Under these assumptions, the distribution of solute concentration in the liquid is governed by the advection-diffusion equation. Intergranular diffusion effects are here neglected. The fluid domain Ω_l is partitioned into two distinct sub-regions, Ω_β and Ω_γ, *i.e.*, $\Omega_l \equiv \Omega_\beta \cup \Omega_\gamma$. These can be identified as a function of the relative importance of the (advective and diffusive) mechanisms acting on transport of the diluted species.

We introduce here the local Pèclet number $Pe = \hat{t}_D / \hat{t}_A = |\hat{\mathbf{u}}(\hat{\mathbf{x}})| \hat{a} / \hat{D}$, where $\hat{a}$ is a characteristic spatial dimension of the pore space, and $\hat{t}_A(\hat{\mathbf{x}}) = \hat{a} / |\hat{\mathbf{u}}(\hat{\mathbf{x}})|$ and $\hat{t}_D = \hat{a}^2 / \hat{D}$ are characteristic time scales of advective and diffusive processes, respectively. Advective transport is described through the spatially variable velocity field and the diffusion coefficient $\hat{D}$ is assumed to be constant in Ω_l. For convenience, we refer to Ω_β and Ω_γ as mobile and immobile regions, respectively. These can be identified through the local value of $Pe(\hat{\mathbf{x}})$, *i.e.*, $\Omega_\beta = \{\hat{\mathbf{x}} \in \Omega_l : Pe(\hat{\mathbf{x}}) > K\}$, $\Omega_\gamma = \{\hat{\mathbf{x}} \in \Omega_l : Pe(\hat{\mathbf{x}}) < K\}$. The boundary surface between Ω_β

and Ω_γ can be defined as $\Gamma_{\beta\gamma} = \{\hat{\mathbf{x}} \in \Omega_l : Pe(\hat{\mathbf{x}}) = K\}$. We consider transport to be advection dominated if $Pe(\hat{\mathbf{x}}) > 10$ and set K = 10 in our application.

We introduce two characteristic lengths of the pore scale medium structure, $\hat{a}_\beta$ and $\hat{a}_\gamma$, respectively related to Ω_β and Ω_γ. The appropriate choice of these scales may be problem dependent and is intrinsically linked to the key transport features associated with the geometry considered. For example, $\hat{a}_\gamma$ may be related to the size of relatively large cavities or small regions surrounding the grains, depending on which one of these is expected to play the dominant role in governing mass exchanges between the identified mobile and immobile zones. We introduce $\hat{U}_\beta$ and $\hat{U}_\gamma$, which are defined as the average velocities in the fluid phase within Ω_β and Ω_γ, respectively, the advective time scale, $\hat{t}_\beta^A = \hat{a}_\beta / \hat{U}_\beta$ and a characteristic concentration scale, $\hat{c}_0$. The latter is, *e.g.*, provided by the initial concentration distribution or through the boundary conditions acting on the external boundary, Γ_{ext}, of the porous medium.

Solute transport within the pore space is governed by the following system of equations

$$\frac{\partial c_\beta}{\partial t} + \hat{a}_\beta \hat{\nabla} \cdot [\mathbf{u}_\beta c_\beta] = \frac{\hat{a}_\beta^2}{Pe_\beta} \hat{\nabla}^2 c_\beta \qquad \mathbf{x} \in \Omega_\beta \tag{1.12}$$

$$\eta_\gamma \frac{\partial c_\gamma}{\partial t} + \hat{a}_\gamma \hat{\nabla} \cdot [\mathbf{u}_\gamma c_\gamma] = \frac{\hat{a}_\gamma^2}{Pe_\gamma} \hat{\nabla}^2 c_\gamma \qquad \mathbf{x} \in \Omega_\gamma \tag{1.13}$$

Here, $c_i = \hat{c}_i / \hat{c}_0$ is (dimensionless) concentration in Ω_i, $c_i = \vartheta_i c$ (c and ϑ_i respectively being concentration in Ω_l and the phase function, $\vartheta_i = 1$ for $\hat{\mathbf{x}} \in \hat{V}_i$, $i = \beta, \gamma$ and $\vartheta_i = 0$ otherwise) $t = \hat{t} / \hat{t}_\beta^A$, $\mathbf{u}_i = \hat{\mathbf{u}}_i / \hat{U}_i$, $Pe_i = \hat{U}_i \cdot \hat{a}_i / \hat{D}$ and $\eta_\gamma = (\hat{a}_\gamma \hat{U}_\beta) / (\hat{a}_\beta \hat{U}_\gamma)$. Note that (1.12)-(1.13) is

set in a dimensionless temporal reference frame, while spatial derivatives are kept in dimensional form for convenience. The dimensionless time is expressed in terms of the advective time scale in the mobile phase, because this process is considered to have a relevant influence on the overall transport scenario. The corresponding boundary conditions at the liquid-liquid and liquid-solid interfaces within Ω_l are

$$\begin{aligned} &\mathbf{n}_{\gamma\alpha} \cdot \hat{\nabla} c_\gamma = 0 \quad \hat{\mathbf{x}} \in \Gamma_{\alpha\gamma}; \\ &\mathbf{n}_{\gamma\beta} \cdot \hat{\nabla} c_\gamma = \mathbf{n}_{\gamma\beta} \cdot \hat{\nabla} c_\beta, \qquad \hat{\mathbf{x}} \in \Gamma_{\beta\gamma}\,. \\ &c_\beta = c_\gamma \end{aligned} \tag{1.14}$$

Here, $\Gamma_{\alpha\gamma}$ identifies the liquid-solid boundary interface; unit vector $\mathbf{n}_{\beta\gamma}$ is normal to $\Gamma_{\beta\gamma}$ and directed from Ω_β towards Ω_γ, and $\mathbf{n}_{\gamma\beta} = -\mathbf{n}_{\beta\gamma}$. Boundary conditions (1.14) ensure the continuity of the flux and solute concentration at the boundary $\Gamma_{\beta\gamma}$ between the two regions.

The system (1.12)-(1.13) is completed by the following boundary conditions on Γ_{ext}

$$\mathrm{n}_e \cdot \hat{\nabla} c_i = 0 \qquad \hat{\mathbf{x}} \in \Gamma_{out}, \Gamma_{imp} \tag{1.15}$$

$$\mathbf{u} \cdot \mathbf{n}_e c_i + \frac{\hat{a}_i}{Pe_i} \mathbf{n}_e \cdot \hat{\nabla} c_i = N_i, \qquad \hat{\mathbf{x}} \in \Gamma_{in} \tag{1.16}$$

where $i = \gamma, \beta$, $\mathbf{n}_e$ is the inward unit normal to the external boundary, and N_i is a (non dimensional) flux term. Here, Γ_{ext} has been decomposed into three parts, *i.e.*, the inflow and outflow boundaries, respectively indicated as Γ_{in} and Γ_{out}, and an impermeable boundary Γ_{imp}. We assume concentration to be constant in the domain at the initial time, *i.e.*,

$$c_i(\hat{\mathbf{x}}, t = 0) = C \tag{1.17}$$

3. *Volume averaging*

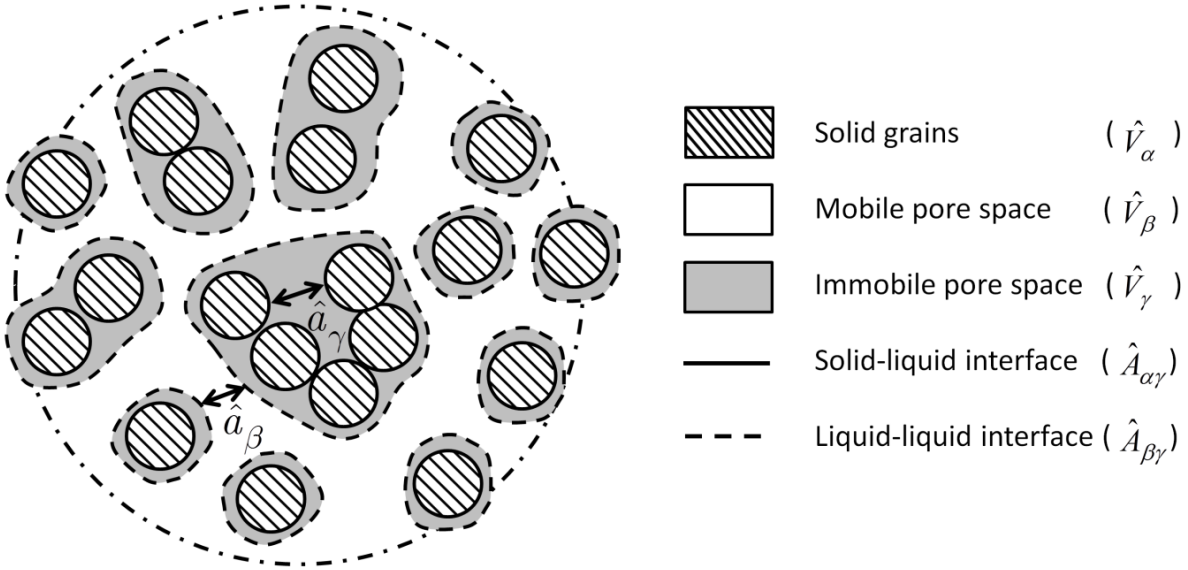

Figure 3. Sketch of the pore scale partition of the averaging volume .

We adopt the volume averaging method [*Whitaker*, 1999] and average (1.12)-(1.13) over a volume, $\hat{V} \in \Omega$, that includes solid, $\hat{V}_\alpha \in \Omega_\alpha$, and mobile, $\hat{V}_\beta \in \Omega_\beta = \{\hat{\mathbf{x}} \in \Omega_l : Pe(\hat{\mathbf{x}}) > K\}$, and immobile, $\hat{V}_\gamma \in \Omega_\gamma = \{\hat{\mathbf{x}} \in \Omega_l : Pe(\hat{\mathbf{x}}) < K\}$, liquid sub-regions. A sketch of the averaging volume is reported in Figure 3. The characteristic length scale of $\hat{V}$ is $\hat{r}_0 \gg \hat{a}_i$.

Considering the scalar field ψ, the superficial ($\langle \psi_i \rangle$) and intrinsic ($\langle \psi_i \rangle^i, i = \beta, \gamma$) averages of $\psi_i = \vartheta_i \psi$ within $\hat{V}_\beta$ and $\hat{V}_\gamma$ are defined as

$$\langle \psi_i \rangle^i = \langle \psi_i \rangle^i \Big|_x = \frac{1}{\left|\hat{V}_i(\hat{\mathbf{x}})\right|} \int_{\hat{V}_i(\hat{\mathbf{x}})} \psi_i(\hat{\mathbf{x}} + \hat{\mathbf{y}})\, d\hat{\mathbf{y}}, \qquad i = \beta, \gamma \tag{1.18}$$

It then follows that $\langle\psi\rangle = \phi_i \langle\psi_i\rangle^i$, $\phi_i = \left|\hat{V}_i\right| / \left|\hat{V}\right|$ and $\phi_\alpha + \phi_\beta + \phi_\gamma = 1$, where $\phi_\alpha = \phi_i = \left|\hat{V}_\alpha\right| / \left|\hat{V}\right|$.

We then introduce [*Whitaker*, 1999]

$$\left\langle \hat{\nabla}\psi_\beta \right\rangle = \hat{\nabla}\left\langle \psi_\beta \right\rangle + \frac{1}{\left|\hat{V}\right|}\int_{\hat{A}_{\beta\gamma}} \left(\psi_\beta \, \mathbf{n}_{\beta\gamma}\right) d\hat{A}_{\beta\gamma} = \hat{\nabla}\left(\phi_\beta \left\langle \psi_\beta \right\rangle^\beta\right) + \frac{1}{\left|\hat{V}\right|}\int_{\hat{A}_{\beta\gamma}} \left(\psi_\beta \, \mathbf{n}_{\beta\gamma}\right) d\hat{A}_{\beta\gamma} \tag{1.19}$$

$$\begin{aligned} \left\langle \hat{\nabla}\psi_\gamma \right\rangle = \hat{\nabla}\left\langle \psi_\gamma \right\rangle + \frac{1}{\left|\hat{V}\right|}\int_{\hat{A}_{\beta\gamma}} \left(\psi_\gamma \, \mathbf{n}_{\gamma\beta}\right) d\hat{A}_{\beta\gamma} + \frac{1}{\left|\hat{V}\right|}\int_{\hat{A}_{\alpha\gamma}} \left(\psi_\gamma \, \mathbf{n}_{\alpha\gamma}\right) d\hat{A}_{\alpha\gamma} = \\ = \hat{\nabla}\left(\phi_\beta \left\langle \psi_\beta \right\rangle^\beta\right) + \frac{1}{\left|\hat{V}\right|}\int_{\hat{A}_{\beta\gamma}} \left(\psi_\beta \, \mathbf{n}_{\gamma\beta}\right) d\hat{A}_{\beta\gamma} + \frac{1}{\left|\hat{V}\right|}\int_{\hat{A}_{\alpha\gamma}} \left(\psi_\gamma \, \mathbf{n}_{\alpha\gamma}\right) d\hat{A}_{\alpha\gamma} \end{aligned} \tag{1.20}$$

Here, $\hat{A}_{\alpha\gamma}$ and $\hat{A}_{\beta\gamma}$ are the internal surfaces delimiting volumes $\hat{V}_i$ $(i = \beta, \gamma)$ within $\hat{V}$ and $\mathbf{n}_{\alpha\gamma}$, $\mathbf{n}_{\beta\gamma} = -\mathbf{n}_{\gamma\beta}$ are the corresponding outward unit normal vector. Note that $\hat{A}_{\alpha\gamma} = \varnothing$ by definition because fluid velocity vanishes at the liquid-solid boundary (see also Figure 3).

Application of volume averaging requires to decompose the pore scale concentration field into two contributions, *i.e.*,

$$c_i = \langle c_i \rangle^i + \tilde{c}_i \tag{1.21}$$

where $\langle c_i \rangle^i$ $(i = \beta, \gamma)$ is defined according to (1.18) and $\tilde{c}_i$ is a zero-mean fluctuation term representing local deviations from $\langle c_i \rangle^i$ within $\hat{V}_i$. We introduce $\hat{L}_c$, $\hat{L}_\phi$, and $\hat{L}_{c1}$, as the length scales respectively associated with the variations of (averaged) concentration, porosity and concentration gradient, *i.e.*,

$$\hat{\nabla}\langle c_i\rangle^i = O\left(\frac{\Delta\langle c_i\rangle^i}{\hat{L}_c}\right)$$
$$\hat{\nabla}\phi = O\left(\frac{\Delta\phi}{\hat{L}_\phi}\right) \tag{1.22}$$
$$\hat{\nabla}\hat{\nabla}\langle c_i\rangle^i = O\left(\frac{\Delta\left(\hat{\nabla}\langle c_i\rangle^i\right)}{\hat{L}_{c1}}\right)$$

Here, $O(\cdot)$ indicates order of magnitude of the quantities in parenthesis and ΔX is a characteristic magnitude of the spatial variation of X over the length scale $\hat{L}_X$.

We show here the main steps of the volume averaging procedure. Let us integrate equation (1.12) in the volume V

$$\frac{\partial\langle c_\beta\rangle}{\partial t} + \hat{a}_\beta\langle\hat{\nabla}\cdot[\mathbf{u}_\beta c_\beta]\rangle = \frac{\hat{a}_\beta^2}{Pe_\beta}\langle\hat{\nabla}^2 c_\beta\rangle \tag{1.23}$$

Applying definition of the intrinsic average we find

$$\phi_\beta\frac{\partial\langle c_\beta\rangle^\beta}{\partial t} + \hat{a}_\beta\langle\hat{\nabla}\cdot[\mathbf{u}_\beta c_\beta]\rangle = \frac{\hat{a}_\beta^2}{Pe_\beta}\langle\hat{\nabla}^2 c_\beta\rangle \tag{1.24}$$

Now we use volume average theorem (1.20) to obtain

$$\phi_\beta\frac{\partial\langle c_\beta\rangle^\beta}{\partial t} + \hat{a}_\beta\hat{\nabla}\cdot\langle\mathbf{u}_\beta c_\beta\rangle = -\frac{\hat{a}_\beta}{|\hat{V}|}\int_{\hat{A}_{\beta\gamma}} n_{\beta\gamma}\cdot\mathbf{u}_\beta c_\beta d\hat{A} +$$
$$\frac{\hat{a}_\beta^2}{Pe_\beta}\hat{\nabla}\cdot\langle\hat{\nabla}c_\beta\rangle + \frac{1}{|\hat{V}|}\int_{\hat{A}_{\beta\gamma}} n_{\beta\gamma}\cdot\frac{\hat{a}_\beta^2}{Pe_\beta}\hat{\nabla}c_\beta d\hat{A} \tag{1.25}$$

Note that two surface integrals are included in (1.25). Both of them are induced by boundary flux exchange between the two regions. In particular the first one is due to advection through the boundary between two phases and the second one is due to diffusion. Consequently

the volume averaged equation in the β and γ regions will be always coupled to each other through these terms.

Using the volume averaging theorem as in equation (1.25) we get

$$\phi_\beta \frac{\partial \langle c_\beta \rangle^\beta}{\partial t} + \hat{a}_\beta \hat{\nabla} \cdot \langle \mathbf{u}_\beta c_\beta \rangle = -\frac{\hat{a}_\beta}{|\hat{V}|} \int_{\hat{A}_{\beta\gamma}} n_{\beta\gamma} \cdot \mathbf{u}_\beta c_\beta d\hat{A} + \frac{\hat{a}_\beta^2}{Pe_\beta} \hat{\nabla} \cdot \left[\hat{\nabla} \langle c_\beta \rangle + \frac{1}{|\hat{V}|} \int_{\hat{A}_{\beta\gamma}} n_{\beta\gamma} \cdot c_\beta d\hat{A} \right] + \frac{1}{|\hat{V}|} \int_{\hat{A}_{\beta\gamma}} n_{\beta\gamma} \cdot \frac{\hat{a}_\beta^2}{Pe_\beta} \hat{\nabla} c_\beta d\hat{A} \tag{1.26}$$

Then we introduce the following decompositions of concentration and velocity fields

$$c_\beta = \langle c \rangle^\beta + \tilde{c}_\beta \tag{1.27}$$

$$u_\beta = \langle u \rangle^\beta + \tilde{u}_\beta \tag{1.28}$$

where $\tilde{c}_\beta, \tilde{u}_\beta$ are the zero-mean fluctuations of the local concentration and velocity in volume $\hat{V}$ respectively.

After we substitute (1.27), (1.28) into (1.26) one finds

$$\phi_\beta \frac{\partial \langle c_\beta \rangle^\beta}{\partial t} + \hat{a}_\beta \hat{\nabla} \cdot \left(\phi_\beta \langle \mathbf{u}_\beta \rangle^\beta \langle c_\beta \rangle^\beta \right) = -\hat{\nabla} \cdot \left[\phi_\beta \langle \tilde{u}_\beta \tilde{c}_\beta \rangle^\beta \right] + \frac{\hat{a}_\beta^2}{Pe_\beta} \hat{\nabla} \cdot \left[\phi_\beta \hat{\nabla} \langle c_\beta \rangle^\beta + \frac{1}{|\hat{V}|} \int_{\hat{A}_{\beta\gamma}} n_{\beta\gamma} \cdot \tilde{c}_\beta d\hat{A} \right] - \frac{\hat{a}_\beta}{|\hat{V}|} \int_{\hat{A}_{\beta\gamma}} n_{\beta\gamma} \cdot \left(\mathbf{u}_\beta c_\beta - \frac{\hat{a}_\beta}{Pe_\beta} \hat{\nabla} c_\beta \right) d\hat{A} \tag{1.29}$$

Equation (1.29) represents the region-averaged transport equations in the superficial form. We identify several macro-scale terms such as macro-scale dispersion and diffusion also terms that involve the spatial deviation quantities. In addition, the inter-region flux (last term) is specified entirely in terms of pore-scale concentration fields. Our aim is now to develop the closure problem, which will allow us to determine the diffusive and dispersive terms. We start by

decomposing inter-region flux into macro-scale quantities and spatial deviation quantities. It can be shown that

$$\frac{\hat{a}_\beta}{\left|\hat{V}\right|}\int_{\hat{A}_{\beta\gamma}} n_{\beta\gamma}\cdot\left(\mathbf{u}_\beta c_\beta-\frac{\hat{a}_\beta}{Pe_\beta}\hat{\nabla}c_\beta\right)d\hat{A}=\frac{\hat{a}_\beta}{\left|\hat{V}\right|}\int_{\hat{A}_{\beta\gamma}} n_{\beta\gamma}\cdot\left(\mathbf{u}_\beta\tilde{c}_\beta-\frac{\hat{a}_\beta}{Pe_\beta}\hat{\nabla}\tilde{c}_\beta\right)d\hat{A} \tag{1.30}$$

Above we used the divergence theorem to express the area integral over the velocity field and the assumption that velocity is divergence free. Then we use that for spatially periodic system, $\nabla\phi_\beta$ is zero.

Using these assumptions we can write inter-region flux in terms of spatial deviation of the concentration

$$\begin{aligned}&\phi_\beta\frac{\partial\left\langle c_\beta\right\rangle^\beta}{\partial t}+\hat{a}_\beta\hat{\nabla}\cdot\left(\phi_\beta\left\langle\mathbf{u}_\beta\right\rangle^\beta\left\langle c_\beta\right\rangle^\beta\right)=-\hat{\nabla}\cdot\left[\phi_\beta\left\langle\tilde{u}_\beta\tilde{c}_\beta\right\rangle^\beta\right]+\\&\frac{\hat{a}_\beta^2}{Pe_\beta}\hat{\nabla}\cdot\left[\phi_\beta\hat{\nabla}\left\langle c_\beta\right\rangle^\beta+\frac{1}{\left|\hat{V}\right|}\int_{\hat{A}_{\beta\gamma}} n_{\beta\gamma}\,\tilde{c}_\beta d\hat{A}\right]-\frac{1}{\left|\hat{V}\right|}\int_{\hat{A}_{\beta\gamma}} n_{\beta\gamma}\cdot\left(\hat{a}_\beta\mathbf{u}_\beta\tilde{c}_\beta-\frac{\hat{a}_\beta}{Pe_\beta}\hat{\nabla}\tilde{c}_\beta\right)d\hat{A}\end{aligned} \tag{1.31}$$

Following the same steps described above we can write equation for the γ-phase. Then the system for both regions take following form:

$$\begin{aligned}&\frac{\partial\left\langle c_\beta\right\rangle^\beta}{\partial t}+\hat{a}_\beta\hat{\nabla}\cdot\left[\left\langle\mathbf{u}_\beta\right\rangle^\beta\left\langle c_\beta\right\rangle^\beta\right]=-\hat{a}_\beta\hat{\nabla}\cdot\left[\left\langle\tilde{\mathbf{u}}_\beta\tilde{c}_\beta\right\rangle^\beta\right]+\\&\frac{\hat{a}_\beta^2}{Pe_\beta}\hat{\nabla}\cdot\left[\hat{\nabla}\left\langle c_\beta\right\rangle^\beta+\frac{1}{\phi_\beta\left|\hat{V}\right|}\int_{\hat{A}_{\beta\gamma}}\mathbf{n}_{\beta\gamma}\,\tilde{c}_\beta d\hat{A}\right]-\frac{1}{\phi_\beta\left|\hat{V}\right|}\int_{\hat{A}_{\beta\gamma}}\mathbf{n}_{\beta\gamma}\cdot\left(\hat{a}_\beta\mathbf{u}_\beta\tilde{c}_\beta-\frac{\hat{a}_\beta^2}{Pe_\beta}\hat{\nabla}\tilde{c}_\beta\right)d\hat{A}\end{aligned} \tag{1.32}$$

$$\begin{aligned}&\eta_\gamma\frac{\partial\left\langle c_\gamma\right\rangle^\gamma}{\partial t}+\hat{a}_\gamma\hat{\nabla}\cdot\left[\left\langle\mathbf{u}_\gamma\right\rangle^\gamma\left\langle c_\gamma\right\rangle^\gamma\right]=-\hat{a}_\gamma\hat{\nabla}\cdot\left[\left\langle\tilde{\mathbf{u}}_\gamma\tilde{c}_\gamma\right\rangle^\gamma\right]+\\&\frac{\hat{a}_\gamma^2}{Pe_\gamma}\hat{\nabla}\cdot\left[\hat{\nabla}\left\langle c_\gamma\right\rangle^\gamma+\frac{1}{\phi_\gamma\left|\hat{V}\right|}\int_{\hat{A}_{\gamma\beta}}\mathbf{n}_{\gamma\beta}\,\tilde{c}_\gamma d\hat{A}\right]-\frac{1}{\phi_\gamma\left|\hat{V}\right|}\int_{\hat{A}_{\gamma\beta}}\mathbf{n}_{\gamma\beta}\cdot\left(\hat{a}_\gamma\mathbf{u}_\gamma\tilde{c}_\gamma-\frac{\hat{a}_\gamma^2}{Pe_\gamma}\hat{\nabla}\tilde{c}_\gamma\right)d\hat{A}\end{aligned} \tag{1.33}$$

The last integral term appearing on the right hand side of (1.32) and (1.33) represents the concentration flux through the surface $\hat{A}_{\gamma\beta}$. Boundary integrals on the liquid solid surface $\hat{A}_{\alpha\gamma}$ do not appear in the volume averaged equations, due to the corresponding zero-flux boundary condition in (1.14). Equations (1.32)-(1.33) can be derived upon assuming typical scale separation hypotheses for the two concentration fields, namely $\hat{r}_0^2 \ll \hat{L}_c \hat{L}_{c1}$, $\hat{r}_0^2 \ll \hat{L}_{c1} \hat{L}_\phi$, $\hat{a}_i \ll \hat{r}_0 \ll \hat{L}_c$.

4. Equations for fluctuations

The system of equations (1.32)-(1.33) includes terms that depend on the concentration fluctuations $\tilde{c}_\beta$ and $\tilde{c}_\gamma$. Formulation of closure relationships is then required to enable one to express $\tilde{c}_\beta$ and $\tilde{c}_\gamma$ in terms of volume averaged concentrations. Subtracting the volume averaged equations (1.32)-(1.33) from the original pore scale system (1.12)-(1.13) leads to

$$\frac{\partial \tilde{c}_\beta}{\partial t} + \hat{a}_\beta \hat{\nabla} \cdot \left[\mathbf{u}_\beta c_\beta - \left\langle \mathbf{u}_\beta \right\rangle^\beta \left\langle c_\beta \right\rangle^\beta \right] = \hat{\nabla} \cdot \left[\frac{\hat{a}_\beta^2}{Pe_\beta} \hat{\nabla} c_\beta - \frac{\hat{a}_\beta^2}{Pe_\beta} \hat{\nabla} \left\langle c_\beta \right\rangle^\beta \right] +$$
$$\nabla \cdot \left[\frac{\hat{a}_\beta^2}{Pe_\beta} \frac{\phi_\beta^{-1}}{\left|\hat{V}\right|} \int_{\hat{A}_{\beta\gamma}} n_{\beta\gamma} \cdot \tilde{c}_\beta d\hat{A} \right] + \hat{a}_\beta \hat{\nabla} \cdot \left\langle \tilde{\mathbf{u}}_\beta \tilde{c}_\beta \right\rangle^\beta + \tag{1.34}$$
$$\frac{\phi_\beta^{-1}}{\left|\hat{V}\right|} \int_{\hat{A}_{\beta\gamma}} n_{\beta\gamma} \cdot \left[\hat{a}_\beta \mathbf{u}_\beta \tilde{c}_\beta - \frac{\hat{a}_\beta^2}{Pe_\beta} \hat{\nabla} \tilde{c}_\beta \right] dA$$

Let's consider the convective transport term in (1.34). We make use of the velocity decomposition to obtain

$$\mathbf{u}_\beta c_\beta - \left\langle \mathbf{u}_\beta \right\rangle^\beta \left\langle c_\beta \right\rangle^\beta = \mathbf{u}_\beta \tilde{c}_\beta + \tilde{\mathbf{u}}_\beta \left\langle c_\beta \right\rangle^\beta \tag{1.35}$$

Using the divergence theorem and ignoring the deviations of volume fraction one can get

$$\hat{\nabla}\cdot\left\langle \mathbf{u}_\beta \right\rangle^\beta = 0 \tag{1.36}$$

Here we simplify the diffusive flux

$$\frac{\hat{a}_\beta^2}{Pe_\beta}\hat{\nabla}c_\beta - \frac{\hat{a}_\beta^2}{Pe_\beta}\hat{\nabla}\left\langle c_\beta \right\rangle^\beta = \frac{\hat{a}_\beta^2}{Pe_\beta}\hat{\nabla}\tilde{c}_\beta \tag{1.37}$$

As a final simplification we make use of the averaging theorem to write

$$\left\langle \hat{\nabla}\tilde{c}_\beta \right\rangle = \hat{\nabla}\left\langle \tilde{c}_\beta \right\rangle + \frac{1}{\left|\hat{V}\right|}\int_{\hat{A}_{\beta\gamma}} n_{\beta\gamma}\,\tilde{c}_\beta d\hat{A} \tag{1.38}$$

using that the average of the deviation equal to zero we write

$$\frac{\phi_\beta^{-1}}{\left|\hat{V}\right|}\int_{\hat{A}_{\beta\gamma}} n_{\beta\gamma}\,\tilde{c}_\beta d\hat{A} = \left\langle \hat{\nabla}\tilde{c}_\beta \right\rangle^\beta \tag{1.39}$$

These allow us to recast the previous result in more compact form given by

$$\begin{aligned}&\frac{\partial\tilde{c}_\beta}{\partial t} + \hat{a}_\beta\hat{\nabla}\cdot\left[\mathbf{u}_\beta\tilde{c}_\beta\right] + \hat{a}_\beta\tilde{\mathbf{u}}_\beta\cdot\hat{\nabla}\left\langle\tilde{c}_\beta\right\rangle^\beta - \hat{a}_\beta\hat{\nabla}\cdot\left\langle\tilde{\mathbf{u}}_\beta\tilde{c}_\beta\right\rangle^\beta = \hat{\nabla}\cdot\left[\frac{\hat{a}_\beta^2}{Pe_\beta}\hat{\nabla}\tilde{c}_\beta\right] - \\ &\hat{\nabla}\cdot\left[\frac{\hat{a}_\beta^2}{Pe_\beta}\left\langle\hat{\nabla}\tilde{c}_\beta\right\rangle^\beta\right] + \frac{\phi_\beta^{-1}}{\left|\hat{V}\right|}\int_{\hat{A}_{\beta\gamma}} n_{\beta\gamma}\cdot\left[\hat{a}_\beta\mathbf{u}_\beta\tilde{c}_\beta - \frac{\hat{a}_\beta^2}{Pe_\beta}\hat{\nabla}\tilde{c}_\beta\right]dA\end{aligned} \tag{1.40}$$

Now let's estimate and compare diffusive terms

$$\hat{\nabla}\cdot\left[\frac{1}{Pe_\beta}\hat{\nabla}\tilde{c}_\beta\right] = O\left[\frac{\tilde{c}_\beta}{\hat{a}_\beta\hat{a}_\beta Pe_\beta}\right], \quad \hat{\nabla}\cdot\left[\frac{1}{Pe_\beta}\left\langle\hat{\nabla}\tilde{c}_\beta\right\rangle^\beta\right] = O\left[\frac{\tilde{c}_\beta}{\hat{a}_\beta LPe_\beta}\right] \tag{1.41}$$

comparing the orders of magnitude of two terms in (1.41) we can neglect the second one when satisfied the length scale assumption $\hat{a}_\beta << \hat{h}$. We can do the same with the convective terms so that

$$\nabla\cdot<\tilde{u}_\beta\tilde{c}_\beta>=O\left[\frac{<u_\beta>\tilde{c}_\beta}{L}\right],\qquad \nabla\cdot[u_\beta\tilde{c}_\beta]=O\left[\frac{<u_\beta>\tilde{c}_\beta}{l_\beta}\right] \tag{1.42}$$

and the first one in (1.42)can be neglected. On the basis of these simplifications equation for $\tilde{c}_\beta$ may be written in the form of

$$\frac{\partial\tilde{c}_\beta}{\partial t}+\hat{a}_\beta\hat{\nabla}\cdot\left[\mathbf{u}_\beta\tilde{c}_\beta\right]+\hat{a}_\beta\tilde{\mathbf{u}}_\beta\cdot\hat{\nabla}\left\langle c_\beta\right\rangle^\beta = \hat{\nabla}\cdot\left[\frac{\hat{a}_\beta^2}{Pe_\beta}\hat{\nabla}\tilde{c}_\beta\right]+\frac{1}{\phi_\beta\left|\hat{V}\right|}\int_{\hat{A}_{\beta\gamma}}\mathbf{n}_{\beta\gamma}\cdot\left[\hat{a}_\beta\mathbf{u}_\beta\tilde{c}_\beta-\frac{\hat{a}_\beta^2}{Pe_\beta}\hat{\nabla}\tilde{c}_\beta\right]d\hat{A} \tag{1.43}$$

$$\eta_\gamma\frac{\partial\tilde{c}_\gamma}{\partial t}+\hat{a}_\gamma\hat{\nabla}\cdot\left[\mathbf{u}_\gamma\tilde{c}_\gamma\right]+\hat{a}_\gamma\tilde{\mathbf{u}}_\gamma\cdot\hat{\nabla}\left\langle c_\gamma\right\rangle^\gamma = \hat{\nabla}\cdot\left[\frac{\hat{a}_\gamma^2}{Pe_\gamma}\hat{\nabla}\tilde{c}_\gamma\right]+\frac{1}{\phi_\gamma\left|\hat{V}\right|}\int_{\hat{A}_{\beta\gamma}}\mathbf{n}_{\gamma\beta}\cdot\left[\hat{a}_\gamma\mathbf{u}_\gamma\tilde{c}_\gamma-\frac{\hat{a}_\gamma^2}{Pe_\gamma}\hat{\nabla}\tilde{c}_\gamma\right]d\hat{A} \tag{1.44}$$

with boundary and initial conditions

$$\begin{aligned}
&\mathbf{n}_{\alpha\gamma}\cdot\left(\hat{\nabla}\tilde{c}_\gamma\right)=-\mathbf{n}_{\alpha\gamma}\cdot\left(\hat{\nabla}\left\langle c_\gamma\right\rangle^\gamma\right), && \hat{\mathbf{x}}\in\hat{A}_{\alpha\gamma}\\
&\tilde{c}_\beta=\tilde{c}_\gamma+\left(\left\langle c_\gamma\right\rangle^\gamma-\left\langle c_\beta\right\rangle^\beta\right), && \hat{\mathbf{x}}\in\hat{A}_{\beta\gamma}\\
&\mathbf{n}_{\beta\gamma}\cdot\left(\hat{\nabla}\tilde{c}_\beta\right)=\mathbf{n}_{\beta\gamma}\cdot\left(\hat{\nabla}\tilde{c}_\gamma\right)+\mathbf{n}_{\beta\gamma}\cdot\left(\hat{\nabla}\left[\left\langle c_\gamma\right\rangle^\gamma-\left\langle c_\beta\right\rangle^\beta\right]\right) && \hat{\mathbf{x}}\in\hat{A}_{\beta\gamma}
\end{aligned} \tag{1.45}$$

$$\tilde{c}_\beta(\hat{\mathbf{x}},t=0)=0,\qquad \tilde{c}_\gamma(\hat{\mathbf{x}},t=0)=0 \tag{1.46}$$

Note that the terms $\hat{a}_\beta\hat{\nabla}\cdot\left[\left\langle\tilde{\mathbf{u}}_\beta\tilde{c}_\beta\right\rangle^\beta\right]$ and $\hat{a}_\gamma\hat{\nabla}\cdot\left[\left\langle\tilde{\mathbf{u}}_\gamma\tilde{c}_\gamma\right\rangle^\gamma\right]$ are not included in (1.43)-(1.44) following standard volume averaging analyses [*Whitaker*, 1999]. The validity of this assumption in the presence of a Dirichlet boundary condition is discussed in *Golfier et al*. [2002] in the context of upscaling of heat transfer in capillary tubes. Here, we note that, as opposed to the

work of *Golfier et al*. [2002] where the Dirichlet boundary condition for the fluctuation term is expressed in terms of an averaged value, our (1.45) involves the difference between two averaged concentrations, $\langle c_\gamma \rangle^\gamma - \langle c_\beta \rangle^\beta$. Albeit this argument cannot be used in general to compare orders of magnitude of averaged concentration and local deviations, equation (1.43)-(1.44) are consistent with previous studies where volume averaging of two-region transport model is performed in the presence of boundary conditions of the kind (1.45) [*e.g*., *Orgogozo et al*, 2010; *Chastanet and Wood*, 2008].

Following *Whitaker* [1999], the porous medium is conceptualized as a collection of unit cells containing pores of arbitrary shapes. The solution of (1.43)-(1.44) is then performed within a unit cell in the presence of periodic boundary conditions. The system (1.43)-(1.44) is composed by two time dependent equations with time-invariant coefficients. Hence, its solution tends asymptotically towards a steady state condition, *i.e*., a steady closure of the system is valid only for long enough times. The relevance of the transient stage on the solution depends (in general) on the geometry of the problem at the level of the unit cell and on the Péclet number in each sub-region as suggested in *Porta et al*. [2012]. Here, we retain the transient effects in the formulation of the closure problems associated with both mobile and immobile regions. Note that, even as one could (in principle) assume problem (1.44) to reach steady state at early time due to small advective effects ($Pe_\gamma < 10$), boundary conditions (1.45) link the closure problems in the two sub-regions considered. Hence, the solution to the closure problem in the immobile region is likely to be influenced by the mobile region also for relatively long times. As the system is linear in $\tilde{c}_\beta$ and $\tilde{c}_\gamma$, superposition can be invoked. The spatial distribution of the concentration fluctuations can then be written in terms of the source terms appearing in (1.43)-(1.45), which

are expressed as functions of the intrinsic average of the concentrations and their gradients. These latter quantities can be considered as uniform within the averaging volume on the basis of scale separation arguments.

Following *Moyne* [1997], we assume the following relationships to hold

$$\begin{aligned}\tilde{c}_\beta &= \hat{\mathbf{g}}^1_{\beta\beta} * \frac{\partial}{\partial t}\hat{\nabla}\left\langle c_\beta \right\rangle^\beta + \hat{\mathbf{g}}^1_{\beta\gamma} * \frac{\partial}{\partial t}\hat{\nabla}\left\langle c_\gamma \right\rangle^\gamma + g^0_\beta * \frac{\partial}{\partial t}\left(\left\langle c_\gamma \right\rangle^\gamma - \left\langle c_\beta \right\rangle^\beta\right) \\ \tilde{c}_\gamma &= \hat{\mathbf{g}}^1_{\gamma\beta} * \frac{\partial}{\partial t}\hat{\nabla}\left\langle c_\beta \right\rangle^\beta + \hat{\mathbf{g}}^1_{\gamma\gamma} * \frac{\partial}{\partial t}\hat{\nabla}\left\langle c_\gamma \right\rangle^\gamma + g^0_\gamma * \frac{\partial}{\partial t}\left(\left\langle c_\gamma \right\rangle^\gamma - \left\langle c_\beta \right\rangle^\beta\right)\end{aligned} \tag{1.47}$$

Here, dimensional vectors $\hat{\mathbf{g}}^1_{\beta\beta}$, $\hat{\mathbf{g}}^1_{\beta\gamma}$, $\hat{\mathbf{g}}^1_{\gamma\beta}$, $\hat{\mathbf{g}}^1_{\gamma\gamma}$ and dimensionless scalars g^0_β and g^0_γ are closure variables, and $*$ indicates convolution, *e.g.*, $\hat{\mathbf{g}}^1_{\beta\beta} * \frac{\partial}{\partial t}\hat{\nabla}\left\langle c_\beta \right\rangle^\beta = \int_0^t \hat{\mathbf{g}}^1_{\beta\beta}(t-\tau)\cdot\frac{\partial}{\partial \tau}\left(\hat{\nabla}\left\langle c_\beta \right\rangle^\beta\right)d\tau$.

Note that different linear combinations of the source terms appearing in (1.43)-(1.45) are possible and lead to different formulations for the closure variables. Here, we rely on the formulation (1.47), which has been previously suggested and employed for the analysis of heat transport [*Moyne*, 1997] and mass transfer in heterogeneous bimodal porous media [*Ahmadi et al*., 1998; *Quintard et al*., 2001; *Cherblanc et al*., 2003, 2007; *Golfier et al*., 2011].

5. *Closure equation systems*

Here the details of the complete system of equations are presented (*i.e.*, six equations, three of which are defined in $\hat{V}_\beta$ and three in $\hat{V}_\gamma$; note that these equations are coupled in pairs through boundary conditions (1.45)) which is used to compute the closure variables introduced in (1.47).

Problem I

$$\frac{\partial \hat{\mathbf{g}}^1_{\beta\beta}}{\partial t} + \hat{a}_\beta \hat{\nabla} \cdot \left[\mathbf{u}_\beta \hat{\mathbf{g}}^1_{\beta\beta} \right] - \hat{a}_\beta \tilde{\mathbf{u}}_\beta = \hat{\nabla} \cdot \left[\frac{\hat{a}^2_\beta}{Pe_\beta} \hat{\nabla} \hat{\mathbf{g}}^1_{\beta\beta} \right] + \phi_\beta^{-1} \mathbf{v}_{\beta\beta}; \quad \hat{\mathbf{x}} \in \hat{V}_\beta \tag{1.48}$$

$$\eta_\gamma \frac{\partial \hat{\mathbf{g}}^1_{\gamma\beta}}{\partial t} + \hat{a}_\gamma \hat{\nabla} \cdot \left[\mathbf{u}_\gamma \hat{\mathbf{g}}^1_{\gamma\beta} \right] = \hat{\nabla} \cdot \left[\frac{\hat{a}^2_\gamma}{Pe_\gamma} \hat{\nabla} \hat{\mathbf{g}}^1_{\gamma\beta} \right] + \phi_\gamma^{-1} \mathbf{v}_{\gamma\beta}; \qquad \hat{\mathbf{x}} \in \hat{V}_\gamma \tag{1.49}$$

Boundary conditions at the internal surfaces $\hat{A}_{\beta\gamma}$ and $\hat{A}_{\alpha\gamma}$ of the unit cell are

$$\hat{\mathbf{g}}^1_{\beta\beta} = \hat{\mathbf{g}}^1_{\gamma\beta} \qquad \hat{\mathbf{x}} \in \hat{A}_{\beta\gamma} \tag{1.50}$$

$$\mathbf{n}_{\beta\gamma} \cdot (\nabla \hat{\mathbf{g}}^1_{\beta\beta} + \mathbf{I}) = \mathbf{n}_{\beta\gamma} \cdot (\nabla \hat{\mathbf{g}}^1_{\gamma\beta}) \qquad \hat{\mathbf{x}} \in \hat{A}_{\beta\gamma} \tag{1.51}$$

$$\mathbf{n}_{\alpha\gamma} \cdot \left(\hat{\nabla} \hat{\mathbf{g}}^1_{\gamma\beta} \right) = 0 \qquad \hat{\mathbf{x}} \in \hat{A}_{\alpha\gamma} \tag{1.52}$$

We assume that initial solute concentration is uniform within the system. In the presence of, *e.g.*, zero initial concentration, the corresponding initial condition is

$$\hat{\mathbf{g}}^1_{\beta\beta}(t=0) = 0, \qquad \hat{\mathbf{g}}^1_{\gamma\beta}(t=0) = 0 \tag{1.53}$$

The following two conditions are additionally set due to the system periodicity

$$\hat{\mathbf{g}}^1_{\beta\beta}(r + \hat{a}_i) = \hat{\mathbf{g}}^1_{\beta\beta}(r), \quad \hat{\mathbf{g}}^1_{\gamma\beta}(r + \hat{a}_i) = \hat{\mathbf{g}}^1_{\gamma\beta}(r), \quad i = 1,2,3 \tag{1.54}$$

$$\left\langle \hat{\mathbf{g}}^1_{\beta\beta} \right\rangle^\beta = 0, \qquad \left\langle \hat{\mathbf{g}}^1_{\gamma\beta} \right\rangle^\gamma = 0 \tag{1.55}$$

We use vectors $\mathbf{v}_{\beta\beta}$ and $\mathbf{v}_{\gamma\beta}$ to represent the two following quantities

$$\mathbf{v}_{\beta\beta} = \frac{1}{\left|\hat{V}\right|} \int_{\hat{A}_{\beta\gamma}} \mathbf{n}_{\beta\gamma} \cdot \left[\hat{a}_\beta \mathbf{u}_\beta \hat{\mathbf{g}}^1_{\beta\beta} - \frac{\hat{a}^2_\beta}{Pe_\beta} \hat{\nabla} \hat{\mathbf{g}}^1_{\beta\beta} \right] d\hat{A} \tag{1.56}$$

$$\mathbf{v}_{\gamma\beta} = \frac{1}{\left|\hat{V}\right|} \int_{\hat{A}_{\beta\gamma}} \mathbf{n}_{\gamma\beta} \cdot \left[\hat{a}_\gamma \mathbf{u}_\gamma \hat{\mathbf{g}}^1_{\gamma\beta} - \frac{\hat{a}^2_\gamma}{Pe_\gamma} \hat{\nabla} \hat{\mathbf{g}}^1_{\gamma\beta} \right] d\hat{A} \tag{1.57}$$

The definition of the other two coupled systems of equations is reported below and relies on the same type of formulation illustrated above.

Problem II

$$\frac{\partial \hat{\mathbf{g}}^1_{\beta\gamma}}{\partial t} = \hat{\nabla}\cdot\left[\frac{\hat{a}^2_\beta}{Pe_\beta}\hat{\nabla}\hat{\mathbf{g}}^1_{\beta\gamma}\right] + \phi_\beta^{-1}\mathbf{v}_{\beta\gamma}\ \mathbf{x}\in\hat{V}_\beta \tag{1.58}$$

$$\eta_\gamma\frac{\partial \hat{\mathbf{g}}^1_{\gamma\gamma}}{\partial t} + \hat{a}_\gamma\hat{\nabla}\cdot\left[\mathbf{u}_\gamma\hat{\mathbf{g}}^1_{\gamma\gamma}\right] + \hat{a}_\gamma\tilde{\mathbf{u}}_\gamma = \hat{\nabla}\cdot\left[\frac{\hat{a}^2_\gamma}{Pe_\gamma}\hat{\nabla}\hat{\mathbf{g}}^1_{\gamma\gamma}\right] + \phi_\gamma^{-1}\mathbf{v}_{\gamma\gamma}\ \mathbf{x}\in\hat{V}_\gamma \tag{1.59}$$

Internal surface boundary conditions:

$$\hat{\mathbf{g}}^1_{\beta\gamma} = \hat{\mathbf{g}}^1_{\gamma\gamma} \qquad \hat{\mathbf{x}}\in\hat{A}_{\beta\gamma} \tag{1.60}$$

$$\mathbf{n}_{\beta\gamma}\cdot\left(\hat{\nabla}\hat{\mathbf{g}}^1_{\beta\gamma}\right) = \mathbf{n}_{\beta\gamma}\cdot\left(\hat{\nabla}\hat{\mathbf{g}}^1_{\gamma\gamma} + \mathbf{I}\right) \qquad \hat{\mathbf{x}}\in\hat{A}_{\beta\gamma} \tag{1.61}$$

$$\mathbf{n}_{\alpha\gamma}\cdot\left(\hat{\nabla}\hat{\mathbf{g}}^1_{\gamma\gamma}\right) = -\mathbf{n}_{\alpha\gamma}\cdot\left(\mathbf{I}\right) \qquad \hat{\mathbf{x}}\in\hat{A}_{\alpha\gamma} \tag{1.62}$$

Initial conditions:

$$\hat{\mathbf{g}}^1_{\beta\gamma}(t=0) = 0, \qquad \hat{\mathbf{g}}^1_{\gamma\gamma}(t=0) = 0, \tag{1.63}$$

Periodicity:

$$\hat{\mathbf{g}}^1_{\beta\gamma}(r+\hat{a}_i) = \hat{\mathbf{g}}^1_{\beta\gamma}(r), \qquad \hat{\mathbf{g}}^1_{\gamma\gamma}(r+\hat{a}_i) = \hat{\mathbf{g}}^1_{\gamma\gamma}(r), \qquad i=1,2,3 \tag{1.64}$$

Average:

$$\left\langle\hat{\mathbf{g}}^1_{\beta\gamma}\right\rangle^\beta = 0, \qquad \left\langle\hat{\mathbf{g}}^1_{\gamma\gamma}\right\rangle^\gamma = 0 \tag{1.65}$$

We use vectors $\mathbf{v}_{\beta\gamma}$ and $\mathbf{v}_{\gamma\gamma}$ to represent the following quantities

$$\mathbf{v}_{\beta\gamma} = \frac{1}{\left|\hat{V}\right|} \int_{\hat{A}_{\beta\gamma}} \mathbf{n}_{\beta\gamma} \cdot \left[\hat{a}_\beta \mathbf{u}_\beta \hat{\mathbf{g}}^1_{\beta\gamma} - \frac{\hat{a}^2_\beta}{Pe_\beta} \hat{\nabla} \hat{\mathbf{g}}^1_{\beta\gamma} \right] d\hat{A} \tag{1.66}$$

$$\mathbf{v}_{\gamma\gamma} = \frac{1}{\left|\hat{V}\right|} \int_{\hat{A}_{\beta\gamma}} \mathbf{n}_{\gamma\gamma} \cdot \left[\hat{a}_\gamma \mathbf{u}_\gamma \hat{\mathbf{g}}^1_{\gamma\gamma} - \frac{\hat{a}^2_\gamma}{Pe_\gamma} \hat{\nabla} \hat{\mathbf{g}}^1_{\gamma\gamma} \right] d\hat{A} \tag{1.67}$$

Problem III

$$\frac{\partial g^0_\beta}{\partial t} + \hat{a}_\beta \hat{\nabla} \cdot \left[\mathbf{u}_\beta g^0_\beta \right] = \hat{\nabla} \cdot \left[\frac{\hat{a}^2_\beta}{Pe_\beta} \hat{\nabla} g^0_\beta \right] + \phi^{-1}_\beta \alpha_\beta \qquad \mathbf{x} \in \hat{V}_\beta \tag{1.68}$$

$$\eta_\gamma \frac{\partial g^0_\gamma}{\partial t} + \hat{a}_\gamma \hat{\nabla} \cdot \left[\mathbf{u}_\gamma g^0_\gamma \right] = \hat{\nabla} \cdot \left[\frac{\hat{a}^2_\gamma}{Pe_\gamma} \hat{\nabla} g^0_\gamma \right] + \phi^{-1}_\gamma \alpha_\gamma \qquad \mathbf{x} \in \hat{V}_\gamma \tag{1.69}$$

Internal surface boundary conditions:

$$g^0_\beta = g^0_\gamma + 1 \qquad \hat{\mathbf{x}} \in \hat{A}_{\beta\gamma} \tag{1.70}$$

$$\mathbf{n}_{\beta\gamma} \cdot \left(\hat{\nabla} g^0_\beta \right) = \mathbf{n}_{\beta\gamma} \cdot \left(\hat{\nabla} g^0_\gamma \right) \qquad \hat{\mathbf{x}} \in \hat{A}_{\beta\gamma} \tag{1.71}$$

$$\mathbf{n}_{\alpha\gamma} \cdot \left(\hat{\nabla} g^0_\gamma \right) = 0 \qquad \hat{\mathbf{x}} \in \hat{A}_{\alpha\gamma} \tag{1.72}$$

Initial conditions:

$$g^1_\beta(t=0) = 0, \qquad g^1_\gamma(t=0) = 0 \tag{1.73}$$

Periodicity:

$$g^0_\beta(r + \hat{a}_i) = g^0_\beta(r), \qquad g^0_\gamma(r + \hat{a}_i) = g^0_\gamma(r), \qquad i = 1,2,3 \tag{1.74}$$

Average:

$$\left\langle g_\beta^0 \right\rangle^\beta = 0, \qquad \left\langle g_\gamma^0 \right\rangle^\gamma = 0 \tag{1.75}$$

Here, the mass transfer coefficients, α_β and α_γ, are defined by

$$\alpha_\beta = \frac{1}{\left|\hat{V}\right|} \int_{\hat{A}_{\beta\gamma}} \mathbf{n}_{\beta\gamma} \cdot \left[\hat{a}_\beta \mathbf{u}_\beta g_\beta^0 - \frac{\hat{a}_\beta^2}{Pe_\beta} \hat{\nabla} g_\beta^0 \right] d\hat{A} \tag{1.76}$$

$$\alpha_\gamma = \frac{1}{\left|\hat{V}\right|} \int_{\hat{A}_{\beta\gamma}} \mathbf{n}_{\gamma\beta} \cdot \left[\hat{a}_\gamma \mathbf{u}_\beta g_\gamma^0 - \frac{\hat{a}_\gamma^2}{Pe_\gamma} \hat{\nabla} g_\gamma^0 \right] d\hat{A} \tag{1.77}$$

6. *The upscaled two-equation transport model*

Substitution of (1.47) into (1.32)-(1.33) yields the closed form of the desired (upscaled) two-equation model. The continuum scale system driving the evolution of the (volume) averaged concentration can be formulated as

$$\begin{aligned} &\phi_\beta \frac{\partial \left\langle c_\beta \right\rangle^\beta}{\partial t} + \underbrace{\hat{a}_\beta \hat{\nabla} \cdot \left[\phi_\beta \left\langle \mathbf{u}_\beta \right\rangle^\beta \left\langle c_\beta \right\rangle^\beta \right]}_{AD_\beta} - \underbrace{\hat{a}_\beta \hat{\nabla} \cdot \left[\mathbf{d}_\beta * \frac{\partial}{\partial t} \left(\left\langle c_\beta \right\rangle^\beta - \left\langle c_\gamma \right\rangle^\gamma \right) \right]}_{AAD_\beta} \\ &\underbrace{-\hat{a}_\beta \mathbf{v}_{\beta\beta} * \frac{\partial}{\partial t} \hat{\nabla} \left\langle c_\beta \right\rangle^\beta}_{ME1_\beta} - \underbrace{\hat{a}_\beta \mathbf{v}_{\beta\gamma} * \frac{\partial}{\partial t} \hat{\nabla} \left\langle c_\gamma \right\rangle^\gamma}_{ME2_\beta} = \underbrace{\frac{\hat{a}_\beta^2}{Pe_\beta} \hat{\nabla} \cdot \left[\mathbf{D}_{\beta\beta}^* * \frac{\partial}{\partial t} \hat{\nabla} \left\langle c_\beta \right\rangle^\beta \right]}_{D1_\beta} + \\ &\underbrace{\frac{\hat{a}_\beta^2}{Pe_\beta} \hat{\nabla} \cdot \left[\mathbf{D}_{\beta\gamma}^* * \frac{\partial}{\partial t} \hat{\nabla} \left\langle c_\gamma \right\rangle^\gamma \right]}_{D2_\beta} + \underbrace{\alpha_\beta * \frac{\partial}{\partial t} \left(\left\langle c_\gamma \right\rangle^\gamma - \left\langle c_\beta \right\rangle^\beta \right)}_{ME3_\beta} \end{aligned} \tag{1.78}$$

$$\eta_\gamma \phi_\gamma \frac{\partial \left\langle c_\gamma \right\rangle^\gamma}{\partial t} + \underbrace{\hat{a}_\gamma \hat{\nabla} \cdot \left(\phi_\gamma \left\langle \mathbf{u}_\gamma \right\rangle^\gamma \left\langle c_\gamma \right\rangle^\gamma \right)}_{AD_\gamma} - \underbrace{\hat{a}_\gamma \hat{\nabla} \cdot \left[\mathbf{d}_\gamma * \frac{\partial}{\partial t} \left(< c_\beta >^\beta - < c_\gamma >^\gamma \right) \right]}_{AAD_\gamma}$$

$$\underbrace{-\hat{a}_\gamma \mathbf{v}_{\gamma\beta} * \frac{\partial}{\partial t} \hat{\nabla} \left\langle c_\beta \right\rangle^\beta}_{ME1_\gamma} - \underbrace{\hat{a}_\gamma \mathbf{v}_{\gamma\gamma} * \frac{\partial}{\partial t} \hat{\nabla} \left\langle c_\gamma \right\rangle^\gamma}_{ME2_\gamma} = \underbrace{\frac{\hat{a}_\gamma^2}{Pe_\gamma} \hat{\nabla} \cdot \left[\mathbf{D}^*_{\gamma\gamma} * \frac{\partial}{\partial t} \hat{\nabla} \left\langle c_\gamma \right\rangle^\gamma \right]}_{D1_\gamma} + \tag{1.79}$$

$$\underbrace{\frac{\hat{a}_\gamma^2}{Pe_\gamma} \hat{\nabla} \cdot \left[\mathbf{D}^*_{\gamma\beta} * \frac{\partial}{\partial t} \hat{\nabla} \left\langle c_\beta \right\rangle^\beta \right]}_{D2_\gamma} + \underbrace{\alpha_\gamma * \frac{\partial}{\partial t} \left(\left\langle c_\gamma \right\rangle^\gamma - \left\langle c_\beta \right\rangle^\beta \right)}_{ME3_\gamma}$$

Equations (1.78) and (1.79) are nonlocal in time, as they include time convolutions. Terms appearing in (1.78)-(1.79) are indicated and grouped as follows, to highlight their distinct contributions. The terms denoted as AD_i ($i = \beta, \gamma$) are the standard advective terms. Terms indicated as AAD_i ($i = \beta, \gamma$) are additional advective terms, containing the difference between the two averaged concentrations. Terms $ME1_i$ and $ME2_i$ ($i = \beta, \gamma$) represent mass exchange between the two sub-regions considered. Terms $D1_i$ and $D2_i$ ($i = \beta, \gamma$) represent dispersive effects. The resulting upscaled system of equations can then be compared against the DRMT/MRMT formulations in a straightforward manner.

Note that all coefficients appearing in (1.78)-(1.79) are dimensionless. The definition of these coefficients is provided in the following, where we distinguish:

- Advective coefficients. Besides the two mean velocities, $\left\langle \mathbf{u}_\beta \right\rangle^\beta$ and $\left\langle \mathbf{u}_\gamma \right\rangle^\gamma$, the following advective coefficients appear in (1.78)-(1.79)

$$\mathbf{v}_{\beta\beta} = \frac{1}{\left|\hat{V}\right|} \int_{\hat{A}_{\beta\gamma}} \mathbf{n}_{\beta\gamma} \cdot \left[\mathbf{u}_\beta \hat{\mathbf{g}}^1_{\beta\beta} - \frac{\hat{a}_\beta}{Pe_\beta} \nabla \hat{\mathbf{g}}^1_{\beta\beta} \right] d\hat{A} \tag{1.80}$$

$$\mathbf{v}_{\beta\gamma} = \frac{1}{\left|\hat{V}\right|}\int_{\hat{A}_{\beta\gamma}} \mathbf{n}_{\beta\gamma}\cdot\left[\mathbf{u}_\beta \hat{\mathbf{g}}^1_{\beta\gamma} - \frac{\hat{a}_\beta}{Pe_\beta}\nabla\hat{\mathbf{g}}^1_{\beta\gamma}\right] d\hat{A} \tag{1.81}$$

$$\mathbf{v}_{\gamma\gamma} = \frac{1}{\left|\hat{V}\right|}\int_{\hat{A}_{\beta\gamma}} \mathbf{n}_{\gamma\beta}\cdot\left[\mathbf{u}_\gamma \hat{\mathbf{g}}^1_{\gamma\gamma} - \frac{\hat{a}_\gamma}{Pe_\gamma}\nabla\hat{\mathbf{g}}^1_{\gamma\gamma}\right] d\hat{A} \tag{1.82}$$

$$\mathbf{v}_{\gamma\beta} = \frac{1}{\left|\hat{V}\right|}\int_{\hat{A}_{\beta\gamma}} \mathbf{n}_{\gamma\beta}\cdot\left[\mathbf{u}_\gamma \hat{\mathbf{g}}^1_{\gamma\beta} - \frac{\hat{a}_\gamma}{Pe_\gamma}\nabla\hat{\mathbf{g}}^1_{\gamma\beta}\right] d\hat{A} \tag{1.83}$$

The following two coefficients appear due to the introduction of the closure variables g^0_β and g^0_γ

$$\mathbf{d}_\beta = -Pe_\beta\left\langle\tilde{\mathbf{u}}_\beta g^0_\beta\right\rangle^\beta + \frac{1}{\left|\hat{V}\right|}\int_{\hat{A}_{\beta\gamma}} \hat{a}_\beta g^0_\beta \mathbf{n}_{\beta\gamma} d\hat{A} \tag{1.84}$$

$$\mathbf{d}_\gamma = -Pe_\gamma\left\langle\tilde{\mathbf{u}}_\gamma g^0_\gamma\right\rangle^\gamma + \frac{1}{\left|\hat{V}\right|}\int_{\hat{A}_{\beta\gamma}} \hat{a}_\gamma g^0_\gamma \mathbf{n}_{\beta\gamma} d\hat{A} \tag{1.85}$$

These may interpreted as additional convective coefficients which arise as a consequence of mass exchange between the two regions $\hat{V}_\beta$ and $\hat{V}_\gamma$.

- Dispersive coefficients. These are defined as the tensors

$$\mathbf{D}^*_{\beta\beta} = I - \frac{Pe_\beta}{\hat{a}_\beta}\left\langle\tilde{\mathbf{u}}_\beta\hat{\mathbf{g}}^1_{\beta\beta}\right\rangle^\beta + \frac{1}{\left|\hat{V}\right|}\int_{\hat{A}_{\beta\gamma}} \hat{\mathbf{g}}^1_{\beta\beta}\mathbf{n}_{\beta\gamma} d\hat{A} \tag{1.86}$$

$$\mathbf{D}^*_{\gamma\gamma} = I - \frac{Pe_\gamma}{\hat{a}_\gamma}\left\langle\tilde{\mathbf{u}}_\gamma\hat{\mathbf{g}}^1_{\gamma\gamma}\right\rangle^\gamma + \frac{1}{\left|\hat{V}\right|}\int_{\hat{A}_{\beta\gamma}} \hat{\mathbf{g}}^1_{\gamma\gamma}\mathbf{n}_{\beta\gamma} d\hat{A} \tag{1.87}$$

$$\mathbf{D}^*_{\beta\gamma} = -\frac{Pe_\beta}{\hat{a}_\beta}\left\langle\tilde{\mathbf{u}}_\beta\hat{\mathbf{g}}^1_{\beta\gamma}\right\rangle^\beta + \frac{1}{\left|\hat{V}\right|}\int_{\hat{A}_{\beta\gamma}} \hat{\mathbf{g}}^1_{\beta\gamma}\mathbf{n}_{\beta\gamma} d\hat{A} \tag{1.88}$$

$$\mathbf{D}^{*}_{\gamma\beta} = -\frac{Pe_{\gamma}}{\hat{a}_{\gamma}}\left\langle \tilde{\mathbf{u}}_{\gamma}\hat{\mathbf{g}}^{1}_{\gamma\beta}\right\rangle^{\gamma} + \frac{1}{\left|\hat{V}\right|}\int_{\hat{A}_{\beta\gamma}}\hat{\mathbf{g}}^{1}_{\gamma\beta}\mathbf{n}_{\beta\gamma}d\hat{A} \tag{1.89}$$

- Mass transfer coefficients

$$\alpha_{\beta} = \frac{1}{\left|\hat{V}\right|}\int_{\hat{A}_{\beta\gamma}}\mathbf{n}_{\beta\gamma}\cdot\left[\hat{a}_{\beta}\mathbf{u}_{\beta}g^{0}_{\beta} - \frac{\hat{a}^{2}_{\beta}}{Pe_{\beta}}\hat{\nabla}g^{0}_{\beta}\right]d\hat{A} \tag{1.90}$$

$$\alpha_{\gamma} = \frac{1}{\left|\hat{V}\right|}\int_{\hat{A}_{\beta\gamma}}\mathbf{n}_{\gamma\beta}\cdot\left[\hat{a}_{\gamma}\mathbf{u}_{\gamma}g^{0}_{\gamma} - \frac{\hat{a}^{2}_{\gamma}}{Pe_{\gamma}}\hat{\nabla}g^{0}_{\gamma}\right]d\hat{A} \tag{1.91}$$

All these coefficients are directly linked to the pore scale characteristics of the system and can be computed once the pore scale geometry and velocity fields are available for a given geometry of the unit cell. The formulation of the upscaled system presented above is similar to that obtained by application of volume averaging to solute transport in heterogeneous porous media at a larger scales [*e.g.*, *Ahmadi et al.*, 1998; *Quintard et al.*, 2001; *Cherblanc et al.*, 2003, 2007; *Chastanet and Wood*, 2008; *Golfier et al.*, 2011]. Our upscaled coefficients are expressed directly in terms of pore scale quantities and the porous medium is assumed to be homogeneous (in terms of hydraulic conductivity distribution) at the continuum scale.

Our upscaled two-equation system (1.78)-(1.79) can be readily compared against typical dual- and multi-rate mass transfer (DRMT/MRMT) formulations [*Haggerty et al.*, 2000, 2004]. As previously recalled, these models represent pore scale mass fluxes between regions associated with different characteristic velocities through mass transfer processes taking place at a continuum scale and driven by a set of effective parameters. A typical formulation associated with MRMT models is presented by system (1.10)-(1.11)

$$\frac{\partial C_{m}}{\partial t} = L(C_{m}) - \Theta\int_{0}^{\infty} f(\beta)\beta(C_{m} - C_{im})d\beta \tag{1.92}$$

$$\frac{\partial C_{im}}{\partial t} = \beta(C_m - C_{im}) \tag{1.93}$$

Here, C_m and C_{im} are solute concentrations in the mobile and immobile phase, respectively; Θ is the ratio between immobile and mobile phase porosities; $L(C_m)$ is the operator representing solute migration due to advection and dispersion; $f(\beta)$ is a probability distribution function associated with the continuous set of first-order rates controlling mass transfer between mobile and immobile phases and satisfying $\int_0^\infty f(\beta)d\beta = 1$. In this sense, the quantities ϕ_β and ϕ_γ representing in (1.78)-(1.79) the volumetric fractions of the mobile ($\hat{V}_\beta$) and immobile ($\hat{V}_\gamma$) regions within the unit cell are respectively termed as mobile and immobile porosity in the context of traditional MRMT formulations. Note that the liquid-liquid interface integral describing mass transfer between $\hat{V}_\beta$ and $\hat{V}_\gamma$ is split into different components in (1.78)-(1.79). These include (*a*) kinetic mass transfer terms which are expressed through the coefficients α_γ (1.91) and α_β (1.90) that are characterized by the same format of the corresponding terms appearing in MRMT models, and (*b*) advective-like quantities, which include the coefficients (1.80)-(1.83). These latter coefficients account for advective-diffusive exchanges taking place through the boundary between the β- and γ- regions and are usually not included in MRMT models.

The comparison between the volume averaged system (1.78)-(1.79) and the MRMT model (1.92)-(1.93) allows to identify the key hypotheses embedded in the latter. These can be summarized as follows.

1) The advective and dispersive terms appearing in (1.92) and depicting transport in the mobile region are local in time. Our upscaled formulation reduces to a similar format when one introduces in (1.86) the asymptotic solution for the closure variable $\hat{\mathbf{g}}_{1\beta\beta}$, *i.e.*, when the solution of the corresponding quasi-steady closure problem is employed. In this sense, the MRMT scheme implicitly assumes that subdividing the pore space into different sub-regions incorporates nonlocal dispersive effects taking place in the mobile region. The MRMT model retains nonlocal contributions only in the mass exchange terms.
2) All terms associated with advective and dispersive effects and appearing in (1.79) are neglected in (1.93), which describes transport in the immobile region.
3) The additional advective terms of the type AAD_i ($i = \beta, \gamma$) are usually neglected in MRMT formulations. This may be justified on the basis of the following assumptions

$$\hat{\nabla}\langle c_\beta\rangle^\beta \approx \hat{\nabla}\langle c_\gamma\rangle^\gamma ;\ \hat{\nabla}\langle c_\beta\rangle^\beta \gg \hat{\nabla}\left(\langle c_\beta\rangle^\beta - \langle c_\gamma\rangle^\gamma\right);\ \hat{\nabla}\langle c_\gamma\rangle^\gamma \gg \hat{\nabla}\left(\langle c_\beta\rangle^\beta - \langle c_\gamma\rangle^\gamma\right) \qquad (1.94)$$

In other words, if the gradients of concentration within the β- and γ-regions are similar, then the gradient of their difference becomes negligible. Clearly, this might not be a sufficient condition if $\mathbf{d}_i \gg \langle \mathbf{u}_i \rangle^i$; likewise, it might not be a necessary condition if $\mathbf{d}_i \ll \langle \mathbf{u}_i \rangle^i$. The validity of the assumption (34) may depend on the specific case considered as well as pore scale concentration distribution at initial time (*e.g.*, the condition expressed in (1.94) might be attained only for long times) because $\mathbf{d}_i$ depends on pore scale geometry and the ensuing spatial fluctuations of the velocity field. Assuming that (1.94) holds, leads to

$$\mathbf{v}_{\beta\beta} * \frac{\partial}{\partial t}\hat{\nabla}\left\langle c_\beta \right\rangle^\beta + \mathbf{v}_{\beta\gamma} * \frac{\partial}{\partial t}\hat{\nabla}\left\langle c_\gamma \right\rangle^\gamma \approx \left(\mathbf{v}_{\beta\beta} + \mathbf{v}_{\beta\gamma}\right) * \frac{\partial}{\partial t}\hat{\nabla}\left\langle c_\beta \right\rangle^\beta \tag{1.95}$$

$$\mathbf{v}_{\gamma\beta} * \frac{\partial}{\partial t}\hat{\nabla}\left\langle c_\beta \right\rangle^\beta + \mathbf{v}_{\gamma\gamma} * \frac{\partial}{\partial t}\hat{\nabla}\left\langle c_\gamma \right\rangle^\gamma \approx \left(\mathbf{v}_{\gamma\beta} + \mathbf{v}_{\gamma\gamma}\right) * \frac{\partial}{\partial t}\hat{\nabla}\left\langle c_\gamma \right\rangle^\gamma \tag{1.96}$$

$$\hat{\nabla}\cdot\left[\mathbf{D}^*_{\beta\beta} * \frac{\partial}{\partial t}\hat{\nabla}\left\langle c_\beta \right\rangle^\beta\right] + \hat{\nabla}\cdot\left[\mathbf{D}^*_{\beta\gamma} * \frac{\partial}{\partial t}\hat{\nabla}\left\langle c_\gamma \right\rangle^\gamma\right] \approx \hat{\nabla}\cdot\left[\left(\mathbf{D}^*_{\beta\beta} + \mathbf{D}^*_{\beta\gamma}\right) * \frac{\partial}{\partial t}\hat{\nabla}\left\langle c_\beta \right\rangle^\beta\right] \tag{1.97}$$

$$\hat{\nabla}\cdot\left[\mathbf{D}^*_{\gamma\gamma} * \frac{\partial}{\partial t}\hat{\nabla}\left\langle c_\gamma \right\rangle^\gamma\right] + \hat{\nabla}\cdot\left[\mathbf{D}^*_{\gamma\beta} * \frac{\partial}{\partial t}\hat{\nabla}\left\langle c_\beta \right\rangle^\beta\right] \approx \hat{\nabla}\cdot\left[\left(\mathbf{D}^*_{\gamma\gamma} + \mathbf{D}^*_{\gamma\beta}\right) * \frac{\partial}{\partial t}\hat{\nabla}\left\langle c_\gamma \right\rangle^\gamma\right] \tag{1.98}$$

This imply that the two equations of the upscaled model (17)-(18) are coupled only through the difference of the two average concentrations (and not through their gradients) when (1.94)-(1.98) hold, consistent with the MRMT formulation (1.92)-(1.93).

4) Mass exchange terms in (1.78)-(1.79) include the usual mass transfer coefficients α_β and α_γ. They also include two additional terms (*ME1* and *ME2*) representing advective effects, which are not explicitly represented in the standard MRMT model. As a consequence, the effective mass transfer coefficient appearing in traditional MRMT models may implicitly represent the combined effects of the advective (1.80)-(1.83) and standard (1.90)-(1.91) mass transfer coefficients. The relative proportion of mobile and immobile porosity is usually unknown in field or laboratory scale settings and is often considered as a calibration parameter in typical applications of MRMT models. Parameter calibration influences the value of the effective advective coefficient which is considered through application of (1.92). Hence, the calibration of the optimal mobile/immobile porosity partition may embed also the effects of the mass exchange terms *ME1* and *ME2* in (1.78)-(1.79).

5) The mass transfer coefficients appearing in (1.78)-(1.79) depend on velocity, as (1.80)-(1.83) and (1.90)-(1.91) include terms associated with normal velocity components $\mathbf{u}_i \cdot \mathbf{n}_{\beta\gamma}$. The dependence of the effective mass transfer rate coefficients on velocity has been discussed by *Haggerty et al*. [2004]. These authors analyzed a large set of laboratory scale data and concluded that effective mass transfer coefficients display a mild dependence on the system velocity even for long times, when diffusive exchanges are dominant. Moreover, it can be observed that the effective dispersion coefficients, and particularly the dispersion coefficient in the mobile phase, depend on the local distribution of velocity within the averaging volume, as shown in (1.86). Hence, the effective dispersion tensor appearing in (1.78)-(1.79) is a priori influenced by the criterion one selects to partition the pore space into the β- and γ- regions. This feature should be taken into account while calibrating the dispersive term in (1.92).

The DRMT model formulation is a simplification of the MRMT model. The corresponding transport equations can be expressed as

$$\frac{\partial C_m}{\partial t} = L(C_m) - \Theta\beta(C_m - C_{im}) \tag{1.99}$$

$$\frac{\partial C_{im}}{\partial t} = \beta(C_m - C_{im}) \tag{1.100}$$

where mass transfer between the two regions is represented through a linear model. As observed by *Chastanet and Wood* [2008] in the context of transport in (large scale) heterogeneous porous media, different levels of simplifications can be introduced to reduce the mass exchange term $ME2_i$ in (1.78)-(1.79) to the format which is assumed in (1.99)-(1.100). First, if the temporal

variation of the difference $\left(\left\langle c_\gamma \right\rangle^\gamma - \left\langle c_\beta \right\rangle^\beta\right)$ is slower than that associated with the coefficient α_β and α_γ, then the following approximation holds

$$\alpha_i * \frac{\partial}{\partial t}\left(\left\langle c_\gamma \right\rangle^\gamma - \left\langle c_\beta \right\rangle^\beta\right) \approx \alpha_i(t)\left(\left\langle c_\gamma \right\rangle^\gamma - \left\langle c_\beta \right\rangle^\beta\right) \quad i = \beta, \gamma \tag{1.101}$$

The latter is termed as uncoupled transient model by *Chastanet and Wood* [2008]. If a quasi-steady solution can be assumed to hold for the closure variables g_β^0 and g_γ^0, then the coefficients α_i are constant in time and the mass transfer terms *ME3* reduces to the classical form of the DRMT model. This approximation is termed quasi-steady model by *Chastanet and Wood* [2008]. The effect of the mass exchange terms *ME1* and *ME2* is not explicitly considered in (1.99)-(1.100) and the effect of the contribution of these two terms can be considered as embedded in the calibration of the mobile/immobile porosity partition.

The full set of assumptions mentioned above enable one to recover the (local in time) DRMT model from (1.78)-(1.79). Although nonlocal formulations are more rigorous than their localized counterparts from a theoretical viewpoint, solving them is computationally demanding and requires the formulation of complex algorithms. In this sense, one could argue that there are no unique guidelines in terms of the optimal choice between alternative modeling options and one should always balance different factors, including (*i*) model accuracy, (*ii*) mathematical and computational complexity, and (*iii*) availability of characterization information at the scale of interest. In this sense, our work does not claim that the formulation proposed in (1.78)-(1.79) should be employed to model any practical situation. Instead, our key aim is to put into evidence the complete set of assumptions which are implicitly embedded in the well known and widely

used DRMT/MRMT transport models and provide a direct link between the parameters embedded in these models and pore scale transport features.

III. Application

1. Problem setup

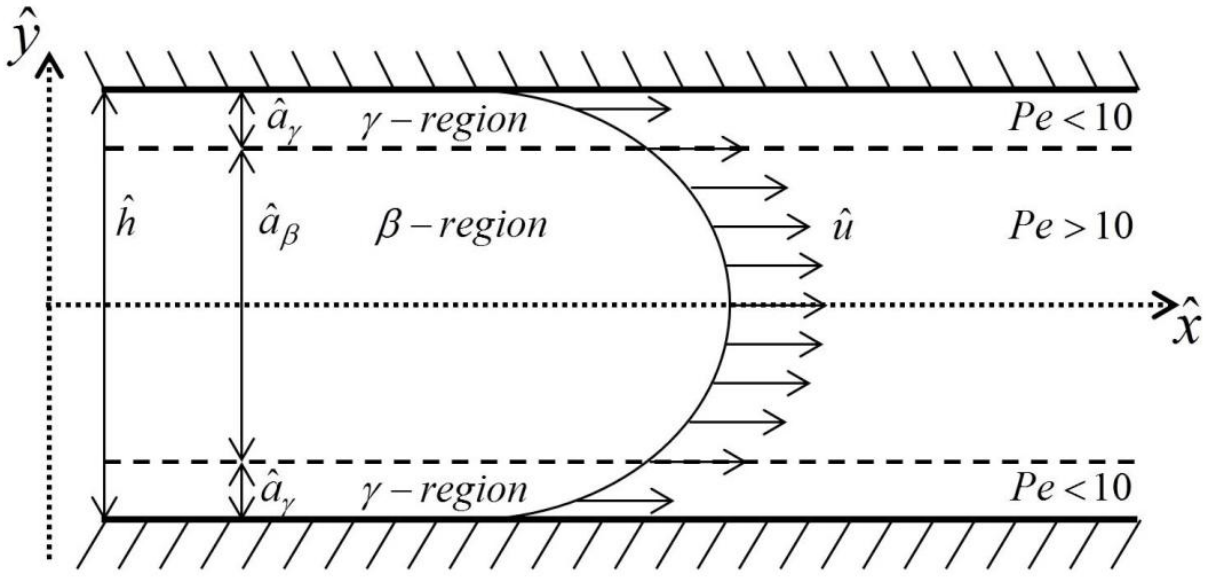

Figure 4. Sketch of the plane channel geometry

Theoretical results of Section II are illustrated here through a scenario where solute transport is taking place within a two-dimensional plane channel. Solute migration in the channel is due to advection (governed by a Poiseuille flow configuration) and molecular diffusion. The transient behavior of the coefficients characterizing the upscaled two-equation model is identified. The latter is obtained through a one-dimensional solution of the unsteady closure system. It is shown that time convolutions do not play a relevant role in this simple case, because asymptotic values

of the coefficients are attained rapidly. The local in time two-equation model is then solved and the relative importance of all terms and associated coefficients appearing in the final two-equation model is quantified through an order-of-magnitude analysis. A compact formulation which can be employed to describe the upscaled system dynamics is finally derived from the full two-equation model and a comparison against classical DRMT/MRMT models is presented.

We solve (1.78)-(1.79) to describe solute transport within a plane channel aligned along the x-direction and characterized by a uniform aperture $\hat{h}$, under steady-state flow conditions. Figure 4 depicts a schematic representation of the problem setup. The distribution of the longitudinal component of velocity, $\hat{u}$, is known analytically and is described by a parabolic expression along the transverse direction, $\hat{y}$. We subdivide the channel space into two low-velocity zones (γ-regions), located near the channel impermeable walls, and a high-velocity zone (β-region), located in between them. The width of the two γ-regions is determined upon setting a threshold for local Péclet number at the value $K = 10$.

We remark that, while this simplified geometry is not fully representative of complex porous media structures, it enables one to clearly show the way pore scale features propagate to DRMT/MRMT models.

2. Closure Problems

Here we present the set of the closure problems (1.48)-(1.77) in case of the plane channel under consideration. In this particular geometry the closure equations can be written in a one-dimensional formulation, i.e. along the channel section.

Problem I

$$\frac{\partial \hat{g}^1_{\beta\beta}}{\partial t} - \hat{a}_\beta \tilde{u}_\beta(y) = \frac{\partial^2}{\partial \hat{y}}\left[\frac{\hat{a}^2_\beta}{Pe_\beta}\hat{g}^1_{\beta\beta}\right] + \phi^{-1}_\beta \nu_{\beta\beta}; \quad |\hat{y}| < \hat{a}_\beta / 2 \tag{1.102}$$

$$\frac{\partial \hat{g}^1_{\gamma\beta}}{\partial t} - \hat{a}_\gamma \tilde{u}_\gamma(y) = \frac{\partial^2}{\partial \hat{y}}\left[\frac{\hat{a}^2_\gamma}{Pe_\gamma}\hat{g}^1_{\gamma\beta}\right] + \phi^{-1}_\gamma \nu_{\gamma\beta}; \quad \hat{a}_\beta / 2 < |\hat{y}| < \hat{h} / 2 \tag{1.103}$$

$$\hat{g}^1_{\beta\beta} = \hat{g}^1_{\gamma\beta} \qquad |\hat{y}| = \hat{a}_\beta / 2 \tag{1.104}$$

$$\frac{\partial \hat{g}^1_{\beta\beta}}{\partial \hat{y}} + 1 = \frac{\partial \hat{g}^1_{\gamma\beta}}{\partial \hat{y}} \qquad |\hat{y}| = \hat{a}_\beta / 2 \tag{1.105}$$

$$\frac{\partial \hat{g}^1_{\gamma\beta}}{\partial \hat{y}} = 0 \qquad |\hat{y}| = \hat{h} / 2 \tag{1.106}$$

Initial conditions of the problem are

$$\hat{g}^1_{\beta\beta}(t=0) = 0, \qquad \hat{g}^1_{\gamma\beta}(t=0) = 0 \tag{1.107}$$

The following conditions are also imposed

$$\left\langle \hat{g}^1_{\beta\beta} \right\rangle^\beta = 0, \qquad \left\langle \hat{g}^1_{\gamma\beta} \right\rangle^\gamma = 0 \tag{1.108}$$

Problem II

$$\frac{\partial \hat{g}^1_{\beta\gamma}}{\partial t} - \hat{a}_\beta \tilde{u}_\beta(y) = \frac{\partial^2}{\partial \hat{y}}\left[\frac{\hat{a}^2_\beta}{Pe_\beta}\hat{g}^1_{\beta\gamma}\right] + \phi^{-1}_\beta \nu_{\beta\gamma} \qquad |\hat{y}| < \hat{a}_\beta / 2 \tag{1.109}$$

$$\eta_\gamma \frac{\partial \hat{g}^1_{\gamma\gamma}}{\partial t} - \hat{a}_\gamma \tilde{u}_\gamma(y) = \frac{\partial^2}{\partial \hat{y}}\left[\frac{\hat{a}^2_\gamma}{Pe_\gamma}\hat{g}^1_{\gamma\gamma}\right] + \phi^{-1}_\gamma \nu_{\gamma\gamma} \qquad \hat{a}_\beta / 2 < |\hat{y}| < \hat{h} / 2 \tag{1.110}$$

$$\hat{g}^1_{\beta\gamma} = \hat{g}^1_{\gamma\gamma} \qquad |\hat{y}| = \hat{a}_\beta / 2 \tag{1.111}$$

$$\frac{\partial \hat{g}^1_{\beta\gamma}}{\partial \hat{y}} = \frac{\partial \hat{g}^1_{\gamma\gamma}}{\partial \hat{y}} + 1 \qquad |\hat{y}| = \hat{a}_\beta / 2 \qquad (1.112)$$

$$\frac{\partial \hat{g}^1_{\gamma\gamma}}{\partial \hat{y}} = -1 \qquad |\hat{y}| = \hat{h} / 2 \qquad (1.113)$$

Initial conditions:

$$\hat{g}^1_{\beta\gamma}(t=0) = 0, \qquad \hat{g}^1_{\gamma\gamma}(t=0) = 0, \qquad (1.114)$$

Average:

$$\left\langle \hat{g}^1_{\beta\gamma} \right\rangle^\beta = 0, \qquad \left\langle \hat{g}^1_{\gamma\gamma} \right\rangle^\gamma = 0 \qquad (1.115)$$

Problem III

$$\frac{\partial g^0_\beta}{\partial t} = \frac{\partial^2}{\partial \hat{y}} \left[\frac{\hat{a}^2_\beta}{Pe_\beta} g^0_\beta \right] + \phi^{-1}_\beta \alpha_\beta \qquad |\hat{y}| < \hat{a}_\beta / 2 \qquad (1.116)$$

$$\eta_\gamma \frac{\partial g^0_\gamma}{\partial t} = \frac{\partial^2}{\partial \hat{y}} \left[\frac{\hat{a}^2_\gamma}{Pe_\gamma} g^0_\gamma \right] + \phi^{-1}_\gamma \alpha_\gamma \qquad \hat{a}_\beta / 2 < |\hat{y}| < \hat{h} / 2 \qquad (1.117)$$

$$g^0_\beta = g^0_\gamma + 1 \qquad |\hat{y}| = \hat{a}_\beta / 2 \qquad (1.118)$$

$$\frac{\partial g^0_\beta}{\partial \hat{y}} = \frac{\partial g^0_\gamma}{\partial \hat{y}} \qquad |\hat{y}| = \hat{a}_\beta / 2 \qquad (1.119)$$

$$\frac{\partial g^0_\gamma}{\partial \hat{y}} = 0 \qquad |\hat{y}| = \hat{h} / 2 \qquad (1.120)$$

Initial conditions:

$$g_\beta^1(t=0)=0, \qquad g_\gamma^1(t=0)=0 \tag{1.121}$$

Average:

$$\left\langle g_\beta^0 \right\rangle^\beta = 0, \qquad \left\langle g_\gamma^0 \right\rangle^\gamma = 0 \tag{1.122}$$

Time dependent solution of the presented closure equations system can be obtained numerically in order to analyze time behavior of the system (1.78)-(1.91). On the other hand the analytical expression of the closure variable can be obtained in the steady state asymptotic solution, which is attained for long times.

3. Analytical solutions

The asymptotic solution of the closure problems and the coefficients (1.80)-(1.91) can be obtained analytically, upon considering that the closure problem is invariant along the *x*-direction.

After the assumptions above the closure system for Problem I becomes a system of ordinary differential equations

$$-\hat{a}_\beta \tilde{u}_\beta(y) = \frac{d^2}{d\hat{y}}\left[\frac{\hat{a}_\beta^2}{Pe_\beta}\hat{g}_{\beta\beta}^1\right] + \phi_\beta^{-1} v_{\beta\beta}; \quad |\hat{y}| < \hat{a}_\beta / 2 \tag{1.123}$$

$$-\hat{a}_\gamma \tilde{u}_\gamma(y) = \frac{d^2}{d\hat{y}}\left[\frac{\hat{a}_\gamma^2}{Pe_\gamma}\hat{g}_{\gamma\beta}^1\right] + \phi_\gamma^{-1} v_{\gamma\beta}; \quad \hat{a}_\beta / 2 < |\hat{y}| < \hat{h} / 2 \tag{1.124}$$

$$\hat{g}^1_{\beta\beta} = \hat{g}^1_{\gamma\beta} \qquad |\hat{y}| = \hat{a}_\beta / 2 \tag{1.125}$$

$$\frac{d\hat{g}^1_{\beta\beta}}{d\hat{y}} + 1 = \frac{d\hat{g}^1_{\gamma\beta}}{d\hat{y}} \qquad |\hat{y}| = \hat{a}_\beta / 2 \tag{1.126}$$

$$\frac{d\hat{g}^1_{\gamma\beta}}{d\hat{y}} = 0 \qquad |\hat{y}| = \hat{h} / 2 \tag{1.127}$$

The following conditions are also imposed

$$\left\langle \hat{g}^1_{\beta\beta} \right\rangle^\beta = 0, \qquad \left\langle \hat{g}^1_{\gamma\beta} \right\rangle^\gamma = 0 \tag{1.128}$$

Solving (1.123) gives

$$\hat{g}^1_{\beta\beta}(\hat{y}) = C_1 + \hat{y}C_2 + \frac{Pe_\beta \hat{y}^2(-2\hat{h}\phi_\beta \hat{y}\hat{a}_\beta + \phi_\beta \hat{y}^2 \hat{a}_\beta - (\hat{h}^2 + 2\hat{h}\hat{a}_\gamma - 2\hat{a}_\gamma^2)(v_{\beta\beta} - \phi_\beta \hat{a}_\beta))}{2\phi_\beta(\hat{h}^2 + 2\hat{h}\hat{a}_\gamma - 2\hat{a}_\gamma^2)\hat{a}_\beta^2} \tag{1.129}$$

$$\frac{d\hat{g}^1_{\beta\beta}}{d\hat{y}}(\hat{y}) = C_2 + \frac{Pe_\beta \hat{y}^2(-2\hat{h}\phi_\beta \hat{a}_\beta + 2\phi_\beta \hat{y}\hat{a}_\beta)}{2\phi_\beta(\hat{h}^2 + 2\hat{h}\hat{a}_\gamma - 2\hat{a}_\gamma^2)\hat{a}_\beta^2} + \frac{Pe_\beta \hat{y}(-2\hat{h}\phi_\beta \hat{y}\hat{a}_\beta + \phi_\beta \hat{y}^2 \hat{a}_\beta - (\hat{h}^2 + 2\hat{h}\hat{a}_\gamma - 2\hat{a}_\gamma^2)(v_{\beta\beta} - \phi_\beta \hat{a}_\beta))}{\phi_\beta(\hat{h}^2 + 2\hat{h}\hat{a}_\gamma - 2\hat{a}_\gamma^2)\hat{a}_\beta^2} \tag{1.130}$$

where C_1 and C_2 are constants.

Solving (1.124) we obtain

$$\hat{g}^1_{\gamma\beta}(\hat{y}) = C_3 + \hat{y}C_4 - \frac{Pe_\gamma v_{\gamma\beta} \hat{y}^2}{2\phi_\gamma \hat{a}_\gamma^2} \tag{1.131}$$

$$\frac{d\hat{g}^1_{\gamma\beta}}{d\hat{y}}(\hat{y}) = C_4 - \frac{Pe_\gamma v_{\gamma\beta} \hat{y}}{\phi_\gamma \hat{a}_\gamma^2} \tag{1.132}$$

where C_3 and C_4 are constants.

Then by applying boundary conditions (1.125)-(1.127) and average constraints (1.128), one can find the C_1, C_2, C_3, C_4, $v_{\beta\beta}$, $v_{\gamma\beta}$.

The analytical expressions for the full set of closure variables can be obtained accordingly. The dull analytical solutions are provided below and graphically in Figures 5-7.

$$\hat{g}^1_{\beta\beta}(\hat{y}) = \frac{1}{360}\Bigg[-60\hat{y}Pe_\beta + \frac{180\hat{y}^2(2+Pe_\beta)}{\hat{a}_\beta} - 5(6+Pe_\beta)\hat{a}_\beta + \frac{30(6+Pe_\beta)(-4\hat{y}+\hat{a}_\beta)\hat{a}_\gamma + 30(12+Pe_\beta)\hat{a}_\gamma^2}{\hat{a}_\beta} + \frac{6(5+Pe_\beta)(-12\hat{y}^2+\hat{a}_\beta^2)}{\hat{a}_\beta+2\hat{a}_\gamma} + \frac{Pe_\beta(180\hat{y}^4 - \hat{a}_\beta^4 - 360\hat{y}^3(\hat{a}_\beta+2\hat{a}_\gamma) + 108\hat{y}^2\hat{a}_\beta(\hat{a}_\beta+2\hat{a}_\gamma) + 24\hat{y}\hat{a}_\beta^2(\hat{a}_\beta+5\hat{a}_\gamma))}{\hat{a}_\beta(\hat{a}_\beta^2+6\hat{a}_\beta\hat{a}_\gamma+6\hat{a}_\gamma^2)}\Bigg] \tag{1.133}$$

$$\hat{g}^1_{\beta\gamma}(\hat{y}) = -\frac{15\hat{a}_\gamma(4+Pe_\gamma)\left[6\hat{y}^2 - 6\hat{y}\hat{a}_\beta + \hat{a}_\beta^2 + 6(-2\hat{y}+\hat{a}_\beta)\hat{a}_\gamma + 6\hat{a}_\gamma^2\right]}{60(\hat{a}_\beta+2\hat{a}_\gamma)(3\hat{a}_\beta+4\hat{a}_\gamma)} - \frac{2\hat{a}_\gamma^2(40+7Pe_\gamma)\left[6\hat{y}^2 - 6\hat{y}\hat{a}_\beta + \hat{a}_\beta^2 + 6(-2\hat{y}+\hat{a}_\beta)\hat{a}_\gamma + 6\hat{a}_\gamma^2\right]}{60\hat{a}_\beta(\hat{a}_\beta+2\hat{a}_\gamma)(3\hat{a}_\beta+4\hat{a}_\gamma)} \tag{1.134}$$

$$\hat{g}^1_{\gamma\beta}(\hat{y}) = \frac{\hat{a}_\beta((-10+Pe_\beta)\hat{a}_\beta^2 - 60\hat{a}_\beta\hat{a}_\gamma - 60\hat{a}_\gamma^2)(-3\hat{y}^2+\hat{a}_\gamma^2)}{60\hat{a}_\gamma(\hat{a}_\beta+2\hat{a}_\gamma)(\hat{a}_\beta^2+6\hat{a}_\beta\hat{a}_\gamma+6\hat{a}_\gamma^2)} \tag{1.135}$$

$$\hat{g}^1_{\gamma\gamma}(\hat{y}) = \frac{\hat{a}_\gamma^3(15(2+Pe_\gamma)\hat{a}_\beta^2 + (40+31Pe_\gamma)\hat{a}_\beta\hat{a}_\gamma + 18Pe_\gamma\hat{a}_\gamma^2)}{60\hat{a}_\gamma^2(\hat{a}_\beta+2\hat{a}_\gamma)(3\hat{a}_\beta+4\hat{a}_\gamma)} - \frac{30\hat{y}^4Pe_\gamma(\hat{a}_\beta+2\hat{a}_\gamma) + 60\hat{y}^3Pe_\gamma(\hat{a}_\beta+2\hat{a}_\gamma)^2}{60\hat{a}_\gamma^2(\hat{a}_\beta+2\hat{a}_\gamma)(3\hat{a}_\beta+4\hat{a}_\gamma)} - \frac{3\hat{y}^2\hat{a}_\gamma(30(1+Pe_\gamma)\hat{a}_\beta^2 + 5(8+17Pe_\gamma)\hat{a}_\beta\hat{a}_\gamma + 66Pe_\gamma\hat{a}_\gamma^2)}{60\hat{a}_\gamma^2(\hat{a}_\beta+2\hat{a}_\gamma)(3\hat{a}_\beta+4\hat{a}_\gamma)} \tag{1.136}$$

$$g^0_\beta(\hat{y}) = \frac{6\hat{y}^2 - 6\hat{y}\hat{a}_\beta + \hat{a}_\beta^2 + 6(-2\hat{y}+\hat{a}_\beta)\hat{a}_\gamma + 6\hat{a}_\gamma^2}{\hat{a}_\beta(\hat{a}_\beta+2\hat{a}_\gamma)} \tag{1.137}$$

$$g_{\gamma}^{0}(\hat{y}) = \frac{-3\hat{y}^2 + \hat{a}_{\gamma}^2}{\hat{a}_{\gamma}(\hat{a}_{\beta} + 2\hat{a}_{\gamma})} \tag{1.138}$$

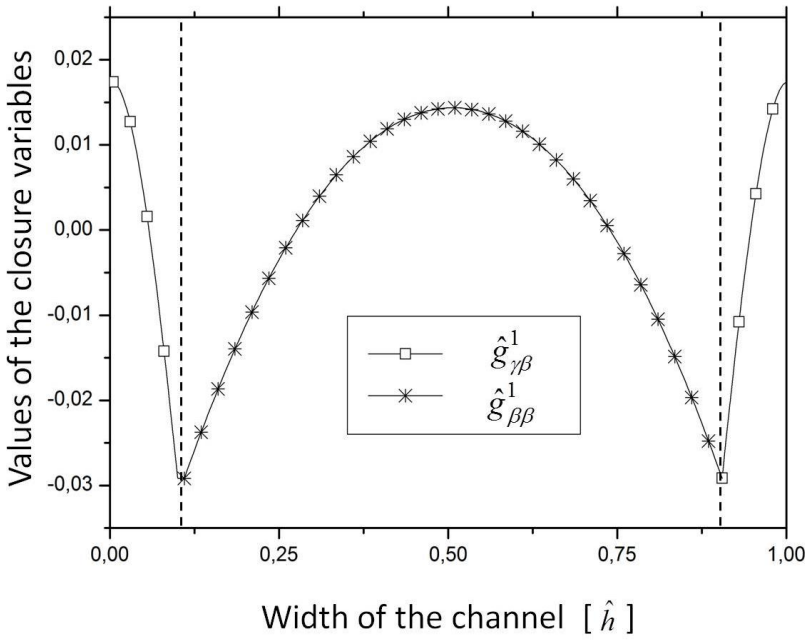

Figure 5. Asymptotic solutions of the closure variables for the Problem I

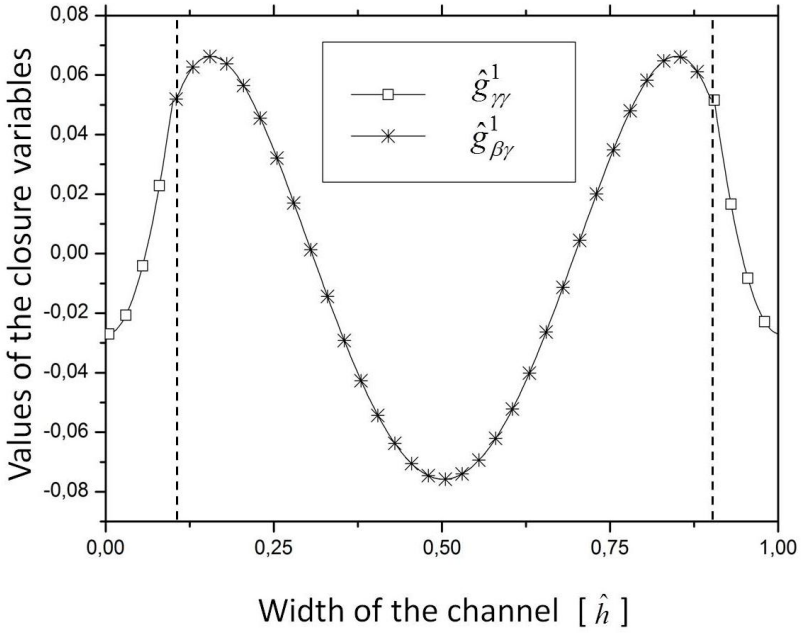

Figure 6. Asymptotic solutions of the closure variables for the Problem II

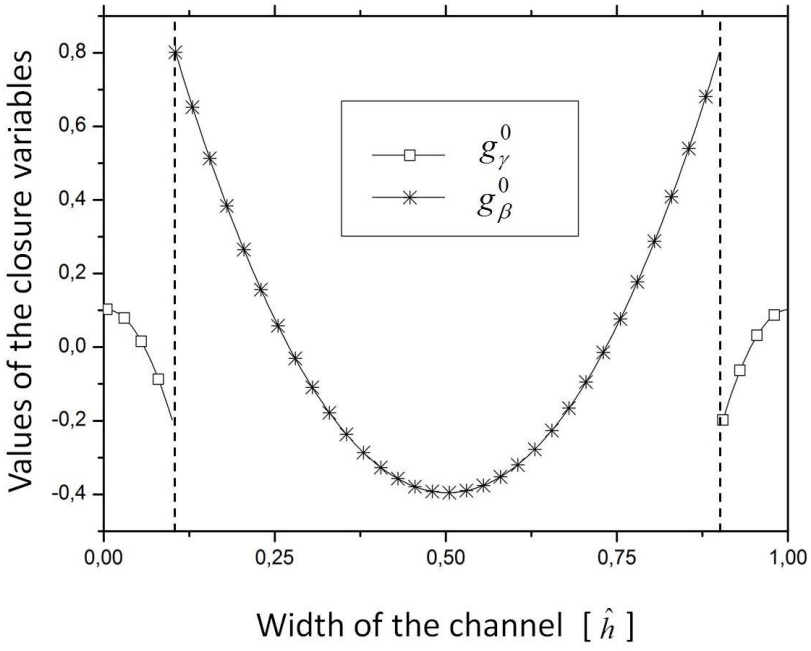

Figure 7. Asymptotic solutions of the closure variables for the Problem III

Upon substitution of (1.133)-(1.138) into (1.80)-(1.91) we obtain the following analytical expression of the coefficients appearing in (1.78)-(1.79)

$$\mathbf{v}_{\beta\beta} = -\frac{\phi_\beta}{5(\hat{a}_\beta + 2\hat{a}_\gamma)}\left(\frac{\hat{a}_\beta^3}{\hat{a}_\beta^2 + 6\hat{a}_\beta\hat{a}_\gamma + 6\hat{a}_\gamma^2} + \frac{20\hat{a}_\gamma}{Pe_\beta}\right) \tag{1.139}$$

$$\mathbf{v}_{\gamma\beta} = \frac{\phi_\gamma \hat{a}_\beta(-60\hat{a}_\beta\hat{a}_\gamma - 60\hat{a}_\gamma^2 + \hat{a}_\beta^2(-10 + Pe_\beta))}{10(\hat{a}_\beta + 2\hat{a}_\gamma)(\hat{a}_\beta^2 + 6\hat{a}_\beta\hat{a}_\gamma + 6\hat{a}_\gamma^2)Pe_\gamma} \tag{1.140}$$

$$\mathbf{v}_{\beta\gamma} = \frac{\phi_\beta \hat{a}_\gamma(15\hat{a}_\beta(4 + Pe_\gamma) + 2\hat{a}_\gamma(40 + 7Pe_\gamma))}{5(\hat{a}_\beta + 2\hat{a}_\gamma)(3\hat{a}_\beta + 4\hat{a}_\gamma)Pe_\beta} \tag{1.141}$$

$$\mathbf{v}_{\gamma\gamma} = \frac{\phi_\gamma}{10(\hat{a}_\beta + 2\hat{a}_\gamma)}\left(\frac{10\hat{a}_\beta}{Pe_\gamma} - \frac{\hat{a}_\gamma(15\hat{a}_\beta + 14\hat{a}_\gamma)}{3\hat{a}_\beta + 4\hat{a}_\gamma}\right) \tag{1.142}$$

$$\mathbf{d}_\beta = \frac{\hat{a}_\beta^4 Pe_\beta}{5(\hat{a}_\beta + 2\hat{a}_\gamma)^2(\hat{a}_\beta^2 + 6\hat{a}_\beta\hat{a}_\gamma + 6\hat{a}_\gamma^2)} \tag{1.143}$$

$$\mathbf{d}_\gamma = \frac{\hat{a}_\gamma^2(15\hat{a}_\beta + 14\hat{a}_\gamma)Pe_\gamma}{5(\hat{a}_\beta + 2\hat{a}_\gamma)^2(3\hat{a}_\beta + 4\hat{a}_\gamma)} \tag{1.144}$$

$$D^*_{\beta\beta} = 1 + \frac{\hat{a}_\beta^3 Pe_\beta(840\hat{a}_\beta\hat{a}_\gamma^2 + 840\hat{a}_\gamma^3 - 20\hat{a}_\beta^2\hat{a}_\gamma(-7 + Pe_\beta) - 3\hat{a}_\beta^3 Pe_\beta)}{2100(\hat{a}_\beta + 2\hat{a}_\gamma)^2(\hat{a}_\beta^2 + 6\hat{a}_\beta\hat{a}_\gamma + 6\hat{a}_\gamma^2)^2} \tag{1.145}$$

$$D^*_{\gamma\beta} = \frac{\hat{a}_\beta\hat{a}_\gamma(15\hat{a}_\beta + 14\hat{a}_\gamma)(-60\hat{a}_\beta\hat{a}_\gamma - 60\hat{a}_\gamma^2 + \hat{a}_\beta^2(-10 + Pe_\beta))Pe_\gamma}{300(\hat{a}_\beta + 2\hat{a}_\gamma)^2(3\hat{a}_\beta + 4\hat{a}_\gamma)(\hat{a}_\beta^2 + 6\hat{a}_\beta\hat{a}_\gamma + 6\hat{a}_\gamma^2)} \tag{1.146}$$

$$D^*_{\beta\gamma} = -\frac{\hat{a}_\beta^3\hat{a}_\gamma Pe_\beta(15\hat{a}_\beta(4 + Pe_\gamma) + 2\hat{a}_\gamma(40 + 7Pe_\gamma))}{300(\hat{a}_\beta + 2\hat{a}_\gamma)^2(3\hat{a}_\beta + 4\hat{a}_\gamma)(\hat{a}_\beta^2 + 6\hat{a}_\beta\hat{a}_\gamma + 6\hat{a}_\gamma^2)} \tag{1.147}$$

$$D^{*}_{\gamma\gamma} = 1 + \frac{\hat{a}_\gamma Pe_\gamma (1188\hat{a}_\gamma^3 Pe_\gamma + 630\hat{a}_\beta^3 (5 + 2Pe_\gamma))}{2100(\hat{a}_\beta + 2\hat{a}_\gamma)^2 (3\hat{a}_\beta + 4\hat{a}_\gamma)^2} + \frac{\hat{a}_\gamma Pe_\gamma (105\hat{a}_\beta^2 \hat{a}_\gamma (68 + 33Pe_\gamma) + 20\hat{a}_\beta \hat{a}_\gamma^2 (196 + 169Pe_\gamma))}{2100(\hat{a}_\beta + 2\hat{a}_\gamma)^2 (3\hat{a}_\beta + 4\hat{a}_\gamma)^2} \tag{1.148}$$

$$\alpha_\beta = -\frac{12\phi_\beta \hat{a}_\beta}{(\hat{a}_\beta + 2\hat{a}_\gamma) Pe_\beta} \tag{1.149}$$

$$\alpha_\gamma = \frac{6\phi_\gamma \hat{a}_\gamma}{(\hat{a}_\beta + 2\hat{a}_\gamma) Pe_\gamma} \tag{1.150}$$

4. Results

In this section we analyze the upscaled two-equation transport system for a plane channel. In particular, we analyze the time and space behavior of the coefficients and terms of the equations. The impact of every term on the global behavior of the system is analyzed and possible simplifications are discussed.

For the purpose of our analysis, we consider a Péclet number, where the average velocity is given by $U = \left(\phi_\gamma \left\langle u_\gamma \right\rangle^\gamma + \phi_\beta \left\langle u_\beta \right\rangle^\beta \right) / \left(\phi_\gamma + \phi_\beta \right)$, to characterize the continuum scale behavior of the system.

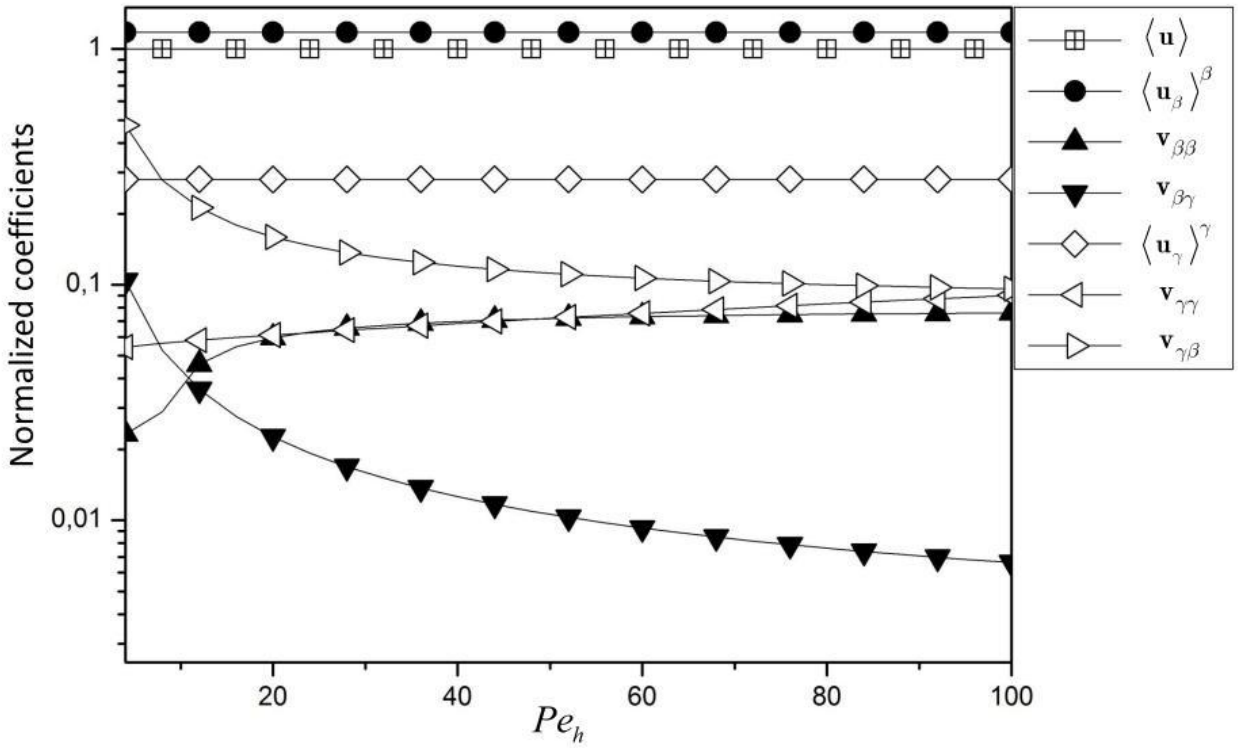

Figure 8. Dependence of the advective coefficients (1.139)-(1.142) on Pe_h.

Figure 8 depicts the dependence of the asymptotic advective coefficients (1.139)-(1.142) on Pe_h. The coefficients are all normalized with respect to U. Note that $\mathbf{u} \cdot \mathbf{n}_{\beta\gamma} = 0$ in this case and the coefficients $\mathbf{v}_{ij}$ in (1.139)-(1.142) essentially represent a diffusive mass exchange between the γ- and β- regions identified. We observe that $\mathbf{v}_{\beta\beta} \gg \mathbf{v}_{\beta\gamma}$ for the full range of considered Pe_h. On the other hand $\mathbf{v}_{\gamma\beta}$ and $\mathbf{v}_{\gamma\gamma}$ are of the same order of magnitude and attain the same value for large Pe_h. All these coefficients reach asymptotic values for large Pe_h, becoming proportional to U, *i.e.*, they depend linearly on Pe_h for $Pe_h \gg 1$.

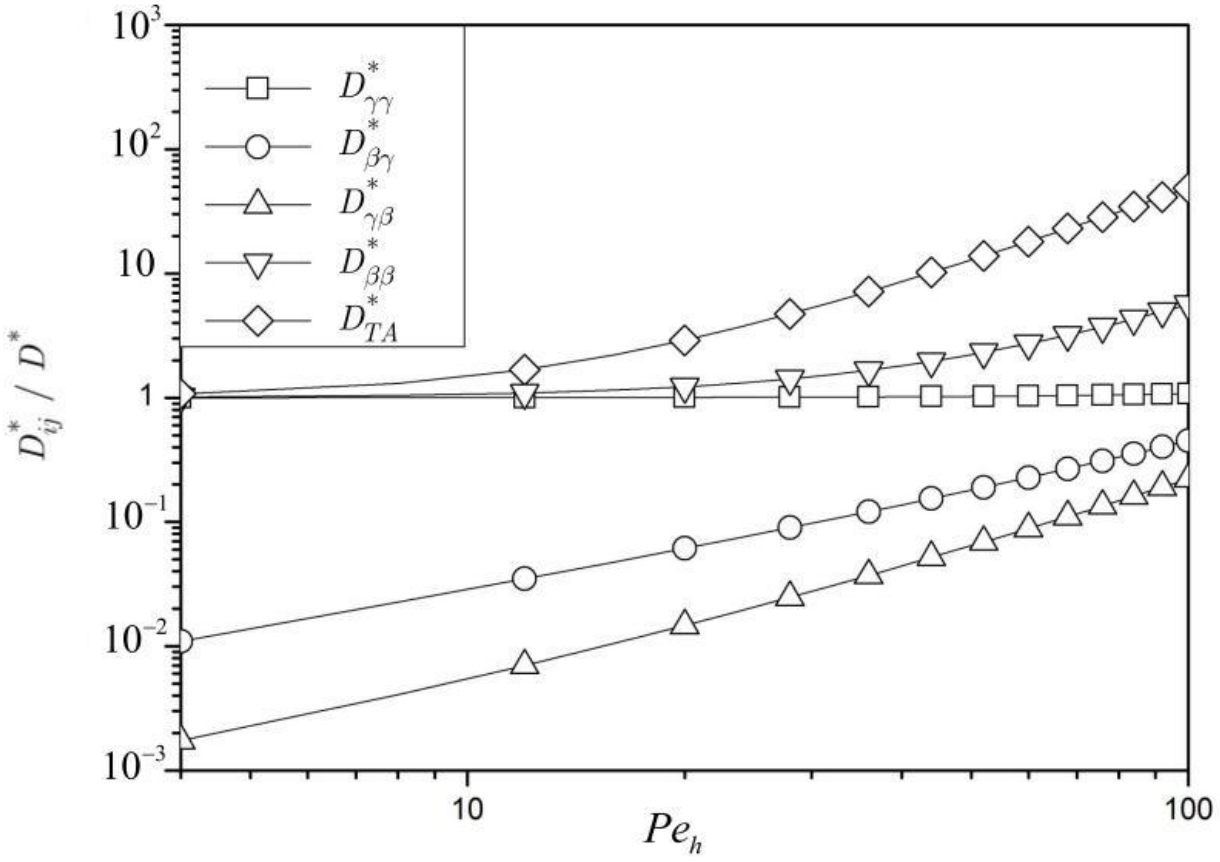

Figure 9. Dependence on Pe_h of the dispersive coefficients introduced in (1.145)-(1.148)

Figure 9 depicts the dependence on Pe_h of the asymptotic dispersive coefficients (1.145)-(1.148). The classical Taylor-Aris expression $D^*_{TA} = 1 + Pe_h^2 / 210$ [*Wooding*, 1960] which is typically included in an ADE-based transport model is also presented as a term of comparison. Note that the dispersion coefficients embedded in the two-equation model (1.78)-(1.79) are proportional to Pe_h^2. All the dispersive coefficients D^*_{ij} (1.145)-(1.148) are considerably smaller than D^*_{TA}. This happens because part of the hydrodynamic dispersion is included in the mass transfer and the additional advective coefficients resulting from the upscaling procedure.

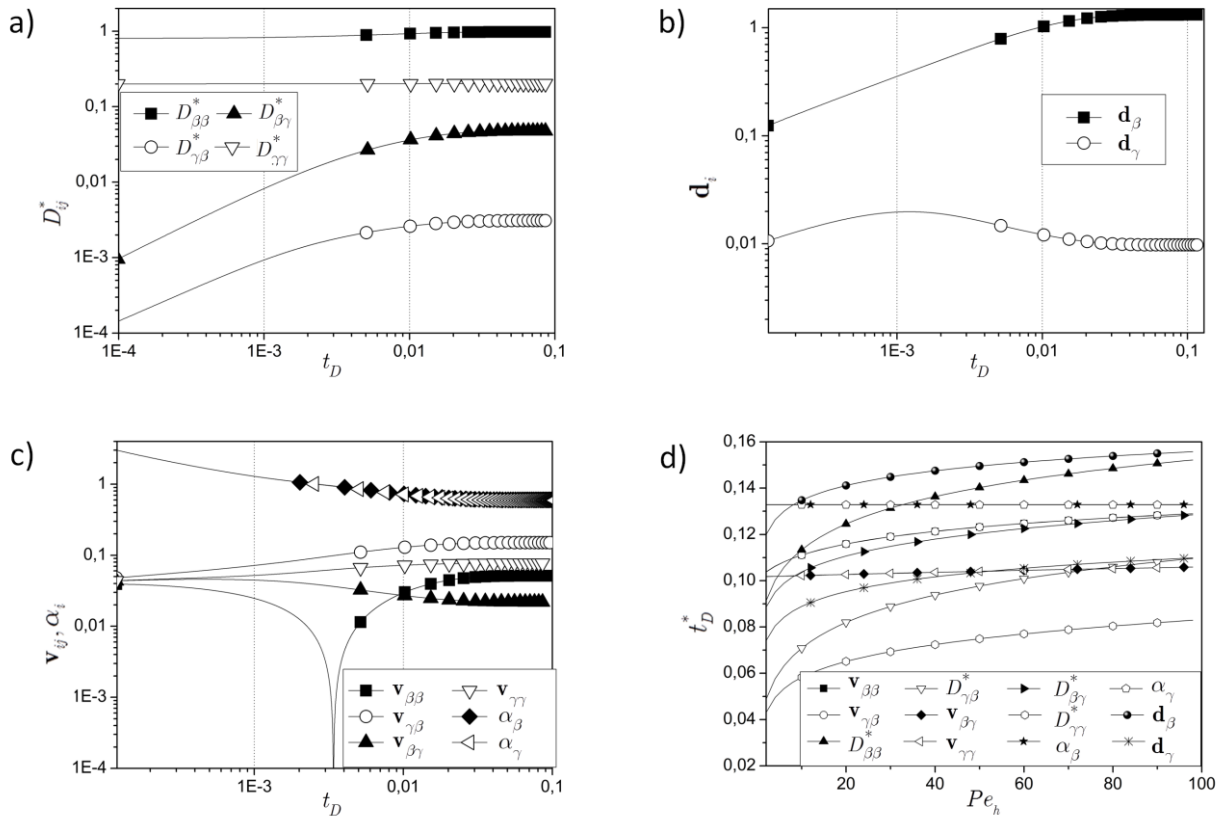

Figure 10. *Time evolution of (a) dispersive coefficients* D^*_{ij} *(*$i, j = \beta, \gamma$*), (b) advective coefficients* $\mathbf{d}_\beta$ *and* $\mathbf{d}_\gamma$*, and (c) mass transfer coefficients for* $Pe_h = 20$*; (d) dependence on* Pe_h *of the asymptotic time (*t^*_D*) at which each of the coefficients attains its asymptotic value. Black and open symbols are associated with coefficients respectively appearing in (1.78)-(1.79).*

Figure 10 depicts the dependence of the model coefficients on the dimensionless time $t_D = \hat{t}\hat{h}^2 / \hat{D}$. Coefficients are grouped into three subsets, depending on their role in the two-equation model. We then quantify the times at which the coefficients attain their asymptotic value as a function of Pe_h.

Figure 10a presents the time evolution of the four dispersive coefficients D_{ij}^{*} $(i, j = \beta, \gamma)$ for $Pe_h = 20$. All dispersive coefficients D_{ij}^{*} reach their asymptotic values at $t_D \approx 0.03$. This result can be compared against the findings of *Wang et al*. [2012], who consider a time varying dispersion coefficient in a single-equation model. The dispersion coefficient appearing in their single-equation model varies in time ranging between the value associated with the diffusion coefficient and the asymptotic value given by the Taylor-Aris expression [*Wooding*, 1960]. In our scenario, the approach towards an asymptotic value takes place in a relatively short time interval because of the small local variability displayed by the velocity field within the β- and γ-regions considered. Hence, the source terms $\tilde{\mathbf{u}}_i$ appearing in (1.48) and (1.49) do not have a strong influence on the problem. This result supports the hypothesis 1) underlying the MRMT model according to which this dispersion term can be considered local in time in the set-up considered. We observe that $D_{\beta\beta}^{*} \gg D_{\beta\gamma}^{*}$ and $D_{\gamma\gamma}^{*} \gg D_{\gamma\beta}^{*}$ during the entire time interval considered. Figure 10b shows the temporal behavior of the two coefficients $\mathbf{d}_\beta$ and $\mathbf{d}_\gamma$. It can be observed that the coefficient $\mathbf{d}_\beta$ exhibits a large variation in time and reaches its asymptotic value (≈ 1.1) at $t_D \approx 0.07$. Conversely, the temporal variability of $\mathbf{d}_\gamma$ appears to be negligible. Figure 10c depicts the time evolution of the coefficients which are related to mass exchange between the two regions β and γ. It can be seen that the two coefficients α_i $(i = \beta, \gamma)$, which are associated with the same closure problem, display the same temporal dynamics and exhibit large variations over time. On the other hand, the coefficients $\mathbf{v}_{ij}$ $(i, j = \beta, \gamma)$ display a limited range of variability between their initial and asymptotic values. The largest time variation is associated

with coefficients $\mathbf{d}_i$ and α_i, all of which are related to closure problem (1.68)-(1.77). Hence, it appears that the asymptotic solution for (1.116)-(1.122) (Problem III) is attained at later times than the solutions of the other closure variable systems (1.102)-(1.108) (problem I) and (1.109)-(1.115) (problem II). Figure 10d depicts the way the asymptotic time (t_D^*) at which each of the coefficients attains its asymptotic value for the considered setting depends on Pe_h. All mass exchange coefficients α_i reach their asymptotic value for a dimensionless time $t_D \approx 0.13$ regardless the value of Pe_h considered. The asymptotic times associated with the remaining coefficients display some dependence on Pe_h. For Pe_h up to 120, the largest (dimensionless) time required by these coefficients to reach an asymptotic value is smaller than 0.16. This shows that temporal variability of the coefficients is confined to a very limited range of times for the example considered, in agreement with the findings of *Orgogozo et al*. [2010] for a similar setting.

5. *Analysis of whole system behavior*

We then analyze the effect of the assumptions which can be invoked to simplify the upscaled system (1.78)-(1.79) and link it to DRMT/MRMT transport models. We do so by solving (1.78)-(1.79) in a one-dimensional setting. The solution is performed numerically through a finite difference method in time and space by employing an explicit method to approximate time derivatives. We consider transport of a finite slug of solute at a given concentration $\hat{c}_0$ which is initially introduced in a finite portion of the plane channel. The channel length is set as a function of Pe_h in a way that the outlet boundary condition does not

influence the solution for the dimensionless times of interest. On the basis of the results shown in Figure 10d and in agreement with previous literature findings for similar settings [*e.g.*, *Orgogozo et al*., 2010], we neglect here the influence of time convolutions and consider the asymptotic values of the coefficients. Our aim is to provide a quantitative analysis of the influence of each term appearing in the system (1.78)-(1.79) and study the appropriateness of the assumptions of DRMT and MRMT models in this simple geometrical setting. For the purpose of our comparison, we compute the L_1-norm

$$\left\|T_i\right\|_{L1} = \int_0^{\hat{L}} \left|\left[T_i\right](\hat{x})\right| d\hat{x} \tag{1.151}$$

Here, $\hat{L}$ is the length of the channel and T_i represents any of the terms appearing in (1.78)-(1.79). The relative contribution of each term is then calculated as

$$\left\|T_i\right\|_{L1}^{R} = \frac{\left\|T_i\right\|_{L1}}{\sum \left\|T_i\right\|_{L1}} \tag{1.152}$$

$\left\|T_i\right\|_{L1}^{R}$ providing a quantitative measure of the relative importance in the whole domain of each term appearing in the upscaled two-equation model.

Figure 11a and Figure 11b show the temporal evolution of (1.151), as calculated with reference to all terms appearing in the transport equations associated with the β- (Figure 11a) and γ- (Figure 11b) regions. A considerable variation in the relative importance of the different terms is observed for short times. One should note that the behavior of the system at these short times is strongly influenced by the initial condition, which is characterized by local discontinuities of the concentration field. Scale separation constraints do not hold under these conditions. Hence,

the upscaled formulation may not be accurate. The relative magnitude of the different terms stabilizes after some time (*i.e.*, $t_D > 1$ in Figure 10).

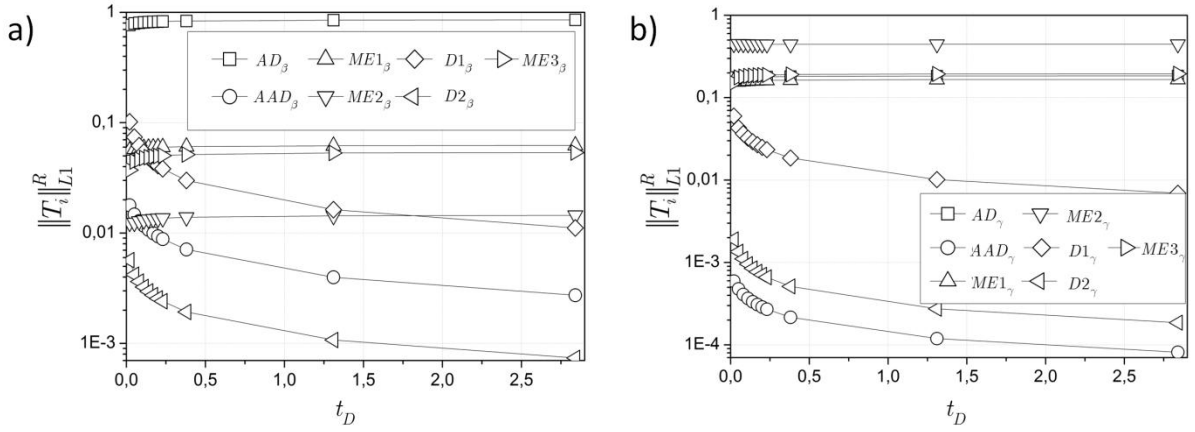

Figure 11. Temporal evolution of the relative magnitude of the terms T_i for the (a) β- and (b) γ-region transport equations. Definitions of the terms are provided in (1.78)-(1.79).

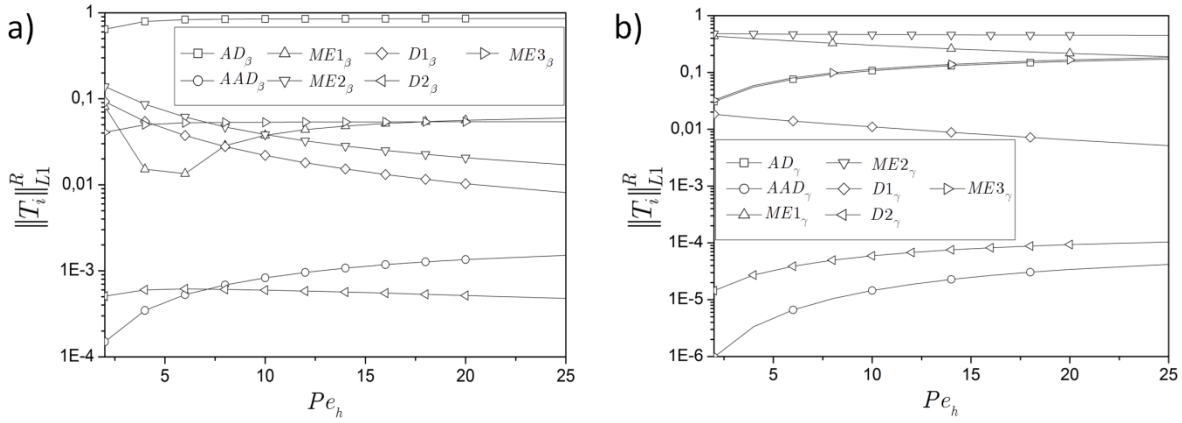

Figure 12. Comparison of the relative influence of the terms T_i for different Péclet numbers and dimensionless time $t_D = 3$. Definitions of the terms are provided in (1.78)-(1.79).

Figure 12a-b compare the relative contribution of the various terms considered for different Péclet numbers at a dimensionless time $t_D = 3$, for which the initial condition does not influence the solution. Figure 12a depicts the results associated with transport equation (1.78) related to the mobile region. We observe that some terms appear to be negligible for all values of Pe_h considered. In particular, the dispersive term ($D2_\beta$) is seen to have a negligible impact on (1.78). The same observation can be made for the additional advective term AAD_β. The relative importance of this term grows with Pe_h. However, it is noted that AAD_β remains of the order of 10^{-3}, regardless the relatively large values associated with its associated coefficient $\mathbf{d}_\beta$ (see Figure 10b; note that dimensionless average velocity $\langle u_\beta \rangle^\beta$ = 1). This result supports the rationale underlying assumption (1.94) and justifies neglecting the term AAD_β in the upscaled model describing the configuration considered. The relative importance of the dispersive term ($D1_\beta$) decreases as Pe_h grows. The standard dispersive term $D1_\beta$ is always dominant with respect to $D2_\beta$. The relative contribution of the two mass exchange terms $ME1_\beta$ and $ME3_\beta$ is always relevant and tends to stabilize at a constant value for large Pe_h. On the other hand, the influence of $ME2_\beta$ decreases with Pe_h.

Figure 12b shows the results of the corresponding analysis for the γ-region transport equation (1.79). Here, mass exchange terms ($ME1_\gamma$, $ME2_\gamma$, $ME3_\gamma$) dominate the problem, while the dispersive terms and the additional advective term are negligible. The relative influence of the advective term increases with Pe_h, to reach a maximum value of about 0.1. We recall that in

our example the subdivision between the β- and γ-region is set by considering that $Pe_\gamma \leq 10$, so that the influence of the advective term in the γ-region is limited by this constraint.

Considering the results reported in Figure 11 and Figure 12 and retaining only the terms which are associated with a relative influence larger that 5% for any of the values of Pe_h considered in Figure 12, the upscaled two-equation model can be recast into the following simplified format

$$\phi_\beta \frac{\partial \left\langle c_\beta \right\rangle^\beta}{\partial t} + \hat{a}_\beta \hat{\nabla} \cdot \left[\phi_\beta \left\langle \mathbf{u}_\beta \right\rangle^\beta \left\langle c_\beta \right\rangle^\beta \right] - \hat{a}_\beta \mathbf{v}_{\beta\beta} \hat{\nabla} \left\langle c_\beta \right\rangle^\beta - \hat{a}_\beta \mathbf{v}_{\beta\gamma} \hat{\nabla} \left\langle c_\gamma \right\rangle^\gamma = \frac{\hat{a}_\beta^2}{Pe_\beta} \hat{\nabla} \cdot \left[D^*_{\beta\beta} \hat{\nabla} \left\langle c_\beta \right\rangle^\beta \right] + \alpha_\beta \left(\left\langle c_\gamma \right\rangle^\gamma - \left\langle c_\beta \right\rangle^\beta \right) \tag{1.153}$$

$$\eta_\gamma \phi_\gamma \frac{\partial \left\langle c_\gamma \right\rangle^\gamma}{\partial t} + \hat{a}_\gamma \hat{\nabla} \cdot \left[\phi_\gamma \left\langle \mathbf{u}_\gamma \right\rangle^\gamma \left\langle c_\gamma \right\rangle^\gamma \right] - \hat{a}_\gamma \mathbf{v}_{\gamma\gamma} \frac{\partial}{\partial t} \hat{\nabla} \left\langle c_\gamma \right\rangle^\gamma - \hat{a}_\gamma \mathbf{v}_{\gamma\beta} \frac{\partial}{\partial t} \hat{\nabla} \left\langle c_\beta \right\rangle^\beta = \alpha_\gamma \left(\left\langle c_\gamma \right\rangle^\gamma - \left\langle c_\beta \right\rangle^\beta \right) \tag{1.154}$$

To verify the appropriateness of the assumptions underlying (1.153)-(1.154) we simulate the transport problem by successively removing different terms from (1.78)-(1.79). Figure 13 compares the solution obtained on the basis of the complete system (1.78)-(1.79) against the results which can be obtained by considering different degrees of simplifications of the problem. System 2 in Figure 13 corresponds to the solution of (1.153)-(1.154), while System 1 is a further simplified formulation which is obtained by dropping also the term $D_{1\beta}$. The latter simplification would be suggested in this case by the relatively limited influence displayed by this dispersive term at late times. System 3 illustrated in Figure 13 is more complex than System 2 and corresponds to neglecting only the dispersive terms $D_{2\beta}$, $D_{1\gamma}$, and $D_{2\gamma}$ from (1.78)-(1.79). The

solution of System 3 is substantially identical to that of the full system, suggesting that the terms $D_{2\beta}$, $D_{1\gamma}$, and $D_{2\gamma}$ do not affect the distribution of solute concentration at the continuum scale.

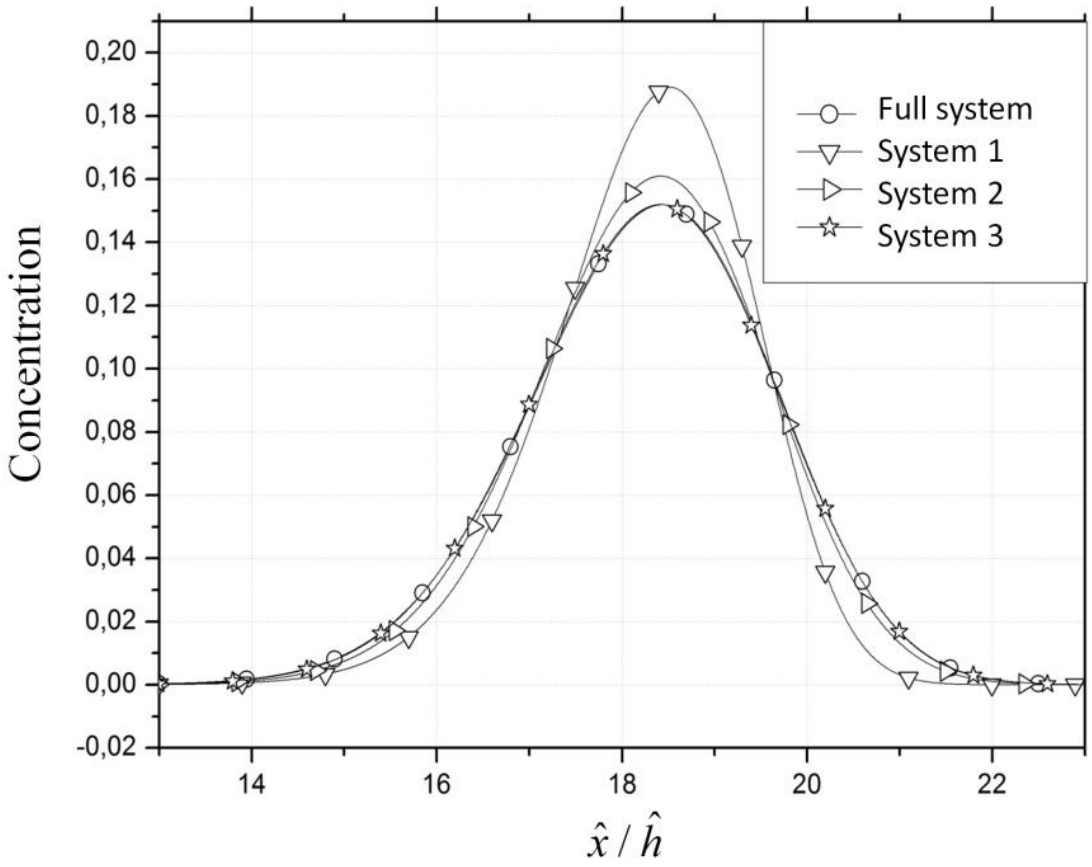

Figure 13. Comparison of (upscaled) concentration fields obtained by solving the full system (1.78)-(1.79) and results associated with different degrees of simplifications of the problem.

Note that the solution of System 2 (1.153)-(1.154) can be found upon neglecting the two additional advective terms AAD_{β} and AAD_{γ} from System 3. We observe that these two terms play some role in the process development even as their influence appears to be limited (Figure 12). The solution associated with System 2 shows a slight under diffusion, even though it appears to

be reasonably accurate. We recall that the formulation of System 2 is compatible with a DMRT model where advection is considered also in the transport equation associated with the immobile region. Including this latter term in the model appears to be necessary in the configuration we examine, because the solute is migrating by advection also in the γ-region. However, stagnant zones where velocity is associated with very small values are likely to play an important role in high complexity geometries and one might assume that advection in the immobile region could be safely disregarded in the upscaled model. The solution of System 1 is notably different from the results of the other models. The concentration peak is highly overestimated and the concentration field is not symmetric, showing a thick backwards tail. This result suggests that the effect of dispersion in the mobile region cannot be disregarded, even though this terms might appear to play a negligible role for large times when compared to mass exchange contributions.

IV. Conclusions

We present theoretical developments grounded on volume averaging and leading form the pore scale advection diffusion equation towards a two-equation continuum (Darcy) scale formulation of conservative transport in macroscopically homogeneous porous media. We contrast our upscaled formulation against the well known and widely used DRMT/MRMT transport models to evidence the complete set of assumptions which are implicitly embedded in these models. Our work leads to the following major conclusions.

1) All coefficients appearing in our upscaled two-equation formulation are explicitly linked to pore scale geometry and velocity distribution. The derived system is more

complex than usual DRMT/MRMT models and is nonlocal in time. The simplifications required to reduce our upscaled formulation to the standard DRMT/MRMT models are illustrated and discussed. Our analysis shows that key assumptions implied by DRMT/MRMT models are that (*i*) The MRMT model retains nonlocal contributions only in the mass exchange terms, while the advective and dispersive terms appearing in (1.92) and describing transport in the mobile region are local in time; (*ii*) the gradients of concentration within the mobile and immobile are similar, thus allowing to neglect the additional advective terms of the type AAD_i ($i = \beta, \gamma$) which appear in our upscaled formulation so that the two equations of the MRMT model are coupled only through the standard mass exchange terms.

2) The effective mass rate exchange parameters included in MRMT models depend on the pore scale velocity normal to the interface between mobile and immobile regions. This result supports previous experimental observation by *Haggerty et al*. [2004], who noted that effective mass transfer coefficients adopted to interpret laboratory scale data tend to display a mild dependence on the system velocity.
3) Mass exchange processes occurring at the pore scale between the mobile and immobile regions give rise to the appearance of advective coefficients (1.80)-(1.83) in the upscaled system of equations which are not typically included in MRMT/DRMT models. These terms might affect (*i*) the calibration of the mobile/immobile proportion and (*ii*) the kernel of the memory function involved in MRMT models.
4) We present the solution of our upscaled model (1.78)-(1.79) and provide a quantitative analysis of the effects of various simplification strategies in the context of a simple illustrative example. The latter involves solute transport within a plane channel

characterized by a uniform aperture under steady-state flow conditions. While this simplified geometry is not fully representative of complex porous media structures, it enables one to clearly show the way pore scale features propagate to DRMT/MRMT models. It also allows obtaining analytical solutions for the asymptotic solution of the closure problems and the system coefficients (1.80)-(1.91). The temporal dynamics of the model coefficients (1.80)-(1.91) is numerically investigated.

5) We provide an assessment of the influence of all the terms included in the our upscaled two-equation model. Our results show that a DRMT model can reproduce the solution of our upscaled model with a reasonable accuracy for the scenario analyzed, provided that advection is retained also in the immobile region.

Our results and observations may provide a useful basis to (*a*) interpret studies of uncertainty propagation, inverse modeling and parameter estimation related to DRMT and MRMT models, and/or (*b*) assess the key elements underpinning the potential/ability of DRMT/MRMT models to interpret upscaled results stemming from pore scale transport simulation or laboratory experiments and exhibiting non-Fickian behavior.

CHAPTER 2. PORE-SCALE SIMULATION OF REACTIVE TRANSPORT

I. Introduction

Efficient simulation of diffusion-controlled chemical reactions in complex media remains a challenge for multiple disciplines, including hydrology [*Dentz et al*,2010. Transport features may significantly affects the reaction rate, driving the spreading and mixing of reactants. Typically averaged concentration models merge the mixing at local and the spreading at a larger scale [*Cirpka,* 2002].This overlapping of reaction and transport at different scales can cause serious errors on the rate of mixing and on reaction rates [*Gramling et al*, 2002*; Kapoor et al,* 1998*; Raje and Kapoor*, 2000].

Traditionally, reactive transport is modeled through a continuum-based approach where all solute concentrations are averaged over a representative elementary volume [*Bear* 1972; *Dagan.*, 1989]. Recent studies indicate that such a continuum-based approach may not be adequate for understanding reactive transport.

The advection diffusion/dispersion reaction equation (ADRE) is a striking example of a continuum formulation which is typically employed to model solute evolution in geological formations [*Bear and Cheng*, 2010; *Rubin*, 1983]. A theoretical analysis based on homogenization [*Battiato and Tartakovsky*, 2011] shows that this formulation is strictly applicable in a relatively narrow region in the phase space identified by the Peclet and Damkohler (*Da*) numbers. In particular, the sufficient conditions for the ADRE to be valid are not met for large *Da* and *Pe*. Formulation and investigation of models which can reliably predict solute evolution outside the range of validity of the ADRE is an active field of research. In this context, micro-scale simulations are a powerful tool to improve our understanding of the key

features of the basic processes affecting the system behavior on multiple scales and consequently to investigate the reliability of existing models and/or to assist in the validation of novel modeling approaches.

Reactive flows in the presence of bimolecular irreversible homogeneous reactions of the kind $A+B \rightarrow C$ are considered in a number of literature studies [*Kang and Redner*, 1985; *Kapoor et al.*, 1997; *Benson and Meerschaert*, 2008; *Willingham et al.*, 2010; *Tartakovsky et al.*, 2009; *Edery et al*., 2012]. This chemical setting is very simple, as compared to the geochemical reaction patterns which can be observed in real porous and fractured systems. Nevertheless, it serves as an ideal benchmark setting to characterize the effects of micro-scale processes on upscaled parameters included in effective formulations. Some works are focused on the description of the process evolution from a global perspective, e.g., [*Kang and Redner*, 1985; *Benson and Meerschaert*, 2008]. These studies highlight the tendency of the system towards a large-time asymptotic behavior characterized by a diffusion/dispersion limited global reaction rate.

The simulation of an irreversible reaction taking place in a plane channel is analyzed in [*Kapoor et al.*, 1997]. This work introduces the definition of a segregation factor, which quantifies the global effect of incomplete solute mixing on the reaction rate. Numerical simulations quantify the influence of local fluctuations of reactant concentrations on a section-averaged effective model. This effect is shown to be particularly relevant for large *Pe* and *Da*. A general one-dimensional effective formulation of the process which includes these effects in the presence of arbitrary initial conditions is still lacking.

A parallel injection of the reactants into artificially built two-dimensional porous media is simulated at the pore scale in [*Willingham et al.*, 2010; *Tartakovsky et al.*, 2009]. The results of

these studies highlight the effects of the pore space geometry and of incomplete mixing of reactants at the pore scale on the reactive process. In particular, it is shown in [*Tartakovsky et al.*, 2009] that an ADRE formulation overestimates the global reaction rate for large *Pe*. Similar results are also compared in [*Tartakovsky*, 2010] against a Langevin model. The latter is found to perform better than the ADRE, its superior predictive capability being attributed to the improved description of the dispersion term.

Experimental works in [*Gramling et al.*, 2002; *Raje and Kapoor*, 2000] consider instead a replacement scenario, i.e., a laboratory column filled with a nonreactive solid matrix is initially saturated with a solution containing chemical species *A* which is progressively replaced by the injection of a solution containing *B*. The reaction takes place as the two reactants *A* and *B* mix. Standard continuum models based on the ADRE lead to a significant overestimation of the reaction product in both studies. These continuum formulations include (i) a constant dispersion coefficient which is calibrated from non reactive experiments, and (ii) a reaction kinetic coefficient derived from batch reactor experiments. The authors suggest that pore scale incomplete mixing is responsible of the failure of the predictive capability of their modeling approach.

Further studies specifically focus on the formulation of interpretative models capable of capturing the key results of the experiment presented in [*Gramling et al.*, 2002]. These modeling approaches include particle tracking Continuous Time Random Walk [*Edery et al*., 2010] and effective continuum approximations based on the ADRE [*Sanchez-Villa et al.*, 2010; *Rubio et al.*, 2008]. A detailed recent review of aspects related to these modeling approaches is available in [*Edery et al*., 2012]. The continuum formulations proposed in [*Sanchez-Villa et al.*, 2010; *Rubio et al.*, 2008] are successful in reproducing the published experimental results through the

introduction of some effective reaction parameters. These are mainly based on heuristic arguments and are not grounded on a firm theoretical analysis.

The theoretical work presented in [*Porta et al.*, 2012] attempts to fill this gap. It shows how adopting a transient closure approximation of volume-averaged advective-diffusive-reactive processes can lead to a volume-averaged formulation of an effective continuum model which includes the traditional ADRE as a special case. Key results of the analysis presented in [*Porta et al.*, 2012] are associated with fast reactions for which the ratio *Da*/*Pe* is much larger than 1. The formulation proposed for this scenario includes (i) a mixing dependent dispersion coefficient for the two reactive species, and (ii) a closed expression for the second order reaction term. The latter is associated with the cross-covariance of solute concentrations within the averaging volume.

The modeling strategies illustrated in [*Sanchez-Villa et al.*, 2010], which are based on considering (i) a dispersion coefficient different from the one estimated through a conservative transport experiment and (ii) a time dependent reaction rate parameter are consistent with the theoretical developments presented in [*Porta et al.*, 2012].

The present work aims at analyzing the behavior of a reactive within the two-dimensional disaggregated porous media in the presence of a homogeneous irreversible bimolecular reaction. The reactive process is simulated through a particle tracking algorithm. The methodology is based on the codes and routines which have been previously employed for the study of several non reactive and reactive transport problems in fractured or porous media [*Salles et al.*, 1993; *Salles et al.*, 1993; *Mourzenko et al.*, 1996; *Debenest et al.*, 2005] and are modified to include the treatment of the chemical reaction. The main objectives of the work are: (i) the development and assessment of a particle based numerical methodology for homogeneous reactive transport

process simulations; (ii) the detailed illustration of the process on the basis of the observation of key quantities on different scales; (iii) the assessment of the validity of closed formulations of a one-dimensional section-averaged model and, in particular, the validation of the upscaled volume averaged equations derived in [*Porta et al.*, 2012]. The analysis is performed considering a wide range of combinations of Peclet and Damkohler numbers, to investigate (a) the effect of the relative strength of these two parameters on the process evolution, and (b) their role in the definition of effective dispersion and reaction coefficients.

This chapter is organized as follows. Section II provides a definition of the problem setting in terms of the key equations governing the system at the micro-scale. Section III describes the particle tracking algorithm and the computation of the velocity field. The selected simulation settings and a multiscale description of the phenomenon evolution is provided in Section IV. Section V is divided into two main parts: (i) the derivation of a section-averaged model is recalled, (ii) the effective coefficients in the equations are computed and compared against the corresponding theoretical predictions.

II. Problem statement

We consider the transport of three diluted chemical species A, B and C within the two-dimensional disaggregated porous media, corresponding to arrays of cylinders. The media is constructed from periodic unit cells (Figure 14).

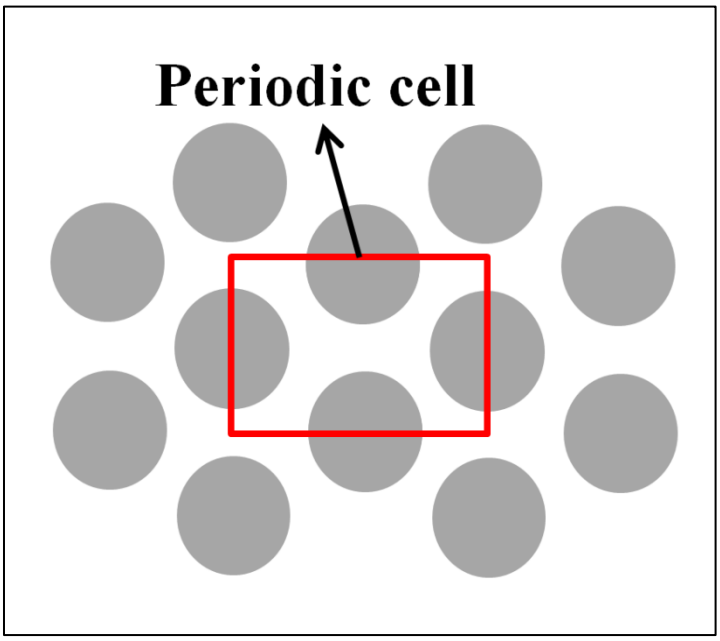

Figure 14. The media constructed from periodic unit cells

We assume an irreversible homogeneous bimolecular reaction is taking place in the liquid phase and solutes A and B react to form the product C, i.e. A + B → C. The initial distributions of concentrations $\hat{c}_A$ and $\hat{c}_B$ of the two species A and B are assumed to be known in the domain. Consider that the reactive process does not produce any change in the porous medium and in the characteristics of the fluid.

It is assumed that the chemical species are sufficiently diluted so that diffusion is described by Fick's Law. The dynamics of solute concentrations are described by

$$\frac{\partial \hat{c}_A}{\partial \hat{t}} + \hat{\mathbf{u}} \cdot \hat{\nabla} \hat{c}_A = \hat{D}_A \hat{\nabla}^2 \hat{c}_A - \hat{r} \tag{2.1}$$

$$\frac{\partial \hat{c}_B}{\partial \hat{t}} + \hat{\mathbf{u}} \cdot \hat{\nabla} \hat{c}_B = \hat{D}_B \hat{\nabla}^2 \hat{c}_B - \hat{r} \tag{2.2}$$

$$\frac{\partial \hat{c}_C}{\partial \hat{t}} + \hat{\mathbf{u}} \cdot \hat{\nabla} \hat{c}_C = \hat{D}_C \hat{\nabla}^2 \hat{c}_C + \hat{r} \tag{2.3}$$

where $\hat{\mathbf{u}}$ is the fluid velocity, $\hat{D}_i$ ($i = A, B, C$) the molecular diffusion coefficient and $\hat{r}$ is the reaction rate. A first order chemical reaction is considered

$$\hat{r} = \hat{k} \hat{c}_A \hat{c}_B \tag{2.4}$$

where $\hat{k}[m^3 / mol \cdot s]$ is the reaction rate coefficient. The diffusion is considered to be isotropic and equal for all the chemical species, i.e. $\hat{D}_A = \hat{D}_B = \hat{D}_C = D$. Then system can be written in dimensionless form

$$\frac{\partial c_A}{\partial t} + \mathbf{u} \cdot \nabla c_A = \frac{1}{Pe} \nabla^2 c_A - \frac{Da}{Pe} c_A c_B \tag{2.5}$$

$$\frac{\partial c_B}{\partial t} + \mathbf{u} \cdot \nabla c_B = \frac{1}{Pe} \nabla^2 c_B - \frac{Da}{Pe} c_A c_B \tag{2.6}$$

$$\frac{\partial c_C}{\partial t} + \mathbf{u} \cdot \nabla c_C = \frac{1}{Pe} \nabla^2 c_C + \frac{Da}{Pe} c_A c_B \tag{2.7}$$

The dimensionless quantities are defined as following

$$x = \frac{\hat{x}}{\hat{l}}, \quad t = \frac{\hat{t}\hat{l}}{\hat{u}^*}, \quad \mathbf{u} = \frac{\hat{\mathbf{u}}}{\hat{u}^*}, \quad Pe = \frac{\hat{u}^* \hat{l}}{\hat{D}}, \quad c_i = \frac{\hat{c}_i}{\hat{c}_0}, \quad Da = \frac{\hat{k} \hat{c}_0 \hat{l}^2}{\hat{D}} \tag{2.8}$$

where $\hat{u}^*$ is the mean fluid velocity, $\hat{c}_0$ is a characteristic concentration value for the problem, $\hat{l}$ is the characteristic length (ex. length of the unit cell, radius of solid grains, cavity aperture, etc).

Then we introduce time scales which influence dynamics of the species concentrations:

a) the advection time scale $\hat{t}_A = \dfrac{\hat{l}}{\hat{u}^*}$

b) the diffusion time scale $\hat{t}_D = \dfrac{\hat{l}^2}{\hat{D}}$

c) the reaction time scale $\hat{t}_R = \dfrac{1}{\hat{k}\hat{c}_0}$

The dispersion time scale $\hat{t}_{D^*} = \dfrac{\hat{l}^2}{\hat{D}D^*}$,where $\hat{D}^*$ is the effective dispersion coefficient.

The following dimensionless time scales are introduced

$$t_D = \frac{\hat{t}}{\hat{t}_D}, \quad t_R = \frac{\hat{t}}{\hat{t}_R}, \quad t_{D^*} = \frac{\hat{t}}{\hat{t}_{D^*}} \tag{2.9}$$

The system (2.5)-(2.7) should be completed by the following boundary and initial conditions:

$$uc_i - \frac{1}{Pe}\frac{\partial c_i}{\partial x} = N_i, \qquad x = 0, y \in [0,1], t > 0 \tag{2.10}$$

$$u\frac{\partial c_i}{\partial y} = 0, \qquad x \in [0, L], y = 0, t > 0 \tag{2.11}$$

$$\frac{\partial c_i}{\partial y} = 0, \qquad x \in [0, L], y = 1, t > 0 \tag{2.12}$$

$$\frac{\partial c_i}{\partial x} = 0, \qquad x = L, y \in [0,1], t > 0 \tag{2.13}$$

$$c_{A0}(x, y) = c_{A0}, \qquad c_{B0}(x, y) = c_{B0}, \qquad x \in [0, L], y \in [0,1], t = 0 \tag{2.14}$$

Here , L is the length of the domain; N_i represents the dimensionless flux of each species at the inflow boundary located at $x = 0$. For simplicity and without any loss of generality, it is assumed that $c_C = 0$ at $t = 0$.

III. Numerical technique

1. Particle tracking

The reactive transport process is simulated via a particle tracking algorithm which is based on a series of routines [*Porta et al.*, 2012] which were used to investigate pore scale reactive transport processes in porous media and fractures in a variety of physical settings. The media space is discretized into elementary cubes K_i of side $\hat{a}$. Three different sets of particles are defined, each corresponding to a different chemical species. Starting from a known location of the particles at time $\hat{t}^k$, the displacement vector for each particle is computed as

$$\hat{\mathbf{d}} = \hat{\mathbf{u}}[\hat{\mathbf{x}}(\hat{t}^k)]\delta t + \hat{\delta}\hat{\mathbf{d}}_D \tag{2.15}$$

where $\hat{\mathbf{u}}$ is the fluid velocity, δt the time step magnitude and $\hat{\delta}\hat{\mathbf{d}}_D$ the diffusive displacement. The last one is associated with a random orientation $\hat{\mathbf{d}}_D$ and a module equal to

$$\hat{\delta} = \sqrt{6\hat{D}\delta t} \tag{2.16}$$

The velocity $\hat{\mathbf{u}}[\hat{\mathbf{x}}(\hat{t}^k)]$ is evaluated at the position of the particles $\hat{\mathbf{x}}(\hat{t}^k)$ at the beginning of the time step, using a second order Taylor series. The Taylor approximation is done separately for the determination of each component of the velocity field. For example, for the *x*-component of $\hat{\mathbf{u}}[\hat{\mathbf{x}}(\hat{t}^k)]$ it can be written as

$$\hat{u}[\hat{\mathbf{x}}(\hat{t}^k)] = \hat{u}_0 + \hat{\nabla}\hat{u}\cdot\left(\hat{\mathbf{x}}(\hat{t}^k) - \hat{\mathbf{x}}_0^{(x)}\right) + \frac{1}{2}\left(\hat{\mathbf{x}}(\hat{t}^k) - \hat{\mathbf{x}}_0^{(x)}\right)\cdot\hat{\nabla}\hat{\nabla}\hat{u}\cdot\left(\hat{\mathbf{x}}(\hat{t}^k) - \hat{\mathbf{x}}_0^{(x)}\right) \tag{2.17}$$

where $\hat{u}_0$, the first, $\hat{\nabla}\hat{u}$, and second gradients, $\hat{\nabla}\hat{\nabla}\hat{u}$, are evaluated at the closest point $\hat{\mathbf{x}}_0^{(x)}$. For the *x*-component of the velocity field $\hat{u}[\hat{\mathbf{x}}(\hat{t}^k)]$, $\hat{\mathbf{x}}_0^{(x)}$ is the center of one of the two faces in *x* (parallel to *x-axis*) of the cube that contains the particle.

The advective displacement in (2.15) is computed with the velocity at $\hat{\mathbf{x}}(\hat{t}^k)$, whereas the fluid velocity theoretically varies along the particle path. To limit the effect of this approximation, an upper bound is set for particle displacements as

$$\hat{\delta} \le \hat{\delta}_M = \max[\hat{u}(\hat{\mathbf{x}})]\delta t + \hat{\delta} = \beta \hat{a} \tag{2.18}$$

where $\beta < 1$. The time discretization step δt is fixed according to (2.18). Note that as β decreases, the accuracy of the simulation and the computational cost increase, as a smaller δt is required in (2.18). A value $\beta = 0.6$ is selected on the basis of preliminary numerical tests for

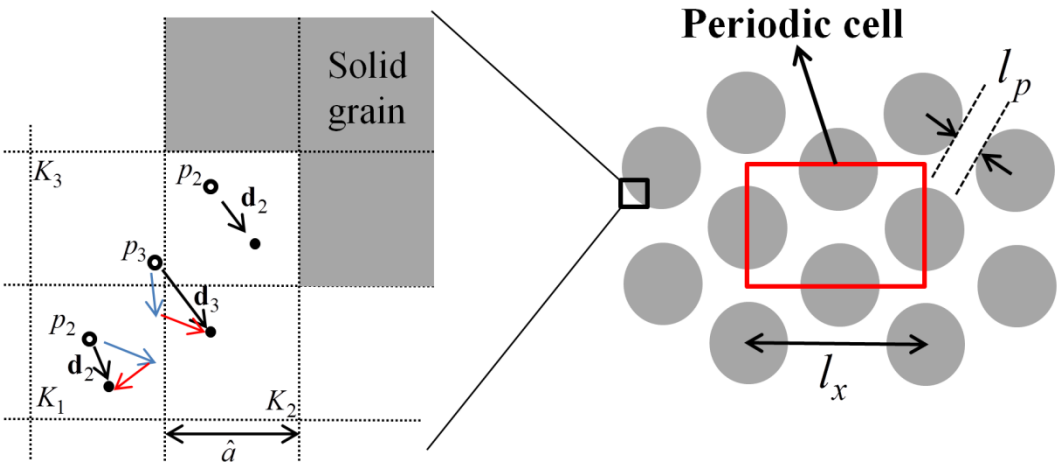

Figure 15. Sketch of possible particle displacements

passive transport conditions. Once the displacement is computed by (2.15), the new particle position is given by

$$\hat{\mathbf{x}}(\hat{t}^k + \delta t) = \hat{\mathbf{x}}(\hat{t}^k) + \hat{\mathbf{d}} \tag{2.19}$$

Reflection boundary conditions are imposed at the solid walls, preserving the modulus of the complete displacement $\hat{\mathbf{d}}$. Critical steps of the proposed procedure include (a) the representation of the bimolecular reaction process and (b) the update of the ensuing concentration fields. The probability of A and B particles to react inside a cube is proportional to (i) the concentration of the reacting species, (ii) the particles residence time inside the cube and (iii) the reaction kinetic coefficient. The procedure illustrated in the following aims at providing the best approximation of the first two quantities, as $\hat{k}$ is assumed to be constant. Consider a particle of species A that interacts with the field of $c_B(\hat{t})$. The time evolution of concentration $c_A(\hat{t})$ interacting with $c_B(\hat{t})$ is described by

$$\frac{d\hat{c}_A}{d\hat{t}} = -\hat{k}\hat{c}_0 c_B(\hat{t})\hat{c}_A \tag{2.20}$$

Integration of (2.20) yields the probability of survival of A particles at time $\hat{t} > \hat{t}_0$

$$SP_A = \exp\left[-\int_{\hat{t}_0}^{\hat{t}} \hat{k}\hat{c}_0 c_B(s)ds\right] \tag{2.21}$$

Hence, the probability that reaction takes place is $RP_A = 1 - SP_A$. Assuming that concentration is constant within cube K_i and along the time discretization step δt , the reaction probability can be linearized as

$$RP_A(K_i) = \hat{k}\hat{c}_0 c_B(K_i)T_C(K_i)\delta t, \quad RP_B(K_i) = \hat{k}\hat{c}_0 c_A(K_i)T_C(K_i)\delta t \tag{2.22}$$

for the A and B particles. Here, the factor $T_C(K_i)$ is the fraction of the time step δt spent by the particle in cube K_i. Note that the linearized formulations (2.22) are accurate if the

condition $\delta t < \hat{t}_R$ is fulfilled. In order to avoid any artificial mixing between the two reactants A and B

$$Da_K = \frac{\hat{t}_D^K}{\hat{t}_R^K} = \frac{\hat{a}^2 \hat{k} \hat{c}_0}{\hat{D}} < 1 \tag{2.23}$$

must be satisfied, where Da_K is the Dahmkohler number based on the grid size. Figure 15 depicts the location of three particles of species A at time $\hat{t}_0$. During δt , particle p_1 remains within K_1 so that $T_C = 1$. The concentration $c_B(K_i)$ in (2.22) is known from the previous time step computation or by the initial condition. A Bernoulli trial is then performed and the probability RP_A is compared with a uniformly distributed random number, $RN \in [0, 1]$. If $RN > RP_A$, the reaction takes place, the A particle disappears and is replaced by a C particle. On the other hand, if $RN < RP_A$, the reaction does not take place and particle A remains in the system. If the particle reacts, the location of the reaction and the newly formed *C* particle are randomly assigned along the path described by the displacement $\mathbf{d}_1$. In these cases, the factor T_C in (2.22) accounts for the fact that the particles paths are split between different cubes. The fractions of the time step spent by a particle within a cube along the path are computed upon assuming that particle displacements take place at a constant velocity during δt . Hence, T_C in (2.22) corresponds to the fraction of the total computed displacement inside each cube. Updating of the concentration fields is then based on the residence time of the particles within each cube, i.e. the fractions of the time step δt spent by the particles within a cube is taken into account

through the quantity T_C . The dimensionless concentration of species s ($s = A, B, C$) in cube K_i can be computed as

$$c_s(K_i) = \sum_{j=1}^{N_p} T_C^{p_j}(K_i) \frac{1}{NP_K} \tag{2.24}$$

Here, $T_C^{p_j}(K_i)$ is the fraction of time step spent by particle p_j in cube K_i , NP_K is the number of particles per cube which renders a concentration $\hat{c}_0$, i.e.,

$$NP_K = \hat{a}^3 NP_{mol} \hat{c}_0 \tag{2.25}$$

where NP_{mol} is the number of particles which corresponds to one mole of solute. For simplicity, in the following we assume $\hat{c}_0 = 1\, mol / m^3$. The concentration in (2.24) takes into account the residence time of the particles in each cube. The amount of solute assigned to a single particle can be distributed into different cubes. The procedure described insures that minimum concentration values do not depend on NP_K .

2. Velocity field

Firstly, it is important to note that we consider that the solid phase is considered impermeable to the fluid phase. Therefore, we consider that the flow in the intragranular pore space is government by the Navier-Stokes equations with a condition of adhesion to the wall. In addition, the condition of adhesion to the wall is replaced by a condition of zero velocity at the wall means that the interface is considered to be immobile, or at least its deformation is so slow that an approximation of quasi-static is applicable.

The Reynolds number is defined as;

$$\mathrm{Re} = \frac{\bar{v}R}{\nu} \tag{2.26}$$

and ν is the dynamical viscosity, R is the grain diameter and $\bar{v}$ is the fluid velocity (the average density of the fluid velocity, which is equal to the volumetric flow rate per unit area) . We assume that the flow remains laminar over the entire range of flow regarded in our case. We accept as a general rule that the transition between laminar and turbulent flow occurs for Reynolds numbers greater than 100 (e.g., about 150 to 300 for a three-dimensional random stacking of cylinders according *Dybbs and Edwards*, [1984]) . The fluid is considered incompressible. We impose a constant global flow rate, this implies that the flow is stationary. Therefore, the fluid velocity can be determined before any further calculation and used in our simulations.

Using all the remarks made earlier, the fluid flow is governed by the Stokes equations are:

$$\nabla \mathbf{p} = \mu \nabla^2 \mathbf{v} \tag{2.27}$$

$$\nabla \cdot \mathbf{v} = 0 \tag{2.28}$$

$$\mathbf{v} = 0, \qquad \text{at solid-liquid interface} \tag{2.29}$$

where $\mathbf{v}$ is the local velocity, μ is the dynamic viscosity $\mathbf{p}$ is the pressure.

Equations (2.27)-(2.29) are solved once and the velocity field can be used resulting in all simulations to come. As the geometry of the solid phase is periodic, the velocity field is also, and the problem does not need to be solved in the unit cell periodic pattern. In the absence of inertial effects, the local velocities are proportional to the macroscopic pressure gradient $\nabla \mathbf{p}$. Therefore,

we only need to solve the problem for a particular value of $\nabla \mathbf{p}$. Then, the velocity field for flow or imposes a certain value of the pressure gradient can be obtained simply by readjusting the particular solution with an appropriate multiplicative factor. A first version of a numerical solver for equations of Stokes in a complex 3D environment was made by *Lemaitre et al* [1990]. He used a method of artificial compressibility, with a finite difference scheme. Then, the performance of the code were significantly improved and the fourth order of spatial discretization was introduced by *Coelho*, [1996].

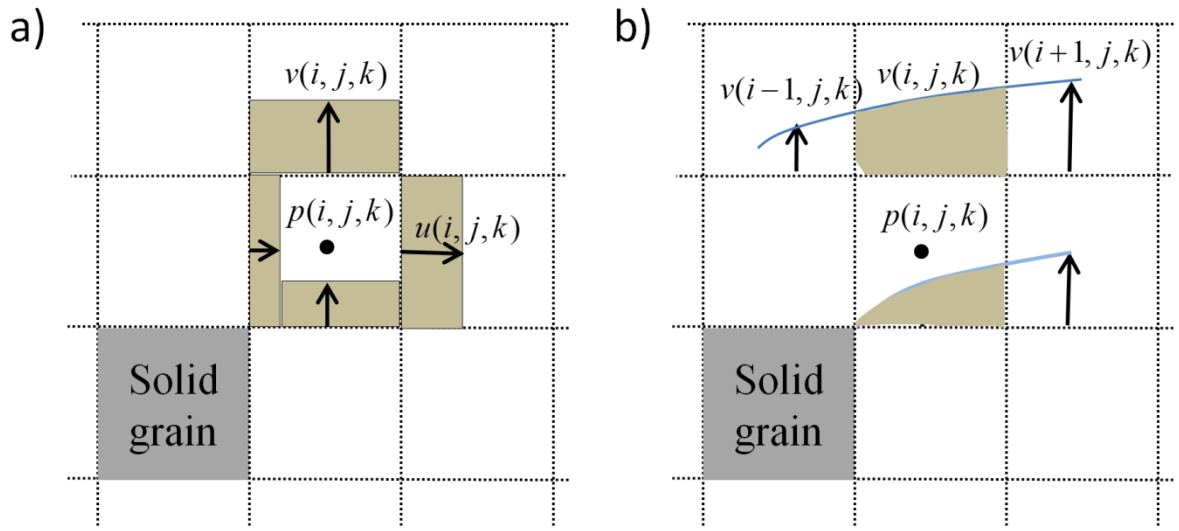

Figure 16. Illustration of the pressure and velocity fields discretization. The pressure $\mathbf{p}$ *is determined at the centers of cubic fluid and components of the velocity field (u, v, w) are determined at the centers of the faces of cubes orthogonally to those above. If we use the second order formulation (a), the balance of matter on the cube is obtained by considering the speed is uniform across each face of the cube. In formulating the fourth order(b), the speed on one side is a quadratic function of position, which depends on speed adjacent faces.*

There are many criteria for convergence in the solver, which are based on the local velocity difference on the overall conservation of the flow and the stability of the average flow in the iterative solution scheme has. Excellent convergence of the velocity field (that is to say, the speed difference negligible) is necessary for a rigorous application of the random walk method. A complete description of the algorithm was made by *Lemaitre et al* [1990] and *Coelho* [1996] and will not be repeated here. However, one aspect is detailed further. Recall that the geometry of the porous medium is partitioned into elementary cubes, identified by integer coordinates (i, j, k), they are either filled with fluid or solid. The pressure $\mathbf{p}$ in the fluid is estimated at the centers of cubic fluids and velocity components (u, v, w) are determined at the centers of faces orthogonal to the corresponding direction, as shown in *Figure 16*. A system of linear equations for these quantities is obtained by discretizing the balance equations that result from the integration of the equation of mass of each elementary cube of fluid. This gives

$$\Omega c \frac{\partial \mathbf{p}}{\partial t} + B = 0, \qquad B = \int_{\partial\Omega} \mathbf{n} \cdot \mathbf{v} ds \tag{2.30}$$

where Ω is the volume of the cube, with its border $\partial\Omega$, $\mathbf{n}$ is the normal vector , and c is the coefficient of compressibility of the fluid. For stationary boundary conditions, we obtain a flow stable, then $\frac{\partial \mathbf{p}}{\partial t}$ vanishes and the equation (2.30) reduces to $B = 0$, in agreement with (2.28) and in accordance with the artificial value c, as it should be. Two versions of the flow solver has been developed, with spatial discretization is second to fourth order either. In the second case the velocity field is obtained with greater precision, but has a greater cost in terms of computation time. Of course, the expression for B depends on the order of discretization and must be chosen in such a way that the balance equation $B = 0$ is consistent with the solute

transport equation. In the second order formulation, B is simply reduced to a sum of the components of the velocity vectors normal to each face of the 4 faces of the cube, as if the flow passing through each face, as shown in *Figure 16*a . In formulating the fourth order, the mass balance is obtained by integrating the normal components of the speed which depend on the position and is a quadratic function of the speed at the center of the face and at the centers of neighboring faces as in *Figure 16*b. The random walk algorithm which has been used in most of our simulations requires that B vanishes in the formulation to fourth order.

IV. Simulations

1. Simulations setup.

The methodology from the previous section is applied to a geometry with a regular distribution of grains. We consider hexagonal packing as the distribution of the grains and cylinders as the grains. All the cylinders have the same radius, r_c , and the distance between the centers of the cylinders is taken as the characteristic length, $\hat{l}$, for this setup.

Numerical simulations are performed for a different combinations of Peclet and Dahmkohler numbers for the hexagonal micro-scale geometry with different porosities. To change the porosity of the system, ϕ, we vary the radius , r_c. The set of the Peclet and Dahmkohler numbers and set of the used porosities is reported in Table 1

Porosities	25%	36%	50%
Peclet numbers	6	24	96
Dahmkohler numbers	8.1	64.8	1038

Table 1. Set of parameters used for the numerical simulations with hexagonal packing

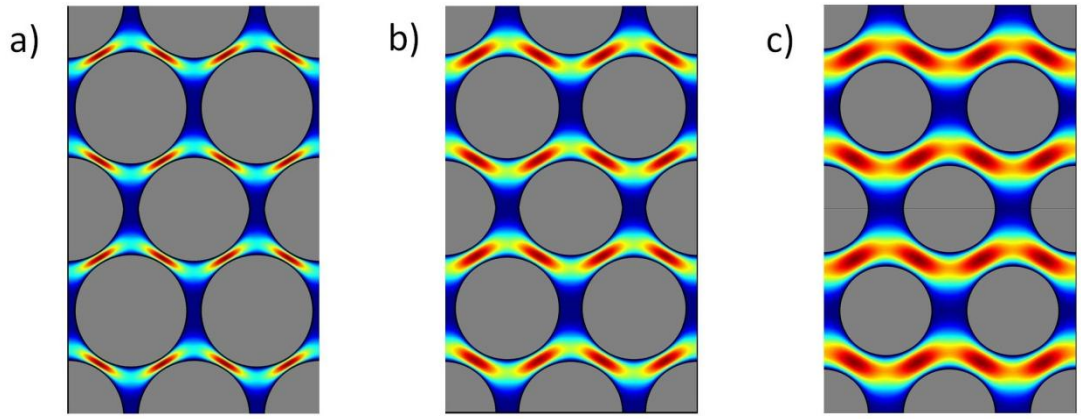

Figure 17.Geometry of the unit cell with hexagonal packing of cylinders with different porosities of the media: a) 0.25; b) 0.36 c) 0.5 .

Figure 17 demonstrates the unit cells with different porosities (a) 25% b) 36% c) 50%.) with calculated distribution of the velocity field.

The pore space is initially filled by a solution with uniform concentration, $c_{A0} = 1$ of species A. Species B is injected into the system as a step input with a fixed concentration $c_B = 1$, at $x = 0$ and time $t = 0$.

With the time, the two reactants move along the channel, reaction between them takes place and a traveling wave of C species moves along the channel. The dimension of the unit cells in the case of hexagonal packing is 72×60 [cubes] with the dimension of cube $\hat{a} = 2 \times 10^{-5} m$. Diffusion coefficient $\hat{D} = 2 \times 10^{-9} m^2 / s$. The length of the domain in the *x*-direction $\hat{L}$ is chosen as a function of the total simulation time, in a way that ensures the reactive process can be observed into the channel for a prescribed time. To avoid any interference of the injection boundary condition on the early time system evolution, we set $c_B = 1$ and $c_A = 0$ for

$x < x_0$ and $t = 0$, and prescribe $x_0 = \hat{l}$ to avoid that B particles exit the system from the inlet section by diffusion.

As the amount of particle per cube value $\mathrm{NP}_K = 50$ has been found to be a good compromise between accuracy and computational. Typical simulation of the reactive transport in this case last from 1 to 6 weeks depending on the parameters. Such the difference in computation time between the simulations is due to the different length of the media needed for different values of Peclet number to reach the asymptotic(diffusion/dispersion limited) regime.

c. Dispersion

The dispersion is an effective transport property of porous media that results from the combination of transport mechanisms convective and diffusive. It plays an important role in the transport of solute.

Quantify the mass, the average position and spread-solute cloud can be calculated by the first three moments of the concentration

$$M_0(t) = \int c(\mathbf{r}, t) d\mathbf{r}^3 \tag{2.31}$$

$$\mathbf{M}_1(t) = \int \mathbf{r} c(\mathbf{r}, t) d\mathbf{r}^3 \tag{2.32}$$

$$\mathbf{M}_2(t) = \int \mathbf{r}\mathbf{r} c(\mathbf{r}, t) d\mathbf{r}^3 \tag{2.33}$$

In addition, we define the central second moment $\bar{\mathbf{M}}_2$ as

$$\bar{\mathbf{M}}_2 = \mathbf{M}_2^{'} - \mathbf{M}_1^{'}\mathbf{M}_1^{'} \tag{2.34}$$

where $\mathbf{M}_1^{'} = \mathbf{M}_1 / M_0$ and $\mathbf{M}_2^{'} = \mathbf{M}_2 / M_0$.

The main point is the intuitive idea that, after a certain time, the solute samples all statistics of the microstructure and flow. This is possible thanks to the molecular diffusion. In addition, if the time is long enough, the solute has "forgotten" the details of the initial spatial distribution and moves at the same speed as the fluid.

$$\lim_{t\to\infty} \frac{d\mathbf{M}_1}{dt} = \mathbf{v}^* \tag{2.35}$$

where $\mathbf{v}^*$ is the interstitial velocity.

$$\frac{1}{2}\lim_{t\to\infty} \frac{d\bar{\mathbf{M}}_2'}{dt} = \mathbf{D}^* \tag{2.36}$$

where $\mathbf{D}^*$ is called the dispersion tensor. It can be shown that this tensor is symmetric, positive definite, but it is not spherical. Anisotropy is introduced by the direction of the flow.

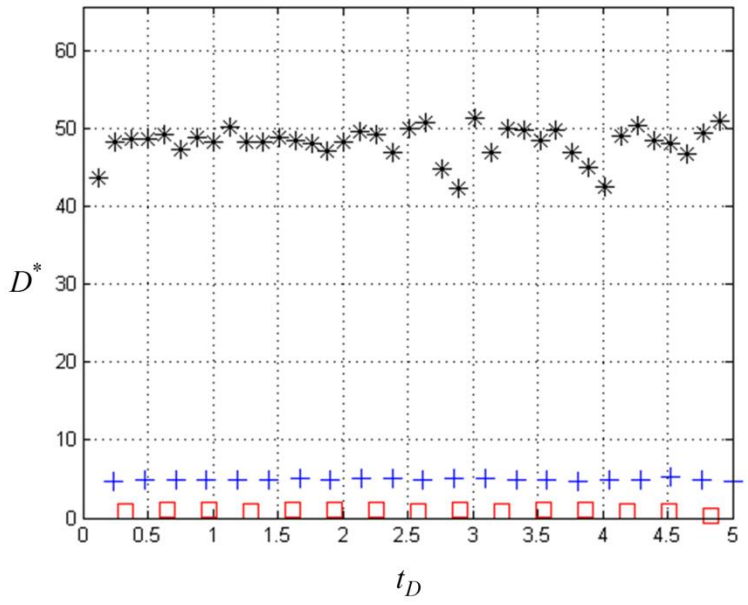

Figure 18. Evolution of dispersion coefficient D^* for three Peclet numbers: Pe=6(□), Pe=24 (+) , Pe=96 (✳).

To evaluate the dispersion coefficients we fill several unit cells in the simulation domain with a solute. Then we apply equation (2.36) to the solute plume. Figure 18 depicts time evolution of the dispersive coefficients for 3 Peclet numbers over diffusion time t_D .

To fully characterize the media for the simulations, we present longitudinal effective dispersion coefficients, D^*, for different simulations' parameters in Table 2.

	$Pe = 6$	$Pe = 24$	$Pe = 96$
$\phi = 0.25$	**0.964**	**4.962**	**48.591**
$\phi = 0.36$	**0.983**	**5.088**	**45.851**
$\phi = 0.50$	**0.976**	**4.260**	**34.604**

Table 2. Dispersion coefficients for the simulations

2. *Results of the simulations*

The time evolution of the total amount of the reaction product C is given by

$$TC_C^*(t) = \int_\Omega c_C(t) d\Omega \tag{2.37}$$

The global reaction rate or global production rate of C can be written as a time derivative of $TC_C^*(t)$ .Depending on the reference time scale the global reaction rate expressed as

$$R_D^*(t_D) = \frac{dTC_C^*}{dt_D}, \quad R_R^*(t_R) = \frac{dTC_C^*}{dt_R} = \frac{R_D^*}{Da}, \quad R_{D^*}^*(t_{D^*}) = \frac{dTC_C^*}{dt_{D^*}} = R_D^* D^* \tag{2.38}$$

Figure 19 depicts the temporal evolution of $TC_C^*(t)$ and R_R^* for all values Da and Pe reported at Table 1. The porosity of the system for the results at Figure 19 is $\phi = 0.25$.

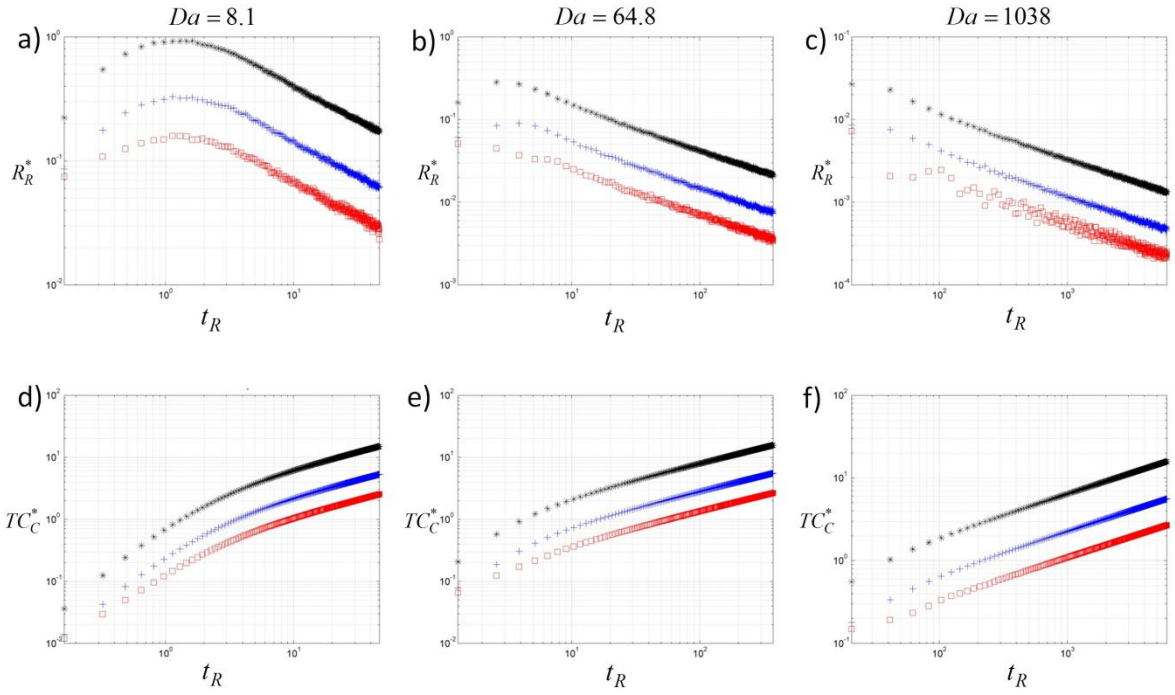

Figure 19. Temporal evolution (t_R) of TC_C^* and R_R^* for different Da values: Da = 8.1 - a) and d); Da = 64.8 - b) and e); Da = 1038 - c) and f). Every subplot presents the evolution for three values of Pe: Pe=6(□), Pe=24 (+) , Pe=96 (✳).The porosity of the system $\phi = 0.5$.

It should be noted temporal dynamics of R_R^* are characterized by a reaction limited regime, that is associated with an early time increase of R_R^*. This phase is then followed by a diffusion limited regime. The latter corresponds to the decreasing trend of R_R^* which is observed after the peak value occurring at a transition time $t_R = t_R^* = 1$. It is observed that R_R^* is proportional to $t_R^{-0.5}$ for long times ($t_R \gg t_R^*$). As a consequence, the time evolution of TC_C^* also exhibits a clear change in the slope around $t_R = t_R^*$ (Figure 19a) and is proportional to $t_R^{0.5}$ at late time. Advective processes cause R_R^* and TC_C^* to increase with the Peclet number. The reaction and diffusion limited regimes can still be clearly identified as the transition time t_R^* increases

with Pe . All values of Pe explored are characterized by a similar late time behavior, associated with $R_R^* \propto t_R^{-0.5}$ and $TC_C^* \propto t_R^{0.5}$. These asymptotic results related to the diffusion limited regime are consistent with previous works presented in [*Kang and Redner,* 1985*; Benson and Meerschaert,*2008].

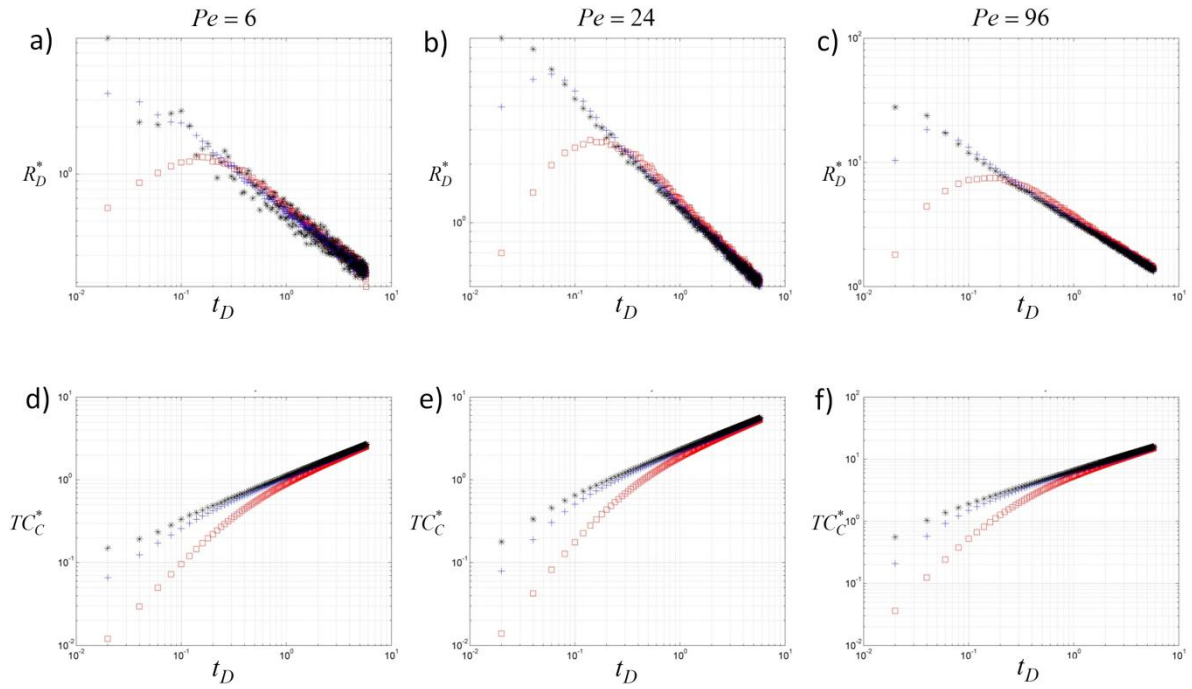

Figure 20. Temporal evolution ( ) of and for different Pe values : Pe = 6 - a) and d); Pe= 24 - b) and e); Pe = 96 - c) and f). Every subplot presents the evolution for three values of Da: Da=8.1(□), Da= 64.8 (✳) , Da= 1038 (+).The porosity of the system $\phi = 0.5$.

Figure 20 displays the evolution of R_D^* and TC_C^* for different combinations of Pe and Da. It should be noted that to emphasize the influence of Pe on the reactive process R_D^* is considered instead of R_R^*. The reaction rate R_D^* is independent of Da for $t_D > 1$ (Figure 20a–c). As a consequence, TC_C^* at the end of the simulation is only slightly dependent on Da, because its influence is confined to the early times ($t_D < 1$,Figure 20d–f). The dimensionless

time $t_D^* = t_R^* / Da$ is here introduced to identify the occurrence of the peak of R_D^*. The behavior of the system for $t_D < t_D^*$ depends on the particular set of initial conditions. The problem tends to become limited by diffusion/dispersion as the reaction time decreases. This is reflected by the observation that t_D^* decreases with Da. The time t_D^* defining the transition between the reaction and diffusion limited regions depends on both Pe and Da.

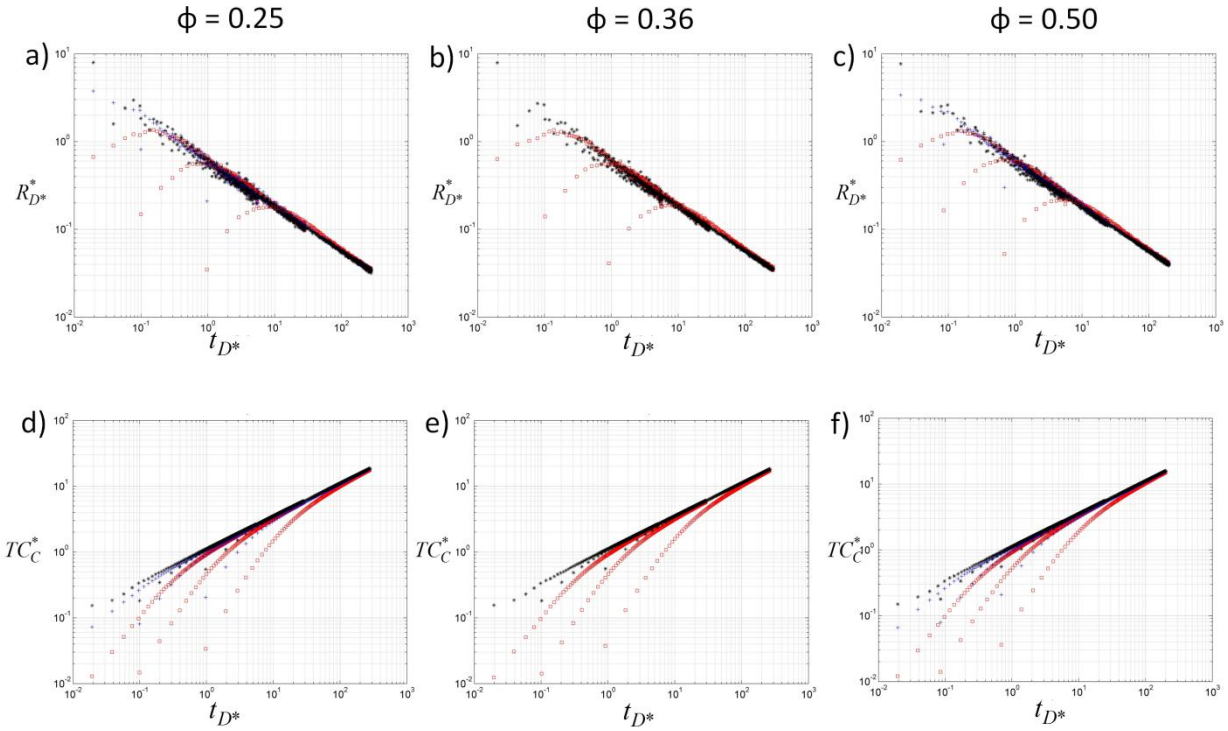

Figure 21. Temporal evolution (t_{D*}) of TC_C^* and R_{D*}^* for different values of ϕ : $\phi = 0.25$ - a) and d); $\phi = 0.36$ - b) and e); $\phi = 0.50$ - c) and f). Every subplot presents the evolution for all values of Pe and Da: 8.1(□), 64.8 (✳) , 1038 (+).

Figure 21 presents the set of simulation results as a function of the dimensionless time t_{D*}. It can be noted that in the asymptotic regime $TC_C^* \propto t_{D*}^{0.5}$ and $R_{D*}^* \propto t_{D*}^{-0.5}$ collapse onto the same curves for all the investigated (Da , Pe) pairs. Hence, the dependence of TC_C^* and R_{D*}^* on Pe can be expressed by the dispersion coefficient D^*. The evolution of the reactive process and

the longitudinal dispersive mass exchanges are characterized by the same time scale in the late time asymptotic regime.

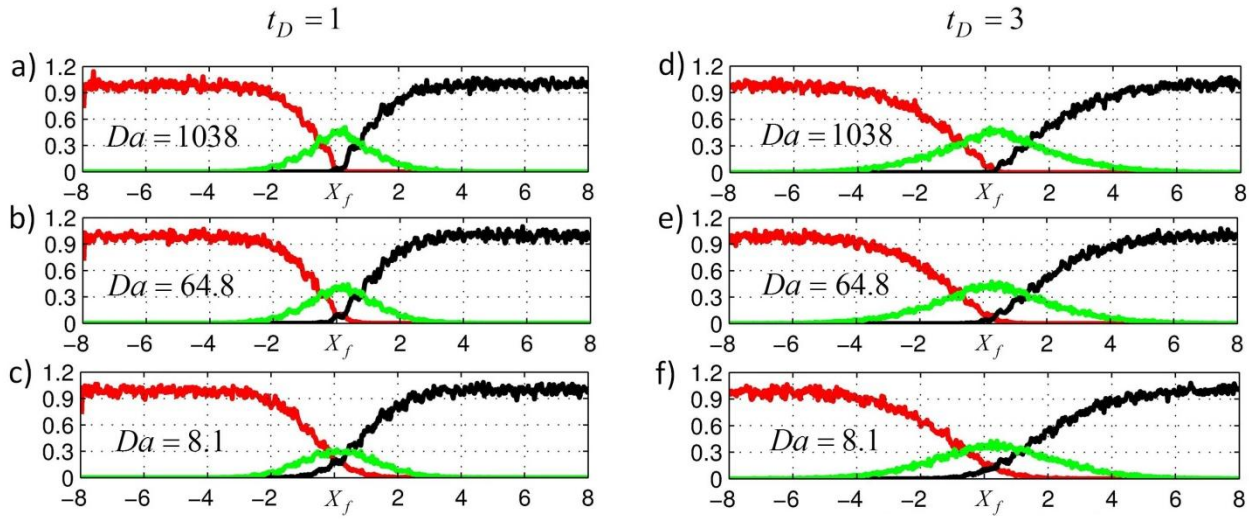

Figure 22 Temporal evolution of the section-averaged concentration of the two reactants c_A *(black curve) and* c_B *(red curve)and of the reaction product* c_C *(green curve), centered at XF . Numerical results are for Pe = 6 and* $\phi = 0.25$

Figure 22 shows the longitudinal distribution of the section-averaged concentrations along the channel for selected combinations of Pe and Da. The results are presented for different observation times by adopting the reference frame X_f, where $X_f = \hat{u}\hat{t} / \hat{h}$, to allow a direct comparison between the concentration snapshots. Da strongly influences the spatial distribution of the three species mean concentrations along the channel. It can be noticed from the Figure 22a and Figure 22d that(in case of high values of Da) distribution of reactant C is mainly localized near reaction front X_f. However in case of low Da numbers solute C spreads more. Indeed, R_D^* for $t_D > 1$ is the same for the values of Da (Figure 22a) which means that for high values of Da the reaction front will be thinner than for small values of Da.

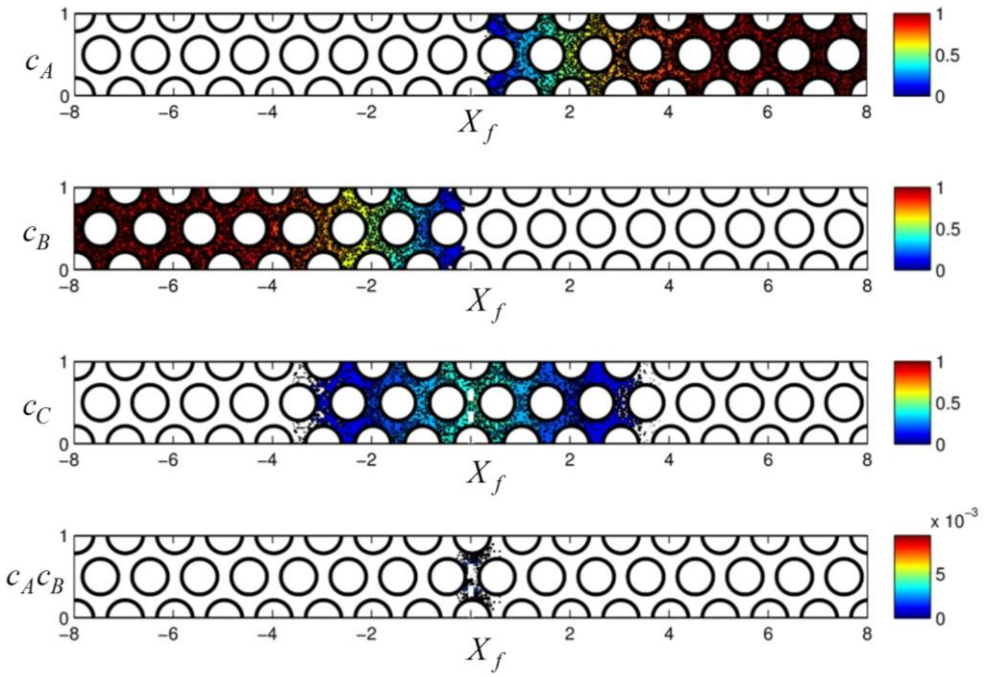

Figure 23. Snapshot of the simulation for Pe=6, Da=1038, $t_D = 3$.

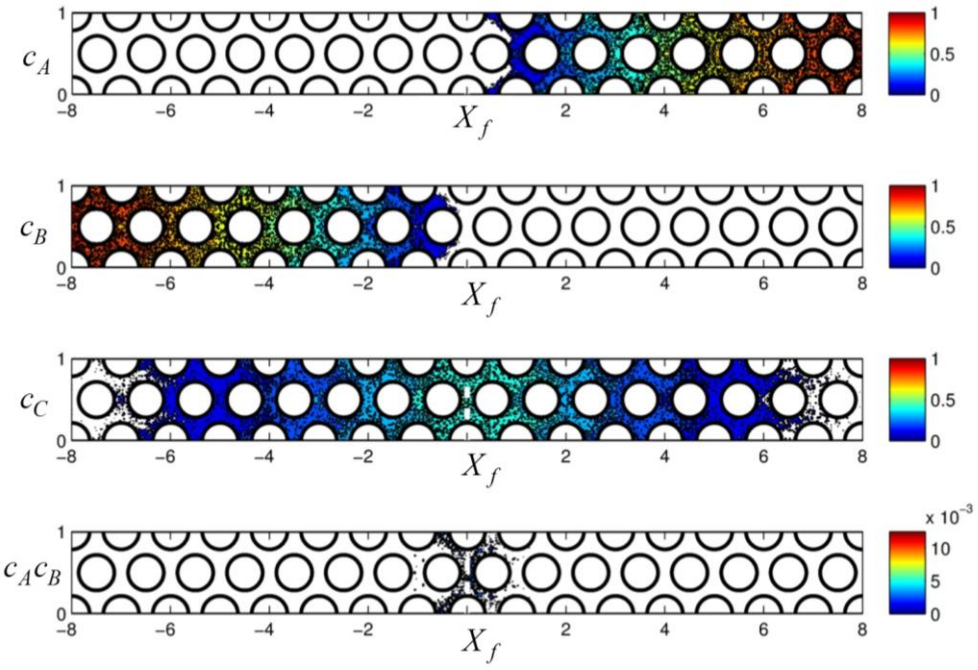

Figure 24.Snapshot of the simulation for Pe=24, Da=1038, $t_D = 3$.

Figure 23- Figure **24** depict the distribution within the channel of the solutes and mixing intensity $c_A c_B$ of the reactants for selected observation times and combinations of Pe and Da . This allows a detailed investigation of the micro-scale spatial features of the region where mixing of the two reactants A and B takes place. The size of the mixing zone highly depends on Pe and Da. Generally, $c_A c_B$ is maximum at $x = X_f$. The presence of immobile zones induces a stretching of the reaction zone with time. This, in turn, causes an increase of the contact surface between the two reactants. This, in turn, causes an increase of the contact surface between the two reactants.

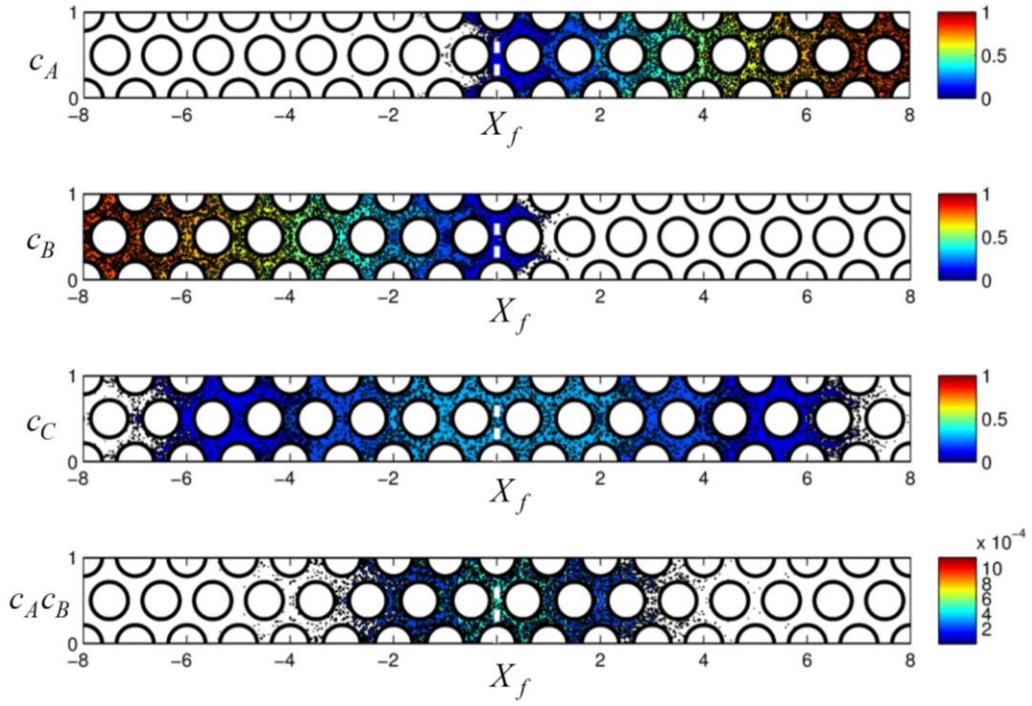

.

Figure 25.Snapshot of the simulation for Pe=24, Da=8, $t_D = 3$.

This mechanism explains the dependence of t_R^* on Pe observed before, i.e., the stretching of the mixing zone induces a global increase of R_R^*. The fingerprint of the velocity

field is recognizable in the mixing zone. The product $c_A c_B$ may vary by one order of magnitude over a single cross section. As lateral mixing does not have time to take place in the presence of a fast reaction, the two reactants are incompletely mixed over the cross section. On the other hand, for small Da , lateral mixing induced by diffusion smoothes out the product $c_A c_B$ along the y-direction (Figure 25).

The initial stretching of the front (Figure 23-Figure 24) obviously increases with Pe , i.e. when the velocity variations over the channel section are largest. Two combined effect of longitudinal mixing and front stretching and the fingerprint of the velocity field with a persistent incomplete mixing of the reactants over the channel section become more evident for large Pe. To summarize, for the adopted initial conditions the evolution of the reactive process appears to be driven by the Damkohler and the Peclet numbers for short times. At this stage, the global reaction rate continuously increases as the diffusive (or dispersive) fluxes exceed the capability of the reaction to consume the reactants at the front. As time increases, dispersion (or diffusion) becomes the limiting factor and Pe governs the evolution of the global reaction rate in the channel through the effective dispersion coefficient D^*. Transition towards this late time regime takes place for $t_R > t_R^*(Pe)$. Nevertheless, Da always displays an important and persistent influence on the spatial distribution of the reactants along the channel and on the local features of the mixing zone, where reaction takes place. In particular, a fast reaction induces a clear correlation between the velocity field and the spatial patterns of the mixing of the reactants.

V. Upscaling of parameters

An effective model of the reactive transport process described in Section II is derived through averaging of the governing equations across the section of the simulation media. The analysis relies on the developments illustrated by *Porta et al*.[2012] and based on volume averaging. Then, effective model coefficients are introduced and calculated from the particle tracking numerical simulations.

1. Theoretical framework. Volume averaging.

Firstly we introduce two new concentration fields $c_D = c_B - c_A$ and $c_E = c_C - c_B$ to simplify the initial system. Then the expressions for the concentrations are introduced into the system (2.5)-(2.3) and after some manipulations system takes following form

$$\frac{\partial c_B}{\partial t} + \mathbf{u} \cdot \nabla c_B = \frac{1}{Pe} \nabla^2 c_B - \frac{Da}{Pe} \left(c_B - c_D \right) c_B \tag{2.39}$$

$$\frac{\partial c_D}{\partial t} + \mathbf{u} \cdot \nabla c_D = \frac{1}{Pe} \nabla^2 c_D \tag{2.40}$$

$$\frac{\partial c_E}{\partial t} + \mathbf{u} \cdot \nabla c_E = \frac{1}{Pe} \nabla^2 c_E \tag{2.41}$$

It should be noted that (2.40) and (2.41) are not coupled with other equations and can be solved independently. Applying the volume averaging (described at Chapter I) to (2.40) leads to

$$\begin{aligned} &\phi \frac{\partial \left\langle c_i \right\rangle^l}{\partial t} + \phi \left\langle \mathbf{u} \right\rangle^l \cdot \nabla \left\langle c_i \right\rangle^l = \\ &\frac{1}{Pe} \left[\phi \nabla^2 \left\langle c_i \right\rangle^l + \nabla \phi \cdot \nabla \left\langle c_i \right\rangle^l + \nabla \cdot \left(\frac{1}{|V|} \int_{A_{SL}} \tilde{c}_i \mathbf{n} dA \right) \right] - \nabla \cdot \left\langle \tilde{\mathbf{u}} \tilde{c}_i \right\rangle \end{aligned} \tag{2.42}$$

where index l - means that averaging is being performed over liquid phase, $i = D, E$, A_{SL} - solid-liquid interface.

Following *Porta et al.*[2012] we present two different volume averaged equations for the reactive species B corresponding to 1) $Da \gg Pe$ and 2) $O(Da) \approx O(Pe)$.

Hence, the equation in the case of $Da \gg Pe$ is

$$\phi \frac{\partial \langle c_B \rangle^l}{\partial t} + \phi \langle \mathbf{u} \rangle^l \cdot \nabla \langle c_B \rangle^l = \frac{1}{Pe}\left[\phi \nabla^2 \langle c_B \rangle^l + \nabla \phi \cdot \nabla \langle c_B \rangle^l + \nabla \cdot \left(\frac{1}{|V|} \int_{A_{SL}} \tilde{c}_B \mathbf{n} dA \right) \right] \quad (2.43)$$
$$-\phi \frac{Da}{Pe}\left[\langle c_B \rangle^l \left(\langle c_B \rangle^l - \langle c_D \rangle^l \right) + \langle \tilde{c}_B \left(\tilde{c}_B - \tilde{c}_D \right) \rangle \right] - \nabla \cdot \langle \tilde{\mathbf{u}} \tilde{c}_B \rangle$$

In the second case when $O(Da) \approx O(Pe)$ the corresponding equation is

$$\phi \frac{\partial \langle c_B \rangle^l}{\partial t} + \phi \langle \mathbf{u} \rangle^l \cdot \nabla \langle c_B \rangle^l = \frac{1}{Pe}\left[\phi \nabla^2 \langle c_B \rangle^l + \nabla \phi \cdot \nabla \langle c_B \rangle^l + \nabla \cdot \left(\frac{1}{|V|} \int_{A_{SL}} \tilde{c}_B \mathbf{n} dA \right) \right] \quad (2.44)$$
$$-\phi \frac{Da}{Pe}\left[\langle c_B \rangle^l \left(\langle c_B \rangle^l - \langle c_D \rangle^l \right) \right] - \nabla \cdot \langle \tilde{\mathbf{u}} \tilde{c}_B \rangle$$

The cross covariance term $\langle \tilde{c}_B \left(\tilde{c}_B - \tilde{c}_D \right) \rangle$ appearing in (2.43) was explored numerically [*Kapoor et al.*, 1997; 1998] for a Poiseuille flow condition taking place within straight conduit. Numerical results show that, in the specific condition examined, the relevance of the so called segregation intensity factor, which is linked to the above mentioned average of the fluctuations product, increases with Da/Pe . Numerical simulations performed *Battiato et al*. [2009] for a diffusion-reaction setting within fully saturated idealized medium, at $Da \gg 1$ ($Da = 27$) and in the vicinity of the reaction front, indicate that neglecting these terms related to non-uniform mixing is not the weakest approximation. For the sake of generality the term $\langle \tilde{c}_B \left(\tilde{c}_B - \tilde{c}_D \right) \rangle$ is

included (2.43). In equation (2.44), related to the condition $O(Da) \approx O(Pe)$, we adopt the simplifying assumption that the influence of the second order term can be neglected. The range of conditions under which this assumption can provide reliable results are examined in next sections. We note that we do not consider here scenarios for which $Da \ll Pe$ because this leads to the standard advection dispersion equation, as it has been shown by, e.g., *Battiato et al*.[2010], in the framework of upscaling via multiple scale expansion of an advection-diffusion problem with heterogeneous reaction.

2. Closure

Equations (2.42)-(2.44) are written in unclosed form since they contain microscopic quantities $\tilde{c}_i$. The closure of (2.42)-(2.44) is obtained by considering the equations satisfied by $\tilde{c}_i$. In the following part of the thesis the closure equations are derived for the concentrations of the conservative components c_D and c_E closure equations for the reactive species c_B for two cases: 1) $Da \gg Pe$ and 2) $O(Da) \approx O(Pe)$.

a. Transport equation for conservative species

To derive equation satisfied by $\tilde{c}_i$ we divide (2.42) by ϕ and subtract the resulting form of the equation from (2.40)-(2.41) which leads to

$$\frac{\partial \tilde{c}_i}{\partial t} + \mathbf{u}\cdot\nabla\tilde{c}_i + \tilde{\mathbf{u}}\cdot\nabla\langle c_i\rangle^l = \frac{1}{Pe}\nabla^2\tilde{c}_i$$
$$-\frac{1}{Pe}\left[\nabla\phi\cdot\nabla\langle c_i\rangle^l + \nabla\cdot\left(\frac{1}{|V|}\int_{A_{SL}}\tilde{c}_i\mathbf{n}dA\right)\right] + \frac{1}{\phi}\nabla\cdot\langle\tilde{\mathbf{u}}\tilde{c}_i\rangle \tag{2.45}$$

The following estimates hold on the basis of the order of magnitude of the terms in (2.45) provided by *Whitaker* [1999]

$$\nabla^2\tilde{c}_B \gg \nabla\cdot\left(\frac{1}{|V|}\int_{A_{SL}}\tilde{c}_i\mathbf{n}dA\right) \geq \nabla\phi\cdot\nabla\langle c_i\rangle^l \tag{2.46}$$

$$\frac{1}{\phi}\nabla\cdot\langle\tilde{\mathbf{u}}\tilde{c}_i\rangle \ll \mathbf{u}\cdot\nabla\tilde{c}_i \tag{2.47}$$

The estimates (2.46)-(2.47) allow to simplify (2.45) as

$$\frac{\partial \tilde{c}_i}{\partial t} + \mathbf{u}\cdot\nabla\tilde{c}_i + \tilde{\mathbf{u}}\cdot\nabla\langle c_i\rangle^l = \frac{1}{Pe}\nabla^2\tilde{c}_i \tag{2.48}$$

The equation (2.48) is subject to the following boundary and initial conditions

$$\mathbf{n}\cdot\nabla\langle c_i\rangle^l = -\mathbf{n}\cdot\nabla\tilde{c}_i \qquad \mathbf{x}\in A_{SL} \tag{2.49}$$

$$\tilde{c}_i(t=0) = \tilde{c}_{i0} \tag{2.50}$$

where $\tilde{c}_{i0}$ is the initial distribution of the spatial deviation of the concentration at the pore scale. Following the *Whitaker* [1999], the problem set (2.48)-(2.50) is solved within a unit cell. $\nabla\langle c_i\rangle^l$ can be considered as uniform within the cell. Assuming periodic structure for the porous medium and a periodic velocity field allows imposing periodic boundary conditions on the external surface of the cell

$$\tilde{c}_i(\mathbf{r}+l_i) = \tilde{c}_i(\mathbf{r}), \quad \langle\tilde{c}_i\rangle^l = 0 \tag{2.51}$$

where l_i are the lattice vectors of the unit cell.

Then a quasi-steady solution of (2.48) is typically derived [*Ochoa-Tapia et al*., 1991; *Whitaker,* 1999; *Battiato,* 2011]. The solution can be written as

$$\tilde{c}_i = \mathbf{b}_{ii} \cdot \nabla \langle \tilde{c}_i \rangle \tag{2.52}$$

where the vectors $\mathbf{b}_{ii}$ are closure variables. By introducing the expression (2.52) into equations (2.48) one can derive the equation for the closure variables

$$\mathbf{u} \cdot \nabla \mathbf{b}_{ii} + \tilde{\mathbf{u}} = \frac{1}{Pe} \nabla^2 \mathbf{b}_{ii} \tag{2.53}$$

$$\mathbf{n} \cdot \nabla \mathbf{b}_{ii} = -\mathbf{n} \tag{2.54}$$

b. Reactive transport equation. Case of $Da \gg Pe$

Subtracting (2.44) from (2.39) and using estimates (2.46)-(2.47) leads to

$$\begin{aligned} &\frac{\partial \tilde{c}_B}{\partial t} + \mathbf{u} \cdot \nabla \tilde{c}_B + \tilde{\mathbf{u}} \cdot \nabla \langle c_B \rangle^l = \frac{1}{Pe} \nabla^2 \tilde{c}_B - \\ &- \frac{Da}{Pe} \left[c_B \left(c_B - c_D \right) - \langle c_B \rangle^l \left(\langle c_B \rangle^l - \langle c_D \rangle^l \right) - \left\langle \tilde{c}_B \left(\tilde{c}_B - \tilde{c}_D \right) \right\rangle \right] \end{aligned} \tag{2.55}$$

The reaction term in (2.55) can be reformulated as

$$\begin{aligned} &\left[c_B \left(c_B - c_D \right) - \langle c_B \rangle^l \left(\langle c_B \rangle^l - \langle c_D \rangle^l \right) - \left\langle \tilde{c}_B \left(\tilde{c}_B - \tilde{c}_D \right) \right\rangle \right] = \\ &\left[\tilde{c}_B \left(\langle c_B \rangle^l - \langle c_D \rangle^l \right) + \langle c_B \rangle^l \left(\tilde{c}_B - \tilde{c}_D \right) + \tilde{c}_B \left(\tilde{c}_B - \tilde{c}_D \right) - \left\langle \tilde{c}_B \left(\tilde{c}_B - \tilde{c}_D \right) \right\rangle \right] \end{aligned} \tag{2.56}$$

The closure problem is nonlinear in $\tilde{c}_B$ due to the format of the reaction term. We consider here a linearized form of (2.55) by using assumption

$$\tilde{c}_B\left(\langle c_B\rangle^l-\langle c_D\rangle^l\right)+\langle c_B\rangle^l\left(\tilde{c}_B-\tilde{c}_D\right)\gg\tilde{c}_B^2-\left\langle\tilde{c}_B^2\right\rangle-\left\langle\tilde{c}_B\tilde{c}_D-\left(\tilde{c}_B-\tilde{c}_D\right)\right\rangle \tag{2.57}$$

according to which the local variation of the second order terms is neglected. By the virtue of (2.57), the closure equation (2.55) becomes

$$\frac{\partial\tilde{c}_B}{\partial t}+\mathbf{u}\cdot\nabla\tilde{c}_B+\tilde{\mathbf{u}}\cdot\nabla\langle c_B\rangle^l=\frac{1}{Pe}\nabla^2\tilde{c}_B-\frac{Da}{Pe}\left[\tilde{c}_B\left(\langle c_B\rangle^l-\langle c_D\rangle^l\right)+\langle c_B\rangle^l\left(\tilde{c}_B-\tilde{c}_D\right)\right] \tag{2.58}$$

When $Da\gg Pe$ the following estimates hold

$$\frac{Da}{Pe}\left[\tilde{c}_B\left(\langle c_B\rangle^l-\langle c_D\rangle^l\right)+\langle c_B\rangle^l\left(\tilde{c}_B-\tilde{c}_D\right)\right]\gg\mathbf{u}\cdot\nabla\tilde{c}_B+\tilde{\mathbf{u}}\cdot\nabla\langle c_B\rangle^l \tag{2.59}$$

$$\frac{Da}{Pe}\left[\tilde{c}_B\left(\langle c_B\rangle^l-\langle c_D\rangle^l\right)+\langle c_B\rangle^l\left(\tilde{c}_B-\tilde{c}_D\right)\right]\gg\frac{1}{Pe}\nabla^2\tilde{c}_B \tag{2.60}$$

Assuming that the typical time scale associated with the problem is not small, i.e., $t=O(1)$, leads to

$$\frac{Da}{Pe}\left[\tilde{c}_B\left(\langle c_B\rangle^l-\langle c_D\rangle^l\right)+\langle c_B\rangle^l\left(\tilde{c}_B-\tilde{c}_D\right)\right]\gg\frac{\partial\tilde{c}_B}{\partial t} \tag{2.61}$$

Considering (2.61) allows to simplify (2.58) to the following algebraic relationship

$$\tilde{c}_B=\tilde{c}_D\frac{\langle c_B\rangle^l}{2\langle c_B\rangle^l-\langle c_D\rangle^l} \tag{2.62}$$

This implies that the evolution of $\tilde{c}_D$ drives the distribution of $\tilde{c}_B$. The reaction is locally fast enough so that the amount of available reactant $\tilde{c}_B$ is instantaneously adjusted according to (2.62) as $\tilde{c}_D$ evolves. Finally, substituting (2.53) into (2.62) leads to

$$\tilde{c}_B=\mathbf{b}_{DD}\cdot\nabla\langle c_D\rangle^l\cdot\frac{\langle c_B\rangle^l}{2\langle c_B\rangle^l-\langle c_D\rangle^l} \tag{2.63}$$

c. Reactive transport equation. Case of $O(Da) \approx O(Pe)$

According to the standard derivation, the closure equation for this case is

$$\frac{\partial \tilde{c}_B}{\partial t} + \mathbf{u} \cdot \nabla \tilde{c}_B + \tilde{\mathbf{u}} \cdot \nabla \langle c_B \rangle^l = \frac{1}{Pe} \nabla^2 \tilde{c}_B - \frac{Da}{Pe} \left[\tilde{c}_B \left(\langle c_B \rangle^l - \langle c_D \rangle^l \right) + \langle c_B \rangle^l \left(\tilde{c}_B - \tilde{c}_D \right) \right] \quad (2.64)$$

When $O(Da) \approx O(Pe)$ the time scales characterizing reaction and advection are of the same order of magnitude and (2.64) cannot be further simplified. In this case the closure equation (2.64) for the reactive species B and the equation (2.48) are coupled, as both $\tilde{c}_B$ and $\tilde{c}_D$ appear in (2.64). Making use of superposition leads to

$$\begin{bmatrix} \tilde{c}_B \\ \tilde{c}_D \\ \tilde{c}_E \end{bmatrix} = \begin{bmatrix} \mathbf{b}_{BB} & \mathbf{b}_{BD} & 0 \\ 0 & \mathbf{b}_{DD} & 0 \\ 0 & 0 & \mathbf{b}_{EE} \end{bmatrix} \cdot \begin{bmatrix} \nabla \langle c_B \rangle^l \\ \nabla \langle c_D \rangle^l \\ \nabla \langle c_E \rangle^l \end{bmatrix} \quad (2.65)$$

where $\mathbf{b}_{DD}$ and $\mathbf{b}_{EE}$ can be computed independently through (2.53). We can then write

$$\tilde{c}_B = \mathbf{b}_{BB} \nabla \langle c_B \rangle^l + \mathbf{b}_{BD} \nabla \langle c_D \rangle^l \quad (2.66)$$

This leads to the following equations for the closure variables $\mathbf{b}_{BB}$ and $\mathbf{b}_{BD}$

$$\mathbf{u} \cdot \nabla \mathbf{b}_{BB} + \tilde{\mathbf{u}} = \frac{1}{Pe} \nabla^2 \mathbf{b}_{BB} - \frac{Da}{Pe} \left[\mathbf{b}_{BB} \left(2 \langle c_B \rangle^l - \langle c_D \rangle^l \right) \right] \quad (2.67)$$

$$\mathbf{u} \cdot \nabla \mathbf{b}_{BD} + \tilde{\mathbf{u}} = \frac{1}{Pe} \nabla^2 \mathbf{b}_{BD} - \frac{Da}{Pe} \left[\mathbf{b}_{BD} \left(2 \langle c_B \rangle^l - \langle c_D \rangle^l \right) - \mathbf{b}_{BD} \langle c_B \rangle^l \right] \quad (2.68)$$

$$\mathbf{n} \cdot \mathbf{b}_{BB} = -\mathbf{n} \qquad \mathbf{x} \in A_{SL} \quad (2.69)$$

$$\mathbf{n} \cdot \mathbf{b}_{BD} = 0 \qquad \mathbf{x} \in A_{SL} \quad (2.70)$$

3. *Upscaled system*

In this section developments of Section 1 are coupled with the closure developed in Section 2 to write the closed form of the system being upscaled.

The scheme of this section will be the same as the previous one, i.e. : 1) the nonreactive transport 2) case when $Da \gg Pe$ and 3) case when $O(Da) \approx O(Pe)$.

a. Nonreactive transport

Making use equation (2.52) and putting it into (2.42) gives the closed form of equations (2.40)-(2.41):

$$\phi \frac{\partial \langle c_i \rangle^l}{\partial t} + \left[\langle \mathbf{u} \rangle^l - \frac{\nabla \phi}{\phi Pe} \right] \phi \langle c_i \rangle^l = \frac{\phi}{Pe} \nabla \cdot \left[(\mathbf{I} + \mathbf{D}_i) \nabla \langle c_i \rangle^l \right] \tag{2.71}$$

where $i = D, E$.

The total dispersion in (2.71) is defined as

$$\mathbf{D}_i = \frac{1}{\phi |V|} \int_{A_{SL}} \mathbf{b}_{ii} \mathbf{n} dA - Pe \langle \tilde{\mathbf{u}} \mathbf{b}_{ii} \rangle \tag{2.72}$$

which includes the effect of molecular diffusion, effective diffusion(taking into account the geometry of the unit cell) and hydrodynamic dispersion. The formulation is consistent with that in *Whitaker* [1999] for non-reactive transport.

b. Reactive transport equation. Case of $Da \gg Pe$

Substituting (2.63) into (2.43) leads to

$$\begin{aligned}&\phi\frac{\partial\langle c_B\rangle^l}{\partial t}+\phi\langle\mathbf{u}\rangle^l\cdot\nabla\langle c_B\rangle^l=\frac{\phi}{Pe}\nabla^2\langle c_B\rangle^l+\frac{\phi}{Pe}\nabla\cdot\left[\mathbf{D}_D\nabla\langle c_D\rangle^l M\right]\\&-\phi\frac{Da}{Pe}\langle c_B\rangle^l\left[\left(\langle c_B\rangle^l-\langle c_D\rangle^l\right)-M^2\frac{\langle c_A\rangle^l}{\langle c_B\rangle^l}\left\langle\left(\mathbf{b}_D\nabla\langle c_D\rangle^l\right)^2\right\rangle\right]\end{aligned}\tag{2.73}$$

where $\mathbf{D}_D$ is defined by (2.72) and

$$M=\frac{\langle c_B\rangle^l}{\langle c_B\rangle^l+\langle c_A\rangle^l}\tag{2.74}$$

It can be shown that (2.73) can be reduced to a model describing the dispersion of a conservative component when $c_A\to 0$. Recalling that $c_D=c_B-c_A$ allows rewriting dispersive term in (2.73) as

$$\frac{\phi}{Pe}\nabla\cdot\left[\mathbf{D}_D\nabla\langle c_D\rangle^l M\right]=\frac{\phi}{Pe}\nabla\cdot\left[\mathbf{D}_D\left(\nabla\langle c_B\rangle^l-\nabla\langle c_A\rangle^l\right)M\right]\tag{2.75}$$

Then assuming that $c_A\to 0$ (i.e. $c_D\to c_B, M\to 0$) (2.75) takes form of

$$\lim_{c_A\to\infty}\frac{\phi}{Pe}\nabla\cdot\left[\mathbf{D}_D\nabla\langle c_D\rangle^l M\right]=\frac{\phi}{Pe}\nabla\cdot\left[\mathbf{D}_D\nabla\langle c_B\rangle^l M\right]\tag{2.76}$$

So that equation (2.73) transforms into

$$\phi\frac{\partial\langle c_B\rangle^l}{\partial t}+\phi\langle\mathbf{u}\rangle^l\cdot\nabla\langle c_B\rangle^l=\frac{\phi}{Pe}\nabla\cdot\left[\left(\mathbf{I}+\mathbf{D}_D\right)\nabla\langle c_B\rangle^l\right]\tag{2.77}$$

Equation (2.73) shows that (a) the upscaled dispersive flux (i.e. $\frac{\phi}{Pe}\nabla\cdot\left[\mathbf{I}\nabla\langle c_B\rangle^l+\mathbf{D}_D\nabla\langle c_D\rangle^l M\right]$) is described by a non-Fickian component depicting the interactions between molecular diffusion and effective dispersion, and (b) the dispersive term is

proportional through M to the upscaled concentrations $\langle c_B \rangle^l$ and $\langle c_D \rangle^l$, thus suggesting that chemical reaction and hydrodynamic dispersion are intimately connected.

Equation (2.73) also shows that the effect of dispersion in the case of reactive transport can be different from what observed for conservative solutes. This result is consistent with recent developments [*Valdes-Parada et al.,* 2011]. This suggests that upscaled dispersion coefficients calibrated on the basis of conservative transport settings cannot be systematically adopted to model reactive transport in the same flow conditions.

c. Reactive transport equation. Case of $O(Da) \approx O(Pe)$

Substituting (2.66) into (2.43) leads to

$$\phi \frac{\partial \langle c_B \rangle^l}{\partial t} + \phi \langle \mathbf{u} \rangle^l \cdot \nabla \langle c_B \rangle^l = \frac{\phi}{Pe} \nabla \cdot \left[\mathbf{D}_B \nabla \langle c_B \rangle^l \right] - \phi \frac{Da}{Pe} \langle c_B \rangle^l \left(\langle c_B \rangle^l - \langle c_D \rangle^l \right) + \frac{\phi}{Pe} \nabla \cdot \left(\mathbf{H}_{BD} \nabla \langle c_D \rangle^l \right) \tag{2.78}$$

Here, $\mathbf{D}_B$ is defined by (2.72) and the interactive dispersion tensor $\mathbf{H}_{BD}$ is defined as

$$\mathbf{H}_{BD} = \frac{1}{\phi |V|} \int_{A_{SL}} \mathbf{b}_{BD} \mathbf{n} dA - Pe \langle \tilde{\mathbf{u}} \mathbf{b}_{BD} \rangle \tag{2.79}$$

We note that all dispersive fluxes in (2.78) are spatially dependent through $\langle c_B \rangle^l$ and $\langle c_D \rangle^l$. Equations (2.67) and (2.68) become independent in the limit for $Da \to 0$ and the interactive dispersion tensor $\mathbf{H}_{BD}$ vanish from the resulting upscaled equation. It means that the importance of the interactive dispersion term tends to increase with the reaction rate.

4. *Results. Numerical upscaling.*

This section is devoted to the numerical computation of the dispersive and reactive coefficients presented in previous section (Chapter 2 Section V.3.). The upscaled coefficients are going to be compared with the results of the simulations presented in Chapter 2 Section IV.

We start the analysis from the solution of the closure equation in the case of non-reactive transport, i.e. equation (2.53).

The upscaled dispersion coefficient, D_U^* , is computed using the equation (2.72) and compared with the real one that is computed via particle tracking simulations, D_R^*, and presented before (Figure 18) .

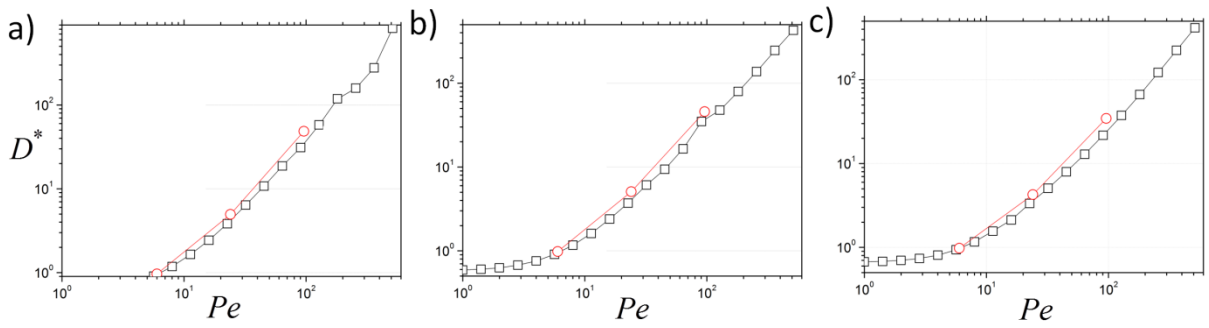

Figure 26. Comparison of the real dispersion coefficients D_R^* *(○) and the upscaled coefficients* D_U^* *(□) with different porosity of the unit cell* ϕ *: a)* $\phi = 0.25$ *b)* $\phi = 0.36$ *c)* $\phi = 0.50$

Figure 26 shows that the values of the upscaled coefficients calculated by equation (2.72) are very close to the real values of dispersion calculated through particle tracking algorithm. The fitting is quite good for the all values of porosity.

The reaction-related term appearing in (2.73) includes contribution of the product of the volume averaged concentrations and the second order term. We focus here on the latter. A single closure variable, $\mathbf{b}_D$, is employed to close (2.43). Consequently, the second order term

$\left\langle \tilde{c}_B \left(\tilde{c}_B - \tilde{c}_D \right) \right\rangle$ is proportional to the volume average of $\mathbf{b}_D^2$. This implies that the upscaled reaction term is intimately linked to the micro-scale behavior of a nonreactive species, as $\mathbf{b}_D$ provides the solution for the closure of a conservative transport problem and emphasizes the interaction between dispersion and reaction under these conditions. In previous studies [*Porta et al.*, 2012] it was shown that in the case of plane channel geometry the incomplete mixing is proportional to Pe^{β} with $\beta = 2$ (i.e. $\left\langle \mathbf{b}_D^2 \right\rangle \propto Pe^2$). Figure 27 shows that in the case of our geometry the volume average of $\mathbf{b}_D^2$ is proportional to Pe^{β} with $\beta \approx 1.5$ (i.e. $\left\langle \mathbf{b}_D^2 \right\rangle \propto Pe^{1.5}$).

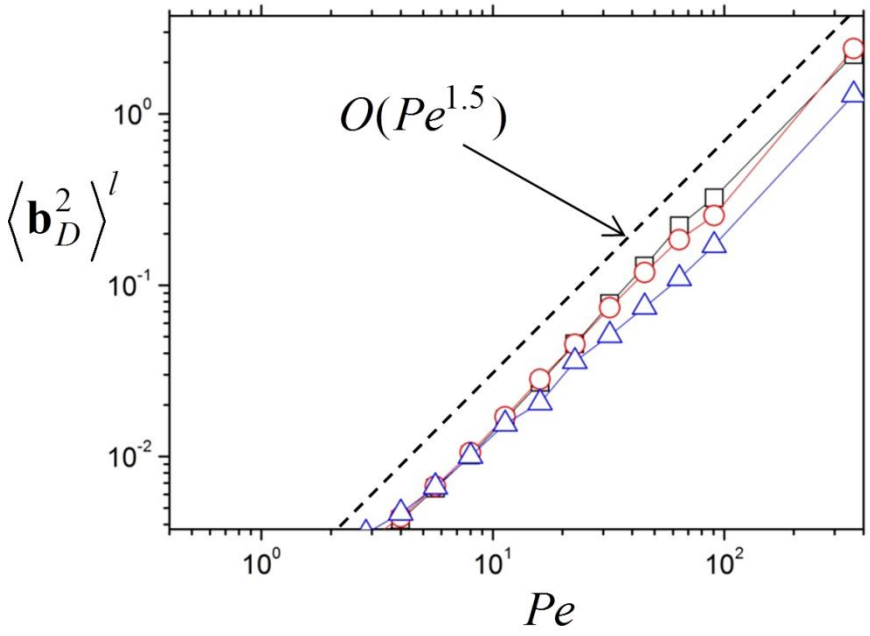

Figure 27. Volume average of $\mathbf{b}_D^2$ *as a function of* Pe *with different porosity of the unit cell* ϕ *:* $\phi = 0.25$ *(* □*);* $\phi = 0.36$ *(* ○*); c)* $\phi = 0.50$ *(* △*)*

The next step of the analysis is to assess the predictive performance of the effective reaction coefficient appearing in the upscaled equation (2.73) against the results of the micro-

scale simulations. In the volume averaged equation (2.43), the reaction rate, $r = \langle c_A c_B \rangle^l$, is expressed as the sum of the two following terms

$$r_1 = \langle c_A \rangle^l \langle c_B \rangle^l \tag{2.80}$$

and

$$r_2 = \langle \tilde{c}_A \tilde{c}_B \rangle^l \tag{2.81}$$

If the scale separation constraints ($\mathbf{r}_0^2 \ll L_c L_{c1}$, $\mathbf{r}_0 \ll L_c$ - reported at Chapter 1) for averaging the reaction term are met then the reaction rate is

$$r_{1+2} = \langle c_A \rangle^l \langle c_B \rangle^l + \langle \tilde{c}_A \tilde{c}_B \rangle^l \approx \langle c_A c_B \rangle^l = r \tag{2.82}$$

It mean that if the reactant concentration gradient is large the scale separation condition is not respected and the reaction term cannot be averaged. Previously it was reported [*Battiato et al.*, 2009] that the scale separation is not met in the case of a fast bimolecular reaction in a batch system.

To define the domain where the constraints are valid we define the error averaging function

$$E = \frac{\int_\Omega |r_{1+2} - r| d\Omega}{\int_\Omega |r| d\Omega} = f(t, Pe, Da, \phi, l_{av}) \tag{2.83}$$

where l_{av} - is the dimension of the averaging volume in the transversal direction. The dimension of l_{av} is [cubes] (Chapter 2 Section IV) and the minimum value in our case is 16 [cubes] that is the length of periodicity.

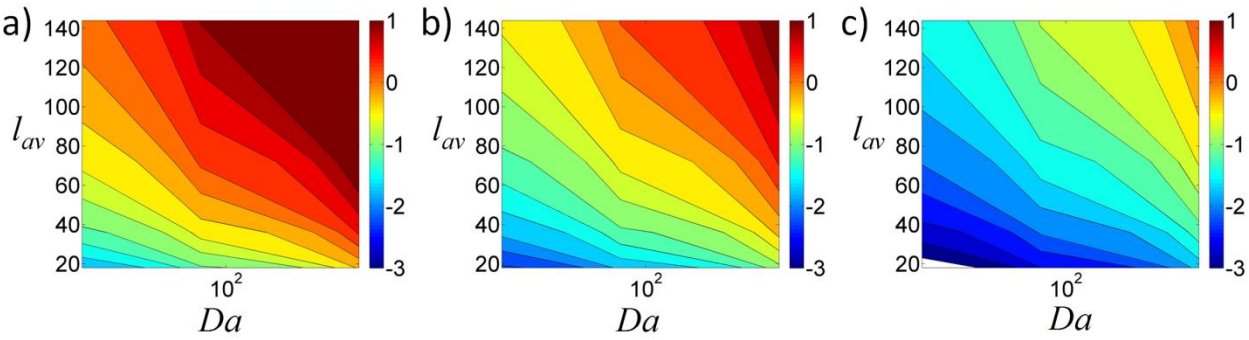

Figure 28. Map of the averaging error function for the case of porosity $\phi = 0.5$ *and values of Pe number: a)* $Pe = 6$ *b)* $Pe = 24$ *c)* $Pe = 96$.

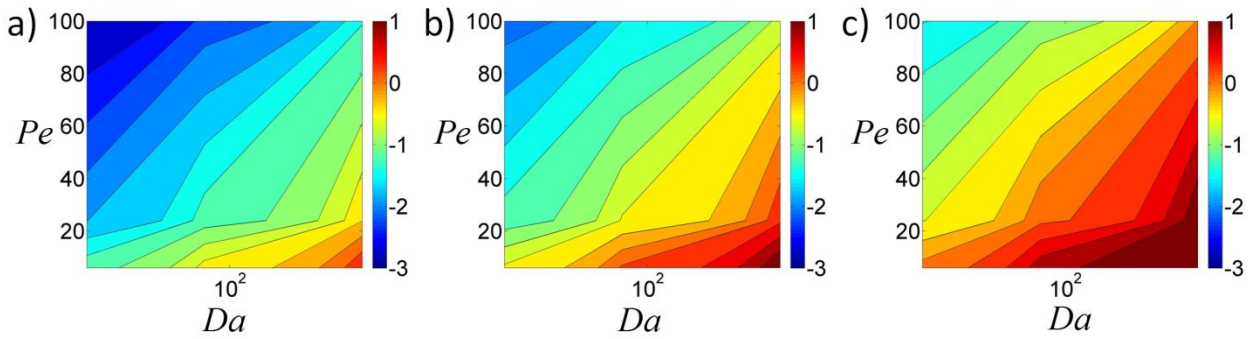

Figure 29. Map of the averaging error function for the case of porosity $\phi = 0.25$ *and values of the averaging length* l_{av} *: a)* $l_{av} = 36$ *b)* $l_{av} = 72$ *c)* $l_{av} = 144$.

Figure 28 and Figure 29 show that the validity of the approximation (2.82) highly depends on the combination of the parameters l_{av}, Pe, Da. Figure 28 depicts that when Pe number is relatively small then the averaging length should small as well. This is in agreement with the observation that for the small value of Pe the reaction takes place in a very small region (since mixing is reduced) so we need short averaging length in order to capture the process with a nice resolution. On the contrary, when Pe is high and the reaction zone spreads through a long distance then we can use bigger values of the averaging volume. The same can be seen from the Figure 29 which shows the dependence of the error function on Da and Pe at constant averaging length. It can be noted that for high Da numbers, when the gradients of reaction rate

are quite high, we need to choose small averaging length or the Pe number should be big enough to stretch the reaction zone.

In the volume averaged equation (2.43), the global reaction rate R_D^* defined by (2.38), is expressed as the sum of the two following terms

$$R^{(1)} = \int_L \langle c_A \rangle^l \langle c_B \rangle^l \, dx \tag{2.84}$$

$$R^{(2)} = \int_L \langle \tilde{c}_A \tilde{c}_B \rangle^l dx \tag{2.85}$$

Here, $R^{(1)}$ is a first order reaction term, which is usually included in standard continuum formulations; $R^{(2)}$ is the second order term taking into account the cross covariance between the concentrations of the reactants along the cross section. The contribution of (2.84) and (2.85) are evaluated through the micro-scale simulations. The closure expression for $R^{(2)}$ is

$$R_U^{(2)} = \int_L M(M-1) \langle b_D^2 \rangle \left(\nabla \langle c_D \rangle^l \right)^2 dx \tag{2.86}$$

Then the upscaled global reaction coefficient can be evaluated as

$$R_U^* = R^{(1)} + R_U^{(2)} \tag{2.87}$$

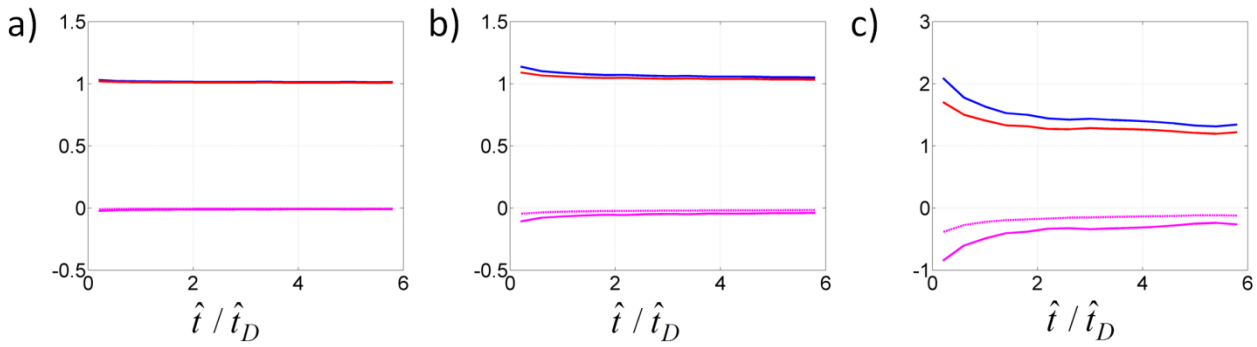

Figure 30. Time evolution of the quantities (2.84)-(2.87) for simulation with parameters: $Pe = 96$, $\phi = 0.5$, $l_{av} = 36$ *and* Da *values : a)* $Da = 8.1$, *b)* $Da = 64.8$, *c)* $Da = 1038$. *The quantities are : (▬)* $R^{(1)} / R_D^*$, *(▬)* R_U^* / R_D^*, *(┅)* $R_U^{(2)} / R_D^*$, *(▬)* $R^{(2)} / R_D^*$.

Figure 30 provides the time evolution of the quantities defined at (2.84)-(2.87) together with R_D^* defined by (2.38). Comparing Figure 30a and Figure 30c allows recognizing the relative contribution of $R^{(1)}$ and $R^{(2)}$ to the global reaction rate for different values of Da number. For small Da, $R^{(1)}$ coincides with R_D^*, as it is always much larger than $R^{(2)}$. In this case, the reaction is not fast enough to preserve the anticorrelation of the concentration field. The effect of $R^{(2)}$ on the global reaction rate is significant for large Da Figure 30c. Hence, neglecting this second order term leads to significantly overestimating the global reaction rate. The values of the term $R_U^{(2)}$ are in a good agreement with $R^{(2)}$. The global upscaled reaction rate, R_U^*, yields an accurate estimate of R_D^*.

VI. Conclusions

The work is focused on the multiscale analysis of a reactive flow in the presence of a homogeneous irreversible reaction. the problem is solved at the micro-scale through a numerical approach based on a particle tracking simulation of the reactive transport process. The purpose of the numerical study was: (a) to provide an accurate description of the reactive process at multiple observation scales, and (b) to characterize dependence on Da and Pe of the upscaled coefficients of effective one-dimensional model. The later is obtained through volume averaging of the micro-scale transport equations. The major conclusions of this work can be summarized as follows:

1. The dynamics of the global production of C are characterized by two distinct stages. In the first stage, the reaction rate increases with the time proportionally to Da and Pe. In the second stage, the global reaction rate is described by a power law decay and is proportional to $t^{-0.5}$. An asymptotic regime is observed for various combinations of Da and Pe. The transition between early time behavior which is influenced by the selected initial conditions and the asymptotic regime occurs for a dimensionless diffusion time t_D^*.

2. An equilibrium between the reactive process and the dispersive flux bringing the reactants at the mixing zone is observed in the asymptotic regime. The Da strongly influences the spatial distribution of the reactants observed in the medium. It also influences the micro-scale patterns of the reactant mixing zone.

3. The influence of the reactive process on the effective dispersion coefficient is assessed through numerical upscaling.

4. The volume averaged model captures the global reaction rate of the system through the sum of two different contributions ,i.e. a first- and a second- order term, respectively given by the product of the two averaged concentrations and the cross correlation of the local concentrations of the reactant. The results demonstrate the role played by Da and Pe on the occurrence of incomplete mixing. Stretching induced by the velocity field is the primary source of the observed incomplete mixing of reactants.

BIBLIOGRAPHY

Ahmadi A., M. Quintard, and S. Whitaker, 1998. Transport in chemically and mechanically heterogeneous porous media V: Two-equation model for solute transport with absorption, Adv. Water Resour., 22, 59-86.

Auriault J.L. and P.M. Adler, 1995. Taylor dispersion in porous media: analysis by multiple scale expansions, Advances in Water Resorces, 18, 4, 217-226

Battiato, D.M. Tartakovsky, A.M. Tartakovsky and T. Scheibe, 2009. On breakdown of macroscopic models of reactive transport in porous media. Adv Water Resour 32, 1664.

Battiato and D.M. Tartakovsky, 2011. Applicability regimes for macroscopic models of reactive transport in porous media. J Contam Hydrol 120, 18.

Bear, J., 1972. Dynamics of Fluids in Porous Media, Dover Science Books, Toronto.

Bear J. and A.H.D. Cheng, 2010. Modelling groundwater flow and contaminant transport, Springer.

Benson D.A. and M.M. Meerschaert, 2008. Simulation of chemical reaction via particle tracking: Diffusion-limited versus thermodynamic rate-limited regimes, Water Resour. Res., 44, W12201, doi:10.1029/2008WR007111.

Berkowitz B., H. Scher and S.E. Silliman, 2000. Anomalous transport in laboratory-scale, heterogeneous porous media, Water Resour. Res., 36, 149– 158.

Berkowitz B., A. Cortis, M. Dentz and H. Scher, 2006. Modeling non-Fickian transport in geological formations as a continuous time random walk, Rev. Geophys., 44, RG2003, doi:10.1029/2005RG000178.

Bjieljic B. and M.J. Blunt, 2006. Pore scale modeling and continuous time random walk analysis of dispersion in porous media, Water Resour. Res., 42, W01202.

Bjieljic B., P. Mostaghimi and M.J. Blunt, 2011. Signature of Non-Fickian Solute Transport in Complex Heterogeneous Porous Media, Phys. Rev. Lett., 107, 204502.

Blunt M.J., 2000. An empirical model for three-phase relative permeability, SPE JOURNAL, Vol:5, Pages:435-445, ISSN:1086-055X

Carrera J., X. Sanchez-Vila, I. Benet, A. Medina, G. Galarza and J. Guimera, 1998. On matrix diffusion: formulations, solution methods and qualitative effects, Hydrogeology Journal, 6, 178–190.

Chastanet J. and B.D. Wood, 2008. Mass transfer process in a two-region medium, Water Resour. Res., 44, W05413.

Cherblanc F., A. Ahmadi, and M. Quintard, 2003. Two-medium description of dispersion in heterogeneous porous media: Calculation of macroscopic properties, Water Resour. Res., 39(6), 1154, doi:10.1029/ 2002WR001559.

Cherblanc F., A. Ahmadi and M. Quintard, 2007. Two-domain description of solute transport in heterogeneous porous media: Comparison between theoretical predictions and numerical experiments, Adv. Water Resour., 20, 1127–1143.

Cirpka O.A., 2002. Choice of dispersion coefficients in reactive transport calculations on smoothed fields, J. Contam. Hydrol., 58, 261–282

Coats K.H. and B.D. Smith, 1964. Dead-end pore volume and dispersion in porous media, Soc.Pet. Eng.J., 4, 73-84.

Coelho D., J.-F. Thovert and P.M. Adler, 1997. Geometrical and transport properties of random packings of spheres and aspherical particles, Phys. Rev. E, 55, 1959-1978.

Cushman J. H. and T. R. Ginn, 2000. Fractional advection-dispersion equation: A classical mass balance with convolution-Fickian flux, Water Resources Research, 36(12):3763–3766.

Cushman J.H., L.S. Bennethum and B.X. Hu, 2002. A primer on upscaling methods for porous media. Adv. Water Resour. 25:1043-1067.

Dagan G., 1989. Flow and Transport in Porous Formations. Springer-Verlag, New York.

Dagan G. and S.C. Lessoff, 2001. Solute transport in heterogeneous formations of bimodal conductivity distribution: 1. Theory, Water Resour. Res., 37(3), 465–472, doi:10.1029/2000WR900225.

Debenest G., V.V. Mourzenko and J.-F. Thovert, 2005. Smoldering in fixed beds of oil shale grains. A three-dimensional micro-scale numerical model, Combust. Theory Modeling, 9,113-135.

Debenest G., V.V. Mourzenko and J.-F. Thovert, 2005. Smoldering in fixed beds of oil shale grains. Governing parameters and global regimes, Combust. Theory Modeling, 9, 301-321.

Dentz M. and B. Berkowitz, 2003. Transport behavior of a passive solute in continuous time random walks and multi-rate mass transfer, Water Resources Research, 39 (5), 1111, doi:10.1029/2001WR001163.

Dentz M., T. Le Borgne, A. Englert and B. Bijeljic, 2010. Mixing, spreading and reaction in heterogeneous media: A brief review, J. Contam. Hydrol., doi:10.1016/j.jconhyd.2010.05.002

Dybbs A. and R.V. Edwards, 1984. A new look at porous media fluid mechanics – Darcy to turbulent. "Fundamentals of transport phenomena in porous media", pages 201–256. Martinus Nijno.

Edery Y., H. Scher and B. Berkowitz, 2010. Particle tracking model of bimolecular reactive transport in porous media, Water Resour. Res., 46, W07524, doi:10.1029/2009WR009017.

Edery Y., A. Guadagnini, H. Scher and B. Berkowitz, 2012. Reactive transport in disordered media: role of fluctuations in interpretation of laboratory experiments, Adv. Water Resour., doi:10.1016/j.advwatres.2011.12.008.

Gelhar L.W., C. Welty and K. R. Rehfeldt, 1992. A critical review of data on field scale dispersion in aquifers, Water Resour. Res., 28(7), 1955-1974.

Golfier F., M. Quintard and S. Whitaker, 2002. Heat and mass transfer in tubes: an analysis using the method of volume averaging, J. Porous Med. (5) 169–85.

Golfier F., M. Quintard and B. D. Wood, 2011. Comparison of theory and experiment for solute transport in weakly heterogeneous bimodal porous media, Adv. Water Resour., 34(7), 899, doi:10.1016/j.advwatres.2011.04.019.

Gramling C. M., C. F. Harvey and L. C. Meigs, 2002. Reactive transport in porous media: A comparison of model prediction with laboratory visualization, Environ. Sci. Technol., 36, 2508–2514.

Gwo J.P., R. O'Brien and P. M. Jardine, 1998. Mass transfer in structured porous media: Embedding meso-scale structure and micro-scale hydrodynamics in a two-region model. J. Hydrology 208(3/4):204-222.

Haggerty R., S.A. McKenna and L.C. Meigs, 2000. On the late-time behavior of tracer test breakthrough curves, Water Resour. Res., 36, 3467-3479.

Haggerty R., C.F. Harvey, C.F. von Schwerin and L.C. Meigs, 2004. What controls the apparent timescales in aquifers and soils? A comparison of experimental results, Water Resour. Res., 40, W01510.

Hornung U., 1997. Homogenization and Porous media, Springer, New York.

Kang K. and S. Redner, 1985. Fluctuation-Dominated Kinetics in Diffusion-Controlled Reactions, Phys. Rev. A 32, 435

Kapoor V., C.T. Jafvert and D.A. Lyn, 1997. Experimental study of a bimolecular reaction in Poiseuille flow, Water Resour. Res., 34(8), 1997–2004.

Landereau P., B.Noetinger and M. Quintard, 2001. Quasi-Steady Two- Equation Models for Diffusive Transport in Fractured Porous Media: Large-Scale Properties for Densely Fractured Systems, Adv. Water Resour. 24, 8, 863-876.

Lemaitre R. and P.M. Adler, 1990. Fractal porous media, IV. Three-dimensional Stokes flow through random media and regular fractals, Transp. Porous Media, 5, 325-340.

Lichtner P.C., D.M. Tartakovsky, 2003. Stochastic analysis of effective rate constant for heterogeneous reactions, 419-429. SERRA, 17 (6).

Neuman S.P. and D. M. Tartakovsky, 2009. Perspective on theories of non-Fickian transport in heterogeneous media, Adv. Water Resour., 32(5), 670-680.

Meakin P. and A.M. Tartakovsky, 2009. Modeling and simulation of pore-scale multiphase fluid flow and reactive transport in fractured and porous media, Rev. Geophys., 47, RG3002.

Metzler R. and J. Klafter, 2000. The random walk's guide to anomalous diffusion: A fractional dynamics approach, Physical reports, 339, 1–77.

Moyne C., 1997. Two-equation model for a diffusive process in porous media using the volume averaging method with an unsteady-state closure, Adv. Water Resour., 20, 63-76.

Mourzenko V.V., S. Bekri, J.F. Thovert, P.M. Adler, 1997. Deposition in fractures, Chem. Eng. Comm., 148-150, 431-464.

Ochoa-Tapia, P. Stroeve and S. Whitaker, 1991. Facilitated transport in porous media. Chem Eng Sci 46, 477.

Orgogozo L., F. Golfier, M. Bues and M. Quintard, 2010. Upscaling of transport processes in porous media with biofilms in non-equilibrium conditions, Adv. Water Resour., 33, 585-600.

Plumb O.A and S. Whitaker, 1988. Dispersion in heterogeneous porous media. Local volume averaging and large scale averaging. Water Resour; 24(7):913-26

Quintard M. and S. Whitaker, 1996. Transport in chemically and machanically heterogenous porous media. I: Theoretical development of region-averaged equations for slightly compressible single-phase flow, Adv Water Res, 19(1), 29-47

Quintard, M., F. Cherblanc and S. Whitaker, 2001. Dispersion in heterogeneous porous media: One-equation non-equilibrium model, Transport Porous Med., 44, 181-203.

Raje D. and V. Kapoor, 2000. Experimental study of bimolecular reaction kinetics in porous media, Environ. Sc. Technol., 34, 1234–1239.

Porta G. M., M. Riva and A. Guadagnini, 2012. Upscaling solute transport in porous media in the presence of an irreversible bimolecular reaction, Adv. Water Resour., 35, 151-162.

Porta G. M., J.-F. Thovert, M. Riva, A. Guadagnini and P. M. Adler, 2012. Micro-scale simulation and numerical upscaling of a reactive flow in a plane channel, Phys. Rev. E 86, 036102

Riva M., A. Guadagnini, D. Fernandez-Garcia, X. Sanchez-Vila and T. Ptak, 2008. Relative importance of geostatistical and transport models in describing heavily tailed breakthrough curves at the Lauswiesen site, J. Contam. Hydrol,101,1-13,doi:10.1016/j.jconhyd.2008.07.004.

Rubin J., 1983. Transport of reacting solutes in porous media: Relation between mathematical nature of problem formulation and chemical nature of reactions, Water Resour. Res., 19(5), 1231–1252, doi:10.1029/WR019i005p01231.

Rubio A.D., A. Zalts, C.D. El Hasi, 2008. Numerical solution of the advection–reaction–diffusion equation at different scales, *Env Mod and Software* vol. 23, p. 90-95

Salles J., J.F. Thovert, R. Delannay, L. Prevors, J.L. Auriault, P.M. Adler, 1993. Taylor dispersion in porous media. Determination of the dispersion tensor , Phys. Fluids A, 5, 2348-2376.

Salles J., J.F. Thovert, P.M. Adler, 1993. Deposition in porous media and clogging, Chem. Eng.Sci., 48, 2839-2858.

Sanchez-Vila X., D. Fernàndez-Garcia, and A. Guadagnini, 2010. Interpretation of column experiments of transport of solutes undergoing an irreversible bimolecular reaction using a continuum approximation, Water Resour. Res., 46, W12510, doi:10.1029/2010WR009539.

Scheibe T.D., Y.-J. Chien, and J.S. Radtke, 2001. Use of quantitative models to design microbial transport experiments in a sandy aquifer, Ground Water,39, 210–222.

Slattery J.C., 1967. Flow in viscoelastic fluids through porous media, AIChEJ, 13(6), 1066-1071

Tartakovsky A.M., G.D. Tartakovsky and T.D. Scheibe, 2009. Effects of incomplete mixing on multi-component reactive transport, Adv in Wat Res 32(11):1674-1679.

Tartakovsky A.M., 2010. Langevin Model for Reactive Transport in Porous Media, Physical Review. E, 82(2 PT 2):Art. No. 026302.

Valdes-Parada F.J., C.G. Aguilar-Madera, J. Alvarez-Ramirez, 2011. On diffusion, dispersion and reaction in porous media. Chem End Sci;66:2177-90.doi:10.1016/j.ces.2011.02.016

Van Genuchten and Dalton, 1986. Models for simulating salt movement in aggregated field soils, Geoderma, 38: 165-183

Wang,L, M. Bayani Cardenas, W. Deng, P.C. Bennett, 2012. Theory for dynamic longitudinal dispersion in fractures and rivers with Poiseuille flow, Geophys. Res. Lett. 39, L05401 doi:10.1029/GL0831.

Whitaker S., 1967. Diffusion and dispersion in porous media, AIChEJ, 13(3), 420-427

Whitaker S., 1999. The method of volume averaging, Netherlands: Kluwer Academic Publishers.

Willingham T., C. Zhang, C.J. Werth, A.J. Valocchi, M.Oostrom, T.Wietsma, 2010. Using dispersivity values to quantify the effects of pore-scale flow focusing on enhanced reaction along a transverse mixing zone, *Adv. Water Resour*., 33(4), 525-535.

Wood B.D., Cherblanc, M. Quintard and S. Whitaker, 2003. Volume averaging for determing the effective dispersion tensor: Closure using periodic unit cells and comparison with ensemble averaging, Water Resour Res., 39(8), 1210, doi:10.1029/2002WR001723

Wood B.D., 2009. The role of scaling laws in upscaling, Adv. Water Resour., 32(5), 723-736

Wood B.D. and F.J. Valdès-Parada, 2012. Local and nonlocal closures using a Green's function approach, Adv. Water Resour., in press, doi:10.1016/j.advwatres.2012.06.008.

Wooding R. A., 1960. Instability of a viscous fluid of variable density in a vertical Hele-Shaw cell, J. Fluid Mech. 7, 501-515.

Zhang Y., D. A. Benson, and D. M. Reeves, 2009. Time and Space nonlocalities underlying fractional-derivative models: Distinction and review of field applications, Adv. Water Resour., 32, 561-581.

Zinn, B. and C. F. Harvey, 2003. When good statistical models of aquifer heterogeneity go bad: A comparison of flow, dispersion, and mass transfer in connected and multivariate Gaussian hydraulic conductivity fields, Water Resources Research, 39 (3), 1051, doi:10.1029/2001WR0